Dissertation
submitted to the
Combined Faculty of Natural Sciences and Mathematics
of the Ruperto Carola University Heidelberg, Germany
for the degree of
Doctor of Natural Sciences

Presented by
M.Sc. Johanna Ripp
Born in: Pforzheim
Oral examination: 22.07.2020

The role of the myosin motor and environmental factors in *Plasmodium* gliding motility

Referees: Prof. Dr. Ulrich Schwarz

Prof. Dr. Friedrich Frischknecht

Summary

Cell migration of *Plasmodium* parasites, the causative agents of malaria, is powered by an actomyosin motor. This substrate-dependent type of movement termed gliding motility is important at different stages throughout the complex life cycle of these parasites and is required to traverse tissues and invade host cells. The motor complex is located beneath the plasma membrane and consists of anchored myosin A proteins that exert forces on actin filaments which can be transmitted to a substrate by transmembrane proteins. How the surrounding environment impacts parasite motility is not fully understood. Furthermore, it is unclear how the actomyosin motor can be modulated to allow for stage-specific regulation of parasite motility. In the first part of this study, I show how substrate elasticity, confinement and pore size affect *Plasmodium* motility using polyacrylamide hydrogels. I found that the parasites were not capable to move persistently on flat soft substrates, while the migratory capacity increased with substrate stiffness. In confined environments on the other hand parasites moved robustly even if the surrounding matrix was extremely soft. *Plasmodium* sporozoites, the stages transmitted into the dermis by a mosquito, could squeeze through the tiny pores of polyacrylamide hydrogels. This 3D hydrogel assay can be used as an *in vitro* model to test drugs or antibodies against the parasite after transmission.

The second part of this thesis deals with the role of myosin A for *Plasmodium* gliding motility. Using a reverse genetic approach, I could demonstrate the importance of amino acids within the unusual N-terminal extension of myosin A for maximum speed of sporozoites *in vitro*. I found that phosphorylation of one of these residues is required for efficient salivary gland invasion of sporozoites *in vivo*. These results show for the first time, how modulation of motor properties by post-translational modification of myosin A could regulate parasite motility to allow for successful transmission from mosquito vector to mammalian host.

Zusammenfassung

Die Zellbewegung der Malariaerreger, Parasiten der Gattung *Plasmodium*, wird von einem Aktomyosin Motor angetrieben. Diese substrat-abhängige Art der gleitenden Fortbewegung ist an mehreren Stellen des komplexen Lebenszyklus wichtig, damit die Parasiten Gewebe durchqueren und in Wirtszellen eindringen können. Der Motorkomplex befindet sich unter der Plasmamembran und besteht aus verankerten Myosin A Proteinen, die Kräfte auf Aktinfilamente ausüben, welche durch Transmembranproteine auf ein Substrat übertragen werden können. Wie die Umgebung die Parasitenbewegung beeinflusst ist noch nicht vollständig bekannt. Zudem ist nicht klar, wie die Anpassung des Aktomyosin Motors eine Stadien-spezifische Regulierung der Zellbewegung ermöglichen könnte. Im ersten Teil dieser Arbeit zeige ich anhand von Polyacrylamid Hydrogelen, wie Substrat Elastizität, eine eingeengte Zellumgebung und Porengröße die Fortbewegung der Parasiten beeinflussen. Die Malariaerreger konnten sich auf ebenen weichen Substraten nicht kontinuierlich bewegen, während die Bewegung mit steigender Steiffigkeit des Substrats zunahm. In einer eingeengten Umgebung bewegten sich die Parasiten jedoch stabil fort, auch wenn diese extrem weich war. *Plasmodium* Sporozoiten, die Stadien welche durch eine Stechmücke in die Dermis übertragen werden, konnten sich durch enge Poren des Polyacrylamid Hydrogels hindurch drücken. Dieses experimentelle System kann dazu dienen, Wirkstoffe oder Antikörper gegen die Parasiten nach der Übertragung zu testen.

Der zweite Teil dieser Arbeit behandelt die Funktion von Myosin A bei der gleitenden Fortbewegung der *Plasmodien*. Mithilfe eines genetischen Ansatzes konnte ich die Rolle spezifischer Aminosäuren innerhalb der ungewöhnlichen N-terminalen Erweiterung von Myosin A für die maximale Geschwindigkeit von Sporozoiten *in vitro* zeigen. Ich fand heraus, dass die Phosphorylierung einer dieser Aminosäuren für ein effizientes Eindringen der Sporozoiten in die Speicheldrüsen *in vivo* nötig ist. Diese Ergebnisse zeigen zum ersten Mal, wie die Anpassung der Motoreigenschaften durch Posttranslationale Modifikation von Myosin A die Parasitenbewegung regulieren könnte.

Contents

Abbreviations

2D	two-dimensional
3D	three-dimensional
5-FC	5-Fluorocytosine
AA	Acrylamide
ADF	Actin depolymerizing factor
AFM	Atomic force microscopy
AMA1	Apical membrane antigen 1
ApiAP2	Apicomplexan Apetala 2
APS	Ammonium persulfate
APTMS	3-Aminopropyltrimethoxysilane
ATP	Adenosine triphosphate
BIS	Bis-acrylamide
BSA	Bovine serum albumin
Cas	CRISPR-associated
CCW	Counter-clockwise
CIP	Calf intestinal phosphatase
cm	Codon modified
CP	Capping protein
CRISPR	Clustered regularly interspaced short palindromic repeats
CS	Circumsporozoite
CSP	Circumsporozoite protein
CTRP	Circumsporozoite- and TRAP-related protein
CW	Clockwise
CytoD	Cytochalasin D
ECM	Extracellular matrix

ELC	Essential light chain
F	Forward
FTTC	Fourier transform traction cytometry
GAP	Gliding-associated protein
GAPM	Gliding associated protein with multiple membrane spans
GIMO	Gene Insertion/Marker Out
GOI	Gene of interest
GPI	Glycosylphosphatidylinositol
gRNA	Guide RNA
hDHFR	Human dihydrofolate reductase
HSP20	Heat shock protein 20
HL sporozoites	Hemolymph sporozoites
IMC	Inner membrane complex
inf	Infected
i.p.	Intraperitoneal
Jas	Jasplakinolide
MG sporozoites	Midgut sporozoites
MTIP	Myosin A tail domain interacting protein
MyoA	Myosin A
NA	Numerical aperture
NHEJ	Non-homologous end joining
NMRI	Naval Medical Research Institute
ORF	Open reading frame
PA	Polyacrylamide
PAM	Protospacer-adjacent motif
PBS	Phosphate-buffered saline
PCR	Polymerase chain reaction
PEG-DA	Poly(ethylene glycol) diacrylate
PFA	paraformaldehyde
PIV	Particle image velocimetry
R	Reverse

recon	Reconstitution
RGD	Arginine-glycine-aspartic acid
RICM	Reflection interference contrast microscopy
ROI	Region of interest
RPMI	Roswell Park Memorial Institute
SDM	Site-directed mutagenesis
SG sporozoites	Salivary gland sporozoites
TEMED	Tetramethylethylenediamine
TFM	Traction force microscopy
TLP	TRAP-like protein
TRAP	Thrombospondin-related anonymous protein
TREP	TRAP-related protein
UTR	Untranslated region
wt	Wild-type
yFCU	Yeast cytosine deaminase-uracil phosphoribosyl transferase fusion protein

1 Introduction

1.1 Apicomplexa

Apicomplexa are a phylum of single-celled eukaryotes comprising medically relevant parasites such as *Plasmodium*, *Toxoplasma*, *Babesia* or *Cryptosporidium*. The members of this phylum contain an apical complex which is made of structural components and organelles that are used for host cell invasion (Dubremetz et al., 1998; Frénal et al., 2017a). Apicomplexa undergo a complex life cycle which typically involves sexual and asexual stages.

1.1.1 The *Plasmodium* life cycle

During their life cycle *Plasmodium* parasites alternate between the *Anopheles* mosquito vector and an intermediate host which can be, depending on the *Plasmodium* species, mammals, reptiles or birds.

When a female mosquito feeds from an infected mammal, it takes up parasites together with the blood meal (Fig 1.1). The sexual stages, called gametocytes, are activated in the mosquito midgut by the change in environmental conditions (Billker et al., 2004; Bennink et al., 2016). Male microgametes egress from the erythrocyte, a process termed exflagellation (Sinden et al., 2010). Then, they move through the midgut lumen until they get in touch with a female macrogamete which they fertilize (Sinden et al., 1976). In this process a zygote is formed which further develops into an ookinete that crosses the peritrophic matrix which forms around the blood bolus and moves through the midgut epithelium (Zieler and Dvorak, 2000; Vlachou et al., 2004; Kumar and Barillas-Mury, 2005; Angrisano et al., 2012; Kan et al., 2014). At the basal lamina the ookinete transforms into an oocyst. Within several days hundreds of sporozoites

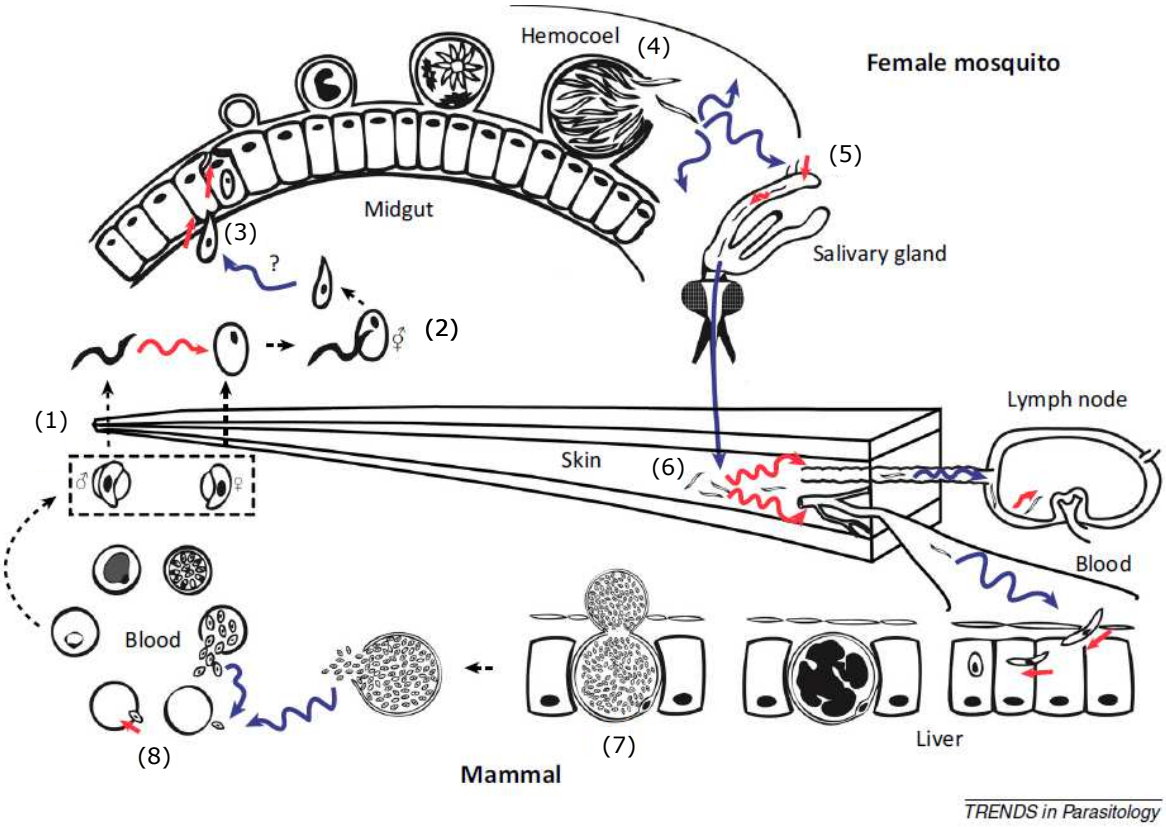

Figure 1.1: The *Plasmodium* life cycle.
Red arrows indicate active migration of the parasites, blue arrows indicated passive transport. Sexual stages taken up together with an infected blood meal (1) become activated in the mosquito midgut. Fertilization occurs (2) and the resulting zygote develops into a motile ookinete that traverses the midgut epithelium (3). At the basal lamina it transforms into an oocyst. Inside the oocyst, sporozoites are formed and released into the mosquitoe's body cavity, the hemocoel (4). They penetrate the salivary glands (5) from where they are transmitted into the skin by an infectious bite (6). There, they migrate to find and invade lymph or blood vessels. With the blood stream, they are transported to the liver, where they transform into schizonts forming thousands of merozoites which are released into the blood stream again (7). These merozoites invade erythrocytes and multiply (8). Some infected erythrocytes differentiate into sexual stages which can infect the next mosquito. Figure modified from Douglas et al. (2015) and reused with permission by the publisher Elsevier.

are built inside the oocyst (Meis et al., 1992). Finally, they egress and reach the salivary glands via the mosquitoes circulatory fluid called the hemolymph (Frischknecht et al., 2006; Klug and Frischknecht, 2017; Pimenta et al., 1994; Wells and Andrew, 2019). The sporozoites invade the salivary glands where they mature (Matuschewski et al., 2002; Hegge et al., 2010; Sato et al., 2014). Like other arthropod-borne pathogens, sporozoites are transmitted into the skin of the next mammalian host (Pimenta et al., 1994; Frischknecht et al., 2004; Frischknecht, 2007). The sporozoites are injected together with the saliva while the mosquito is searching for a blood vessel. In the skin, the sporozoites move at high speeds to find and invade a blood vessel (Amino et al., 2006,

2008; Hopp et al., 2015). Subsequently, they are transported to the liver with the blood flow. There, they exit the blood stream and traverse several hepatocytes before they finally infect a hepatocyte and transform into schizonts (Prudêncio et al., 2006; Tavares et al., 2013). Thousands of merozoites are formed by schizogony, a type of asexual reproduction (Matthews et al., 2018; White and Suvorova, 2018). These are released into the blood stream via vesicles called merosomes (Sturm et al., 2006; Baer et al., 2007; Burda et al., 2017). After merosome rupture, merozoites invade erythrocytes (Cowman and Crabb, 2006; Yahata et al., 2012) and form ring stages, which further develop into trophozoites (Francia and Striepen, 2014). These multiply and transform into schizonts. Again, merozoites are released and infect further erythrocytes. The resulting ring stages can either differentiate into gametocytes (Josling and Llinás, 2015; Bancells et al., 2019) or repeat the asexual reproduction.

1.1.2 Malaria

Malaria is a disease that affected an estimated number of 228 million people and caused 405000 deaths in 2018 (WHO, 2019). The severe form is caused by *Plasmodium falciparum*. Other *Plasmodium* species that can infect humans are *P. malariae*, *P. vivax*, *P. ovale* and *P. knowlesi*. Great efforts to eliminate the disease caused the number of people suffering from malaria to decrease over the years. However, in 2016 the number of cases increased again (WHO, 2019). Especially resistances of the parasite against widely used therapies and resistances of the vector against insecticides impede the progress in elimination of the disease. Until now, there is no effective vaccine that could prevent malaria (Matuschewski, 2017). The most promising vaccine candidate RTS,S which is based on the major surface protein of sporozoites circumsporozoite protein (CSP), has shown poor efficacy in phase III trials (RTSS Clinical Trials Partnership, 2017).

1.2 *Plasmodium berghei* as a model organism

The rodent strain *Plasmodium berghei* is used as a model organism to study cell biological aspects of apicomplexan parasites. Reasons for this are the availability of

fast and efficient genetic tools as compared to human infecting *Plasmodium* species (de Koning-Ward et al., 2015; Matz and Kooij, 2015). Furthermore, the rodent *Plasmodium* strain offers the possibility to study the parasite in its *in vivo* environment and throughout the whole life cycle (Wykes and Good, 2009; Matz and Kooij, 2015).

1.2.1 Gene regulation in *Plasmodium*

Genomic loci consist of open reading frames that define the transcription start site of a gene, intergenic regions upstream of the gene, termed 5' untranslated region (UTR) and intergenic regions downstream of the gene, called 3'UTR. Many genes also contain introns, that are spliced out of the mRNA before translation. Regulation of gene expression via transcriptional, epigenetic and post-transcriptional mechanisms is very important for *Plasmodium* parasites to progress through the life cycle, especially for the transition from one stage to the next (Ruiz and Gómez-Díaz, 2019). Changes in chromatin structure by histone modifications can lead to gene silencing or activation (Duraisingh and Skillman, 2018; Muller et al., 2019). Transcription factors of the Apicomplexan Apetala 2 (ApiAP2) family have been identified as important regulators in *Plasmodium* that bind to cis-regulatory elements within promoter regions upstream of genes (Jeninga et al., 2019). Furthermore, mRNA levels and translation can be modulated by RNA-binding proteins that can for example play a role in stabilization of mRNAs or translational repression (Hughes et al., 2010; Cui et al., 2015). Specific sequence motifs in the UTRs usually mediate this regulation mechanism. Interestingly, gene expression profiles can be altered within short periods of time simply by changing the medium in which the parasites are maintained (Roth et al., 2018) which shows how well the parasites can adapt their gene regulatory program to the microenvironment. In gene dense regions of the genome, UTRs can reach into coding regions of neighboring genes if they are transcribed from complementary strands (van Lin et al., 2001).

1.2.2 Gene editing in *Plasmodium berghei*

P. berghei parasites can be transfected by electroporation of schizonts containing haploid merozoites (Janse and Waters, 2002; Janse et al., 2006; de Koning-Ward et al.,

2015). *Plasmodium* parasites mainly use homologous recombination as DNA repair mechanism, while alternative end joining pathways are rare (Kirkman et al., 2014; Singer et al., 2015). This enables genome editing if a template is introduced into the parasites. For stable transfection, linearized DNA flanked by homology regions is used to trigger incorporation into the *P. berghei* genome (de Koning-Ward et al., 2015). DNA can be introduced by single or double-crossover recombination. Introduction of a selection marker is necessary to select for parasites that integrated the construct. Human dihydrofolate reductase (hDHFR) is used for positive selection as it confers resistance to the antimalarial drugs pyrimethamine and WR99210. For sequential genetic manipulation, the negative selection marker yeast cytosine deaminase-uracil phosphoribosyl transferase fusion protein (yFCU) which makes the parasite prone to selection via 5-fluorocytosine (5-FC) can be used to recycle the positive selection marker.

Site-directed mutagenesis using conventional gene editing

Site-directed mutagenesis of *P. berghei* parasites by gene replacement has been approached in different ways (Fig 1.2 A). All established strategies have the disadvantage of interfering with regulatory DNA elements, which might lead to changes in protein abundance. This might result in mutant phenotypes that do not trace back to the mutation but to the change in regulatory elements. Therefore, it is very important to include the appropriate controls. If only a single or double base pair change should be introduced into the target sequence, alternative homologous recombination events might take place. This leads to parasites that integrated the selection cassette, but not the mutation into the target sequence. To this end, the target sequence can be replaced by a codon modified version, which consists of a different base pair sequence but encodes the same amino acid sequence (Douglas et al., 2018a). Introns are usually deleted in the gene editing process.

This approach harbors the danger, that the change in base pair sequence and the deletion of introns affects transcription and translation resulting in different protein levels compared to wild-type (wt). Differences in protein abundance might then cause mutant phenotypes. Alternatively, the target gene can be replaced by the transcript which leads to a deletion of the introns but keeps the base pair sequence of the exons (Bane et al., 2016). This strategy only works if the gene contains introns and muta-

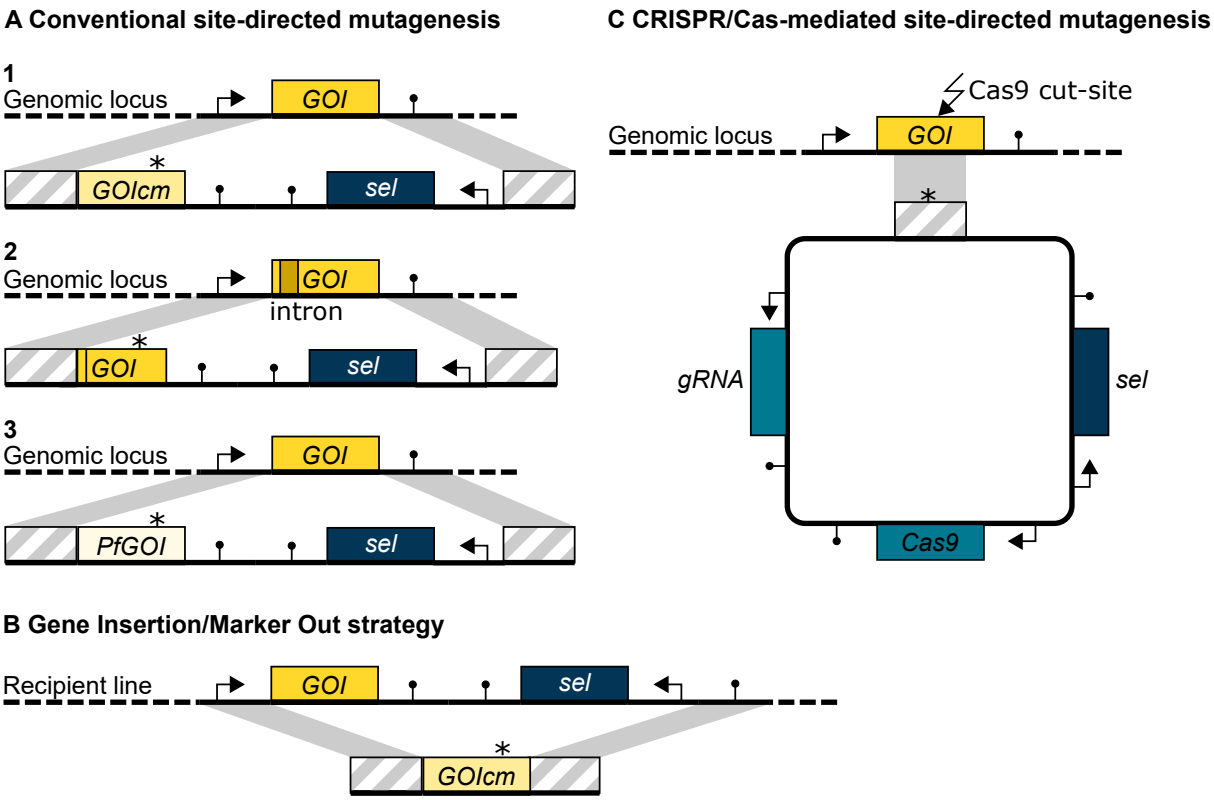

Figure 1.2: Scheme showing the cloning strategies for site-directed mutagenesis in *Plasmodium*.
(**A**) The gene of interest (GOI) is either replaced by a codon modified (cm) version (1), by the transcript (2) or by the *P. falciparum* ortholog (3) using double crossover recombination and positive selection. The star indicates the mutation site. All conventional methods obtain parasite lines that contain a selection marker and interfere with gene regulatory elements. (**B**) A recipient parasite line containing a selection cassette within the GOI locus is used to replace the GOI and selection cassette by a cm version of the GOI using negative selection. (**C**) Cas9 is targeted to the GOI by a gRNA designed to bind close to the mutation site. The nuclease introduces a double strand break which is repaired by the parasites using the repair template containing the mutation.

tions can only be introduced efficiently to one side of the introns, depending on which regions are used as homology regions for integration of the construct and where the selection marker is introduced. Another strategy is a transgenic approach where the target gene is replaced by its orthologous gene from another *Plasmodium* species, for example *P. falciparum* (Moreau et al., 2017). The advantage of this strategy is that amino acid changes can directly be transferred from the *P. falciparum* protein structure without caring if the residue is conserved among *Plasmodium* species. However, the transgene might not complement the gene function and therefore also cause a mutant phenotype.

In case of studying a gene which is non-essential in blood stages but might play a role

in mosquito stages, it is also possible to knockout the gene of interest (GOI) and use this knockout parasite line to introduce a mutated version of the GOI into the respective locus (Kehrer et al., 2016).

Gene Insertion/Marker Out strategy

With the Gene Insertion/Marker Out (GIMO) strategy, parasites that have already integrated a positive and negative selection marker can be modified by transfecting linearized DNA with homology regions to both sides of the locus containing the selection marker (Lin et al., 2011). Negative selection results in integration of the DNA construct via double homologous recombination (Fig 1.2 B). To use this strategy for site-directed mutagenesis, a recipient parasite line needs to be produced first. In a second step, the selection marker is replaced by a DNA construct carrying the mutated version of the gene. Thus the GIMO strategy yields selection marker-free parasite lines. However, the two consecutive cloning steps (generation of recipient line and GIMO-transfection) make the method time consuming, require the use of additional mice and could in principle affect parasite fitness.

CRISPR/Cas9-mediated gene editing

The clustered regularly interspaced short palindromic repeats (CRISPR) / CRISPR-associated (Cas)-mediated gene editing system is derived from an antiviral immune response system of bacteria (Barrangou et al., 2007; Horvath and Barrangou, 2010). It consists of the nuclease Cas9 which specifically introduces a double strand break if it is guided to a target site by a chimeric RNA (Jinek et al., 2012). The chimeric RNA contains a stretch of DNA called the guide RNA (gRNA) which is 20 nucleotides in length and can be designed to target a specific locus. It needs to be next to a protospacer-adjacent motif (PAM) in order to allow for cleavage by the Cas9.

CRISPR/Cas9-mediated gene editing has been used in a wide variety of organisms. Among these are the two *Plasmodium* species *P. falciparum* and *P. yoelii* (Ghorbal et al., 2014; Lee et al., 2014; Zhang et al., 2014, 2017). CRISPR/Cas9-mediated gene editing has the advantage that it yields selection marker free parasite lines if the Cas9 is episomally expressed (Fig 1.2 C). Additionally, single point mutations can be incor-

porated without changing any regulatory DNA elements. Lee and Fidock (2014) generated a single plasmid containing Cas9, a positive selection marker, gRNA expression cassette and a donor sequence which is used as repair template by the parasites. This plasmid is transfected into *Plasmodium*. Due to episomal expression of Cas9, it is only acting transiently during application of a selection pressure. Shortly after removing the selection pressure, the parasites lose the plasmid which reduces the danger of Cas9 off-target effects. Off-target effects are also unlikely because *Plasmodium* is missing the non-homologous end joining (NHEJ) pathway which means that double strand breaks in other loci than the one for which a template is provided cannot be repaired and result in the death of the parasites (Bryant et al., 2019). However, a restriction of CRISPR/Cas-mediated gene editing is the necessity of the PAM motif NGG, which is not as frequent as in other organisms due to the AT-rich genome of some *Plasmodium* species (Lee et al., 2019). The distance between mutation site and gRNA binding site should be as small as possible to prevent alternative homologous recombination events that might lead to the mutation not being incorporated and thus a reduced editing efficiency (Ghorbal et al., 2014). Recodonization of the region between gRNA binding site and the nucleotide which should be substituted reduces the risk of alternative homologous recombination events (Lee et al., 2019).

1.3 Cell migration

Cell migration is important for many physiological processes in multicellular organisms as well as for survival of single-celled organisms. The cytoskeleton comprises the key structural components that determine cell shape and allow for cell migration (Morrissette and Sibley, 2002; Fletcher and Mullins, 2010; Pegoraro et al., 2017). It includes actin filaments, microtubules and intermediate filaments.

Different cells display distinct cell migration modes. These go along with different types of morphologies and mechanisms. While cellular protrusions at the leading edge and the retraction of the rear end are characteristic for mesenchymal cell migration, amoeboid migration typically involves a rounded cell shape and polarization of the cell (Friedl, 2004; Theveneau and Mayor, 2012; Petrie and Yamada, 2016). Both of these migration

modes require deformation of the cell shape. A third type of substrate-dependent locomotion termed gliding motility allows the cells to move over a substrate without visible cellular protrusions and little or no morphological changes (Heintzelman, 2015; Frénal et al., 2017a). This type of substrate-dependent migration is used by apicomplexan parasites. Another form of motility used by the parasites which is not substrate-dependent is the flagellar motility of male gametes which they need to move through the lumen of the mosquito midgut (Sinden et al., 2010; Krüger and Engstler, 2015). Cell migration is powered by molecular motors which move along polymeric tracks. Flagellar motility is tubulin-dynein-based, while gliding motility requires an actomyosin motor. In the following sections I will focus on the latter form of motility.

1.3.1 Gliding motility of apicomplexan parasites

Apicomplexan gliding motility is required for the parasites to move across tissues and invade host cells (Heintzelman, 2015; Frénal et al., 2017a). The molecular machinery needed for this type of locomotion is located beneath the plasma membrane (Fig 1.3). A membrane system made from flattened vesicles and cytoskeletal components called the inner membrane complex (IMC) underlies the parasite's plasma membrane and is further stabilized by a subpellicular network and microtubules (Kudryashev et al., 2010b; Kono et al., 2012; Harding and Meissner, 2014; Spreng et al., 2019). These are thought to be interconnected by gliding associated proteins with multiple membrane spans (GAPMs) (Bullen et al., 2009; Harding et al., 2019). The myosin heavy chain Myosin A (MyoA) is bound to the essential light chain (ELC) and is anchored within the IMC by the light chain myosin A tail domain interacting protein (MTIP) and gliding associated proteins (GAPs) (Bergman et al., 2003; Frenal et al., 2010; Yeoman et al., 2011). Actin monomers are incorporated into short filaments at the apical end of the parasite and moved rearwards by MyoA (Bookwalter et al., 2017; Douglas et al., 2018a; Robert-Paganin et al., 2019). The translocation of actin filaments by myosin has been termed retrograde flow (Welch et al., 1997).

Transmembrane proteins of the thrombospondin-related anonymous protein (TRAP) family of proteins termed adhesins connect the actomyosin motor to the external environment (Morahan et al., 2009). Thereby they allow for the transmission of intracel-

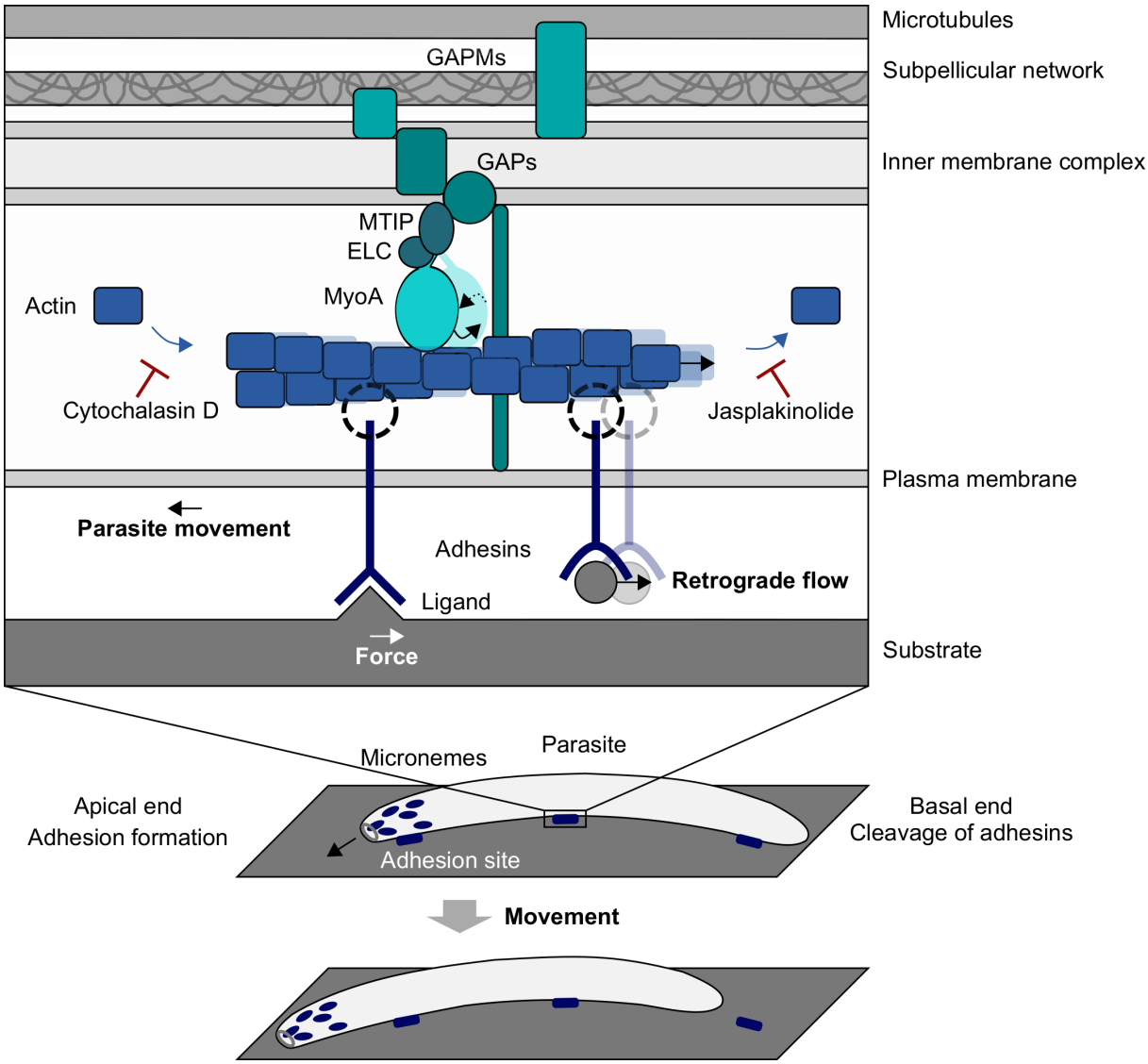

Figure 1.3: Model of the apicomplexan gliding machinery.
The gliding machinery is located beneath the parasite's plasma membrane. Myosin A (MyoA) and its light chains (ELC and MTIP) are anchored to the inner membrane complex and the underlying subpellicular network via adaptor proteins (GAPs). Microtubules provide structural integrity of the cell. The myosin motor produces force on actin filaments, thereby translocating them rearwards, a process termed retrograde flow. Adhesins connect the actomyosin motor to extracellular ligands and thus allow for force transmission to a substrate which results in forward movement of the cell. At the parasite's apical end, adhesins are secreted into the plasma membrane from micronemes and adhesion sites are formed. Over these adhesion sites the parasite can migrate forwards. At the basal end, adhesins are cleaved or ruptured leading to their shedding onto the substrate. Figure adapted from Kratzer (2016).

larly generated forces to an extracellular substrate (Münter et al., 2009; Quadt et al., 2016). It is not clear, how these adhesins are connected to the actin filaments (Shen and Sibley, 2014; Jacot et al., 2016). The transmembrane proteins are stored in intracellular organelles called micronemes (Tomley and Soldati, 2001; Dubois and Soldati-Favre, 2019). These vesicles fuse with the plasma membrane at the apical end of the

parasite during gliding and release the transmembrane proteins which are translocated rearwards by the actomyosin motor (Morahan et al., 2009). The secretion of adhesins is a calcium-dependent process (Carey et al., 2014).

Different *Plasmodium* stages express a unique set of transmembrane proteins to be adapted to their environment. In ookinetes, circumsporozoite- and TRAP-related protein (CTRP) is required for motility (Dessens et al., 1999), while sporozoites need TRAP, TRAP-like protein (TLP) and S6/TRAP-related protein (TREP) for efficient gliding (Sultan et al., 1997; Moreira et al., 2008; Heiss et al., 2008; Steinbuechel and Matuschewski, 2009; Combe et al., 2009). In merozoites, apical membrane antigen 1 (AMA1) (not a member of the TRAP protein family) and other adhesins mediate binding to the host cell and thereby allow for red blood cell invasion (Boucher and Bosch, 2015). The extracellular ligands that adhesins bind to can either be host cell receptors or components of the extracellular matrix (ECM), a network of proteins such as collagen, laminin or fibronectin (Theocharis et al., 2016). For most *Plasmodium* adhesins, the receptors they bind to are unknown or under debate (Pradel et al., 2002; Tossavainen et al., 2006; Coppi et al., 2007; Ghosh et al., 2009; Dundas et al., 2018; O'Brochta et al., 2019). A switch between active and inactive state of adhesins by conformational changes might be involved in the regulation of adhesion and gliding motility (Song et al., 2012; Klug, 2017).

The major structural components of the gliding machinery are thought to be conserved among apicomplexan parasites (Heintzelman, 2015; Frénal et al., 2017a), while the dynamics and output (force, adhesion, retrograde flow, speed and movement trajectories) can vary between species and even between stages of the same species. These parameters can be measured in different ways. Using optical tweezers, the whole parasite can be trapped to probe adhesive forces (Hegge et al., 2012; Crick et al., 2014). In another approach, polystyrene beads can be positioned on the apical end of the parasites which allows for the measurement of retrograde flow speed as the bead is translocated rearwards by the parasites (Quadt et al., 2016; Stadler et al., 2017). Alternatively, the force at which the parasites can pull the bead out of the optical trap can be measured. Adhesive forces of merozoites attaching to erythrocytes are about 40 pN, while those

of hemolymph sporozoites attaching to a glass substrates are higher than 25 pN (Crick et al., 2014; Hegge et al., 2012). Adhesion formation and initiation of motor activity happens within milliseconds in *Plasmodium* sporozoites, while it takes about a minute in *Toxoplasma* tachyzoites (Quadt et al., 2016; Stadler et al., 2017). Furthermore, the forces at which a bead is pulled out of the optical trap are much higher for sporozoites (about 100 pN) than for tachyzoites (about 5 pN). In sporozoites, retrograde flow and force inversely correlate, but changes in these parameters do not necessarily lead to a change in migration speed (Quadt et al., 2016; Moreau et al., 2017, 2020). Retrograde flow is faster than sporozoite speed, indicating that retrograde flow is slowed down under load (Quadt et al., 2016).

During migration, sporozoites do not adhere to the substrate over the whole parasite length, but instead they form small adhesion sites at the apical end over which they move forward (Münter et al., 2009). Finally, the adhesion sites are cleaved by proteases or ruptured at the rear end of the parasites and actin filaments are disassembled (Baker et al., 2006; Ejigiri et al., 2012; Dowse et al., 2008; Douglas et al., 2018a). This leads to shedding of adhesins onto the substrate (Ejigiri et al., 2012). Sporozoites are highly polarized. Their polar ring at the apical end from which the microtubules extend is tilted towards the substrate providing the structural basis for directional movement (Kudryashev et al., 2012). All in all, gliding motility results from a complex interplay between adhesion dynamics, retrograde flow and force generation/transmission (Münter et al., 2009; Quadt et al., 2016; Moreau et al., 2017, 2020). These processes need to be tightly coordinated to allow for fast and robust cell migration.

Although there is a lot of evidence supporting the described model of the apicomplexan gliding machinery, there might be alternative mechanisms that allow apicomplexan parasites to invade host cells and move across tissues (Meissner et al., 2013; Andenmatten et al., 2013; Egarter et al., 2014). However, it is not clear whether these mechanisms are conserved among apicomplexan parasites.

1.3.2 The *Plasmodium* actomyosin motor

As pointed out above, the actomyosin motor is generating the force for apicomplexan gliding motility. It is composed of MyoA which hydrolysis ATP to produce force on actin filaments. MyoA will be introduced in detail in Section 1.4.4. Actin dynamics are key to the function of the actomyosin motor in gliding motility. The double-stranded helical actin filaments have a barbed end (plus end) to which ATP-containing actin monomers bind and a pointed end (minus end) where, after ATP hydrolysis took place, ADP-containing monomers can dissociate from the filament upon release of the inorganic phosphate (Blanchoin et al., 2014). *Plasmodium* parasites possess two actin isotypes, actin I and II (Wesseling et al., 1989; Vahokoski et al., 2014). Actin I is the protein which enables parasite invasion (Das et al., 2017). It displays some unusual biochemical properties when compared to mammalian actins. In the parasite it mainly exists in its monomeric globular form (G-actin) and only polymerizes into short and unstable filaments (F-actin) with a different rotational angle and pitch of the double helix as compared to rabbit skeletal actin (Dobrowolski, Janice M. Niesman and Sibley, 1997; Schmitz et al., 2005, 2010; Vahokoski et al., 2014; Lu et al., 2019). Probably due to these characteristics, parasite F-actin could not be visualized *in vivo* using standard techniques (Melak et al., 2017) for a long time (Kudryashev et al., 2010a). Only recently, parasite actin filaments have been visualized using an actin-chromobody (Periz et al., 2017; Stortz et al., 2019; Del Rosario et al., 2019).

Changing actin dynamics by the actin modulators jasplakinolide (Jas) or cytochalasin D (CytoD) severely impairs force generation/transmission and gliding motility (Mizuno et al., 2002; Siden-Kiamos et al., 2006; Coppi et al., 2007; Münter et al., 2009; Quadt et al., 2016). CytoD binds to the barbed end of F-actin and thereby blocks addition of G-actin which reduces the length of actin filaments (Cooper, 1987). Jas on the other hand stabilizes F-actin by binding to an internal actin pocket which increases lateral contacts between adjacent actin proteins within the filament (Pospich et al., 2017). Studies revealed that Jas impairs merozoite invasion (Mizuno et al., 2002) while both agents interrupt ookinete and sporozoite gliding (Siden-Kiamos et al., 2006; Coppi et al., 2007; Münter et al., 2009). Probably due to the divergence of actin I when compared to

mammalian actins, the actin modulator latrunculin does not affect *Plasmodium* gliding motility (Hegge et al., 2010).

Actin dynamics are regulated by actin-binding proteins which affect nucleation (formation of actin dimers and trimers), filament growth, stability and disassembly (Winder and Ayscough, 2005). This can happen by binding to actin monomers, bundling, crosslinking or capping actin filaments. Several actin-binding proteins regulate actin dynamics in the parasite and play crucial functions throughout different life cycle stages (Schüler and Matuschewski, 2006; Sattler et al., 2011). *Plasmodium* possesses the actin monomer binding proteins profilin and C-CAP, the F-actin binding protein coronin, capping proteins (CPs), actin depolymerizing factors (ADFs) as well as formins and formin-like protein MISFIT which mediate nucleation. Studies have shown that profilin, CPα, ADF1, Formin1 and Formin2 are important in blood stages (Moreau, 2017; Ganter et al., 2015; Schüler et al., 2005; Baum et al., 2008; Stortz et al., 2019). Pofilin, ADF2, C-CAP, CPβ and MISFIT play a role for oocyst formation or development (Moreau, 2017; Doi et al., 2010; Hliscs et al., 2010; Bushell et al., 2009; Ganter et al., 2009). Profilin, coronin and CPβ function in sporozoite motility (Moreau et al., 2017; Bane et al., 2016; Ganter et al., 2009).

Myosins interact with N-terminal acidic residues of actin (Sutoh et al., 1991; Lu et al., 2005). Exchanging the *P. berghei* actin N-terminus by the rabbit actin N-terminus which leads to an additional acidic residue within the N-terminus affects life cycle progression and *in vitro* motility of *Plasmodium* (Douglas et al., 2018a). Mutant parasites show a reduced number of oocysts and impaired salivary gland invasion. Ookinetes as well as sporozoites are slower than wt parasites, probably due to reduced interaction between MyoA and actin.

It is unclear, what mediates directional movement of apicomplexan parasites. Unpublished data by Thomas Blake suggest, that MyoA is not oriented in the IMC. This would explain, why sporozoites are able to perform patch gliding, a type of non-directed motility where the parasite moves back and forth over a single adhesion site (Münter et al., 2009). This implies that the direction of movement is determined by the orientation of

actin filaments. However, it remains elusive what mediates their orientation. One possibility might be, that TRAP aligns actin filaments in sporozoites, as deletion of TRAP results in sporozoites that do not glide in circles any longer but still perform patch gliding (Münter et al., 2009). Alternatively, actin-binding proteins, for example coronin, might be involved in the orientation of actin filaments (Bane et al., 2016).

1.4 Myosin

Myosins are actin-based molecular motors, which are needed for a variety of different cellular processes such as transport of organelles, mitosis and cell motility (Hartman and Spudich, 2012). Eukaryotes possess different myosins, each being recruited to a specific site of action and having a precisely timed enzymatic activity.

1.4.1 Structure, classification and regulation

Myosin heavy chains usually contain a structurally conserved motor or head domain, a neck domain and a tail domain (Sellers, 2000; Sweeney and Houdusse, 2010; Robert-Paganin et al., 2020). The force-generating motor domain is composed of four subdomains (Table 1.1) and contains an ATP binding site as well as regions that interact with filamentous actin. While the nucleotide binding site is conserved among myosins, the actin-binding surface is variable. It consists of five loops from Upper and Lower 50 kDa subdomains (U50 and L50) and changes during the kinetic cycle as the cleft between these subdomains opens and closes. The transducer communicates the closure of the actin-binding cleft to the nucleotide-binding site. Other structural elements connect the subdomains or take part in nucleotide-binding (Table 1.1).

The ATPase activity and the velocity by which actin filaments are moved rearwards can vary a lot between different myosins. The neck domain can interact with light chains or calmodulin and in most myosins contains one or several IQ-motifs (amino acid sequence IQXXXRGXXXR). The tail domain is very diverse in terms of length and sequence. It often contains functional motifs and allows for dimerization of some myosins or binding of cargo. Myosins have been grouped into different classes based

on phylogenetic analysis of the motor domains (Foth et al., 2006; Odronitz and Kollmar, 2007; Sebé-Pedrós et al., 2014; Pasha et al., 2016).

Table 1.1: Myosin subdomains and structural elements

Subdomains	**Role**
N-terminal subdomain	
Upper 50 kDa subdomain (U50)	Actin-binding
Lower 50 kDa subdomain (L50)	Actin-binding
Converter	Amplification of structural changes of the motor domain
Structural elements	**Role**
Transducer	Seven-stranded β-sheet underlying the nucleotide pocket
SH1 helix	Connects N-terminal subdomain and converter
Relay	Connects L50 and converter
Switch I	Nucleotide-binding
Switch II	Connects U50 and L50 and allows for coupling between actin- and nucleotide-binding site
P loop	Nucleotide-binding

1.4.2 The kinetic cycle

The general kinetic or ATPase cycle is the same for myosins of all classes, however the transition from one state to the next happens at different rates (Sweeney and Houdusse, 2010; Walklate et al., 2016; Houdusse and Sweeney, 2016; Robert-Paganin et al., 2020). This allows for the tuning of kinetic properties dependent on the function each myosin performs within the cell (Bloemink and Geeves, 2011). In the rigor state myosin is strongly bound to two adjacent actin monomers which are part of an actin filament (Fig 1.4). During the transition to the postrigor state, the actin-binding cleft between U50 and L50 subdomain opens, F-actin detaches and a new ATP is bound. Next, ATP hydrolysis takes place and the lever arm, which includes the converter and the neck domain with light chains bound to it, is repositioned. The transition from postrigor to prepowerstroke state is termed recovery stroke. Weak binding to F-actin and release of phosphate induces conformational changes. This leads to the lever arm

swing, closure of the actin-binding cleft and ultimately strong binding to F-actin. This series of events is called the powerstroke during which myosin generates force on actin which results in translocation of actin filaments. Afterwards, ADP dissociates from the motor domain and myosin is in the rigor state again. The relative amount of time a myosin spends in strong actin-binding states is called the duty ratio. In order to move quickly along actin filaments, a myosin needs to have a low duty ratio. This property is determined by the rate of transition from prepowerstroke to the rigor state.

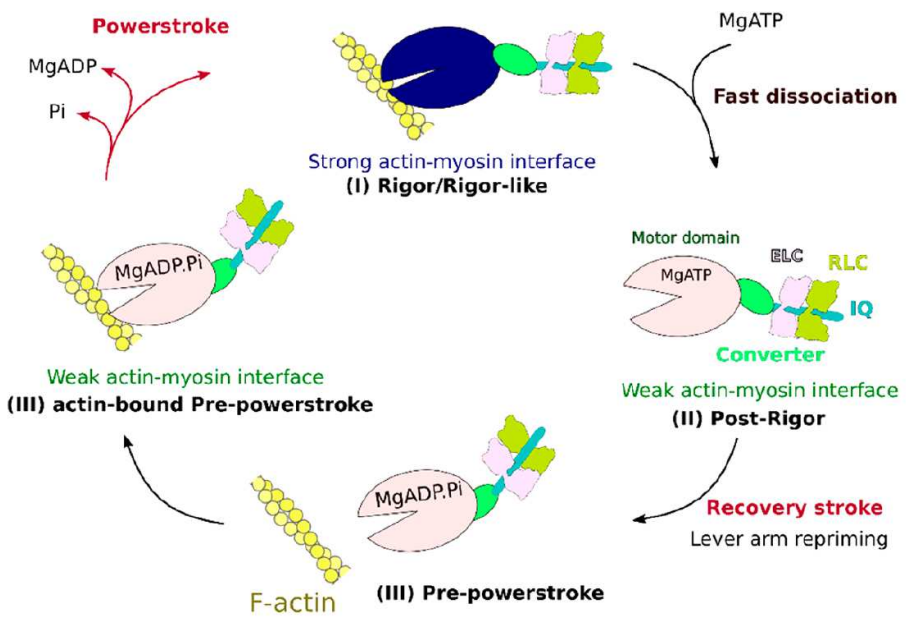

Figure 1.4: Kinetic cycle of the myosin superfamily.
(I) In the rigor state, myosin is strongly bound to actin. Upon ATP-binding, dissociation of myosin from actin occurs creating the post-rigor state (II). The recovery stroke which goes along with ATP hydrolysis and lever arm repriming results in the pre-powerstroke state of myosin (III). Next, myosin weakly associates with F-actin, the hydrolysis products are released and the powerstroke takes place leading to the rigor state again. The motor domain is depicted in light pink (open actin-binding cleft) or dark blue (closed actin-binding cleft). The converter is shown in green and the essential and regulatory light chains ELC and RLC in pink and ocher. The lever arm is illustrated in cyan. Figure reprinted with permission from Robert-Paganin et al. (2020). Copyright (2020) American Chemical Society.

1.4.3 Myosins in Apicomplexa

In *Toxoplasma* 11 myosin isotypes exist (encoded by 10 genes), while there are only 6 isotypes in *Plasmodium* (Chaparro-Olaya et al., 2005; Foth et al., 2006). An overview of all *Plasmodium* and *Toxoplasma* myosin isotypes can be found in Table 1.2. Most of

them belong to apicomplexan-specific myosin classes (Foth et al., 2006; Sebé-Pedrós et al., 2014; Mueller et al., 2017). While there are 6 essential myosin isotypes in *Toxoplasma* (Sidik et al., 2016), high-throughput knockout screens suggest that all isotypes except one are dispensable in *Plasmodium* blood stages (Zhang et al., 2018; Schwach et al., 2015). The most studied myosin isotype in *Plasmodium*, called MyoA, is conserved in Apicomplexa and is thought to be the one producing force for invasion and migration of apicomplexan parasites. Little is known about the other myosin isotypes in *Plasmodium*. MyoB localizes to the apical end of invasive *Plasmodium* stages (Yusuf et al., 2015). Gene deletion of *myoB* does not have an effect on progression through the life cycle in *P. berghei* (Wall et al., 2019). MyoE localizes to the basal end of invasive *Plasmodium* stages and depletion of MyoE results in a defect in salivary gland invasion. MyoJ localizes to the sporoblast in oocysts and seems to be dispensable for life cycle progression. Although MyoF and MyoK were considered dispensable in blood stages in phenotypic screens (Zhang et al., 2018; Schwach et al., 2015), Wall et al. (2019) were not able to knock out these two myosin genes in *P. berghei*. MyoF localizes to the apical end of ookinetes and is distributed homogenously in oocysts, while MyoK forms dotty or rod-like structures in gametocytes.

1.4.4 Myosin A

Structure and function

MyoA belongs to the apicomplexan-specific myosin class XIV. It is a plus-end-directed motor with a step size and velocity similar to myosin II, which produces force for migration of mammalian cells (Herm-Götz et al., 2002). Consistent with its proposed function as part of the gliding machinery, MyoA is located at the periphery of all *Plasmodium* stages that perform gliding motility to invade host cells and/or cross tissues (Green et al., 2017). In blood stages, MyoA is essential (Bushell et al., 2017). In *Plasmodium* it is needed for host cell invasion and in *Toxoplasma* additionally for egress (Perrin et al., 2018; Robert-Paganin et al., 2019; Meissner et al., 2002; Egarter et al., 2014). In *Plasmodium* ookinetes it is required for motility as shown by stage-specific depletion of MyoA (Siden-Kiamos et al., 2011). Except for its localization (Green et al., 2017), nothing is known about the role of MyoA in sporozoites so far. However, *myoA* is one

Table 1.2: Myosins in Apicomplexa

Plasmodium	***Toxoplasma***	**Class**	**Role**
MyoA	MyoA	XIV	Located at the periphery of motile and invasive stages, essential for motility (Perrin et al., 2018; Robert-Paganin et al., 2019; Meissner et al., 2002; Egarter et al., 2014)
-	MyoD	XIV	Unknown
-	MyoB/C	XIV	Unknown
-	MyoE	XIV	Unknown
-	MyoH	XIV	Located at the conoid of motile and invasive stages, necessary for motility (Graindorge et al., 2016)
MyoB	-	XIV	Unknown
MyoE	-	XIV	Salivary gland invasion (Wall et al., 2019)
MyoF	MyoF	XXII	Centrosome positioning, apicoplast segregation and transport of dense granules in *Toxoplasma* (Jacot et al., 2013; Heaslip et al., 2016)
-	MyoG	XXIII	Unknown
-	MyoI	XXIV	Unknown
MyoJ	MyoJ	VI or XXIII	Basal complex constriction and rosette formation in *Toxoplasma* (Frénal et al., 2017b)
MyoK	MyoK	VI or XXIII	Unknown

of the most frequently transcribed genes in *P. falciparum* and *P. yoelii* sporozoites, indicating that it is also important in this stage (Lindner et al., 2019).

The structure of the PfMyoA motor domain (Fig 1.5) has been solved recently (Robert-Paganin et al., 2019). MyoA lacks the tail domain and contains two light chains bound to its neck domain. One is known as Myosin Light Chain (MLC) or Myosin Tail domain Interacting Protein (MTIP) in *Toxoplasma* or *Plasmodium*, respectively while the other one is called Essential Light Chain (ELC) (Bookwalter et al., 2014, 2017; Green et al., 2017). Both light chains are required for maximum velocity of MyoA (Bookwalter et al., 2017; Green et al., 2017). The reason for this might be that the light chains induce conformational changes in MyoA upon binding resulting in stiffening of the lever arm (Pazicky et al., 2019). Light chain MLC/MTIP additionally anchors MyoA to the IMC by binding to GAPs (Frenal et al., 2010). The myosin light chains bind to the

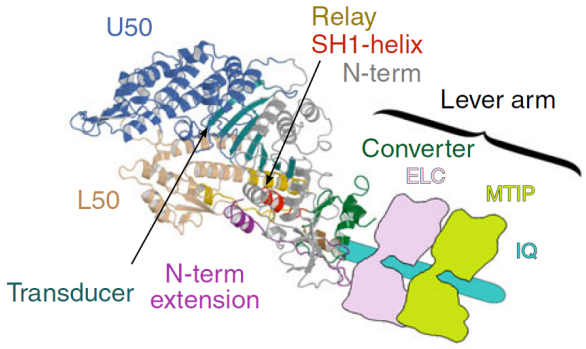

Figure 1.5: Crystallographic structure of *P. falciparum* MyoA.
The subdomains are indicated in different colors: N-terminal subdomain in gray, U50 in blue, L50 in yellow and converter in green. Other structural motifs shown are the transducer (dark cyan), N-terminal extension (purple), SH1-helix (red) and Relay (ocher). The lever arm which consist of the two light chains bound to the neck domain of MyoA is drawn schematically. Image taken from Robert-Paganin et al. (2019). The image is published under a Creative Commons Attribution 4.0 International License (http://creativecommons.org/licenses/by/4.0/).

C-terminus (residues 775-818 in *Toxoplasma*) of MyoA (Powell et al., 2017). Mutagenesis of two arginines within this binding site abolishes the peripheral localization of TgMyoA (Hettmann et al., 2000).

Although the myosin light chain binding site is not conserved between *Toxoplasma* and *Plasmodium*, TgELC can take over the function of PfELC in an *in vitro* gliding assay (Bookwalter et al., 2017). Interestingly, PfMyoA moves skeletal actin filaments at the same speed as *Plasmodium* actin filaments *in vitro* (Bookwalter et al., 2017), despite the differences between *Plasmodium* actin and skeletal actin (Douglas et al., 2018a).

Plasmodium berghei MyoA shares 30% sequence identity with mammalian myosin II, 60% with TgMyoA and 80% with PfMyoA. An alignment of PbMyoA and PfMyoA is depicted in Fig 1.6.

Regulation

Myosins need to be tightly regulated in order to function precisely (Heissler and Sellers, 2016). Therefore, transcriptional and posttranslational regulation of myosin heavy and light chains is very important. Posttranslational regulation can for example happen via phosphorylation or via the binding of divalent cations. Phosphorylation of MyoA, MTIP and other components of the gliding machinery can be carried out by cGMP-dependent and calcium-dependent protein kinases in *Plasmodium* (Sebastian et al., 2012; Alam et al., 2015; Fang et al., 2018).

Two phosphorylation sites affecting motility and egress have been identified in TgMyoA: S21, which is also found in *Plasmodium* and S743, which is not conserved (Gaji et al.,

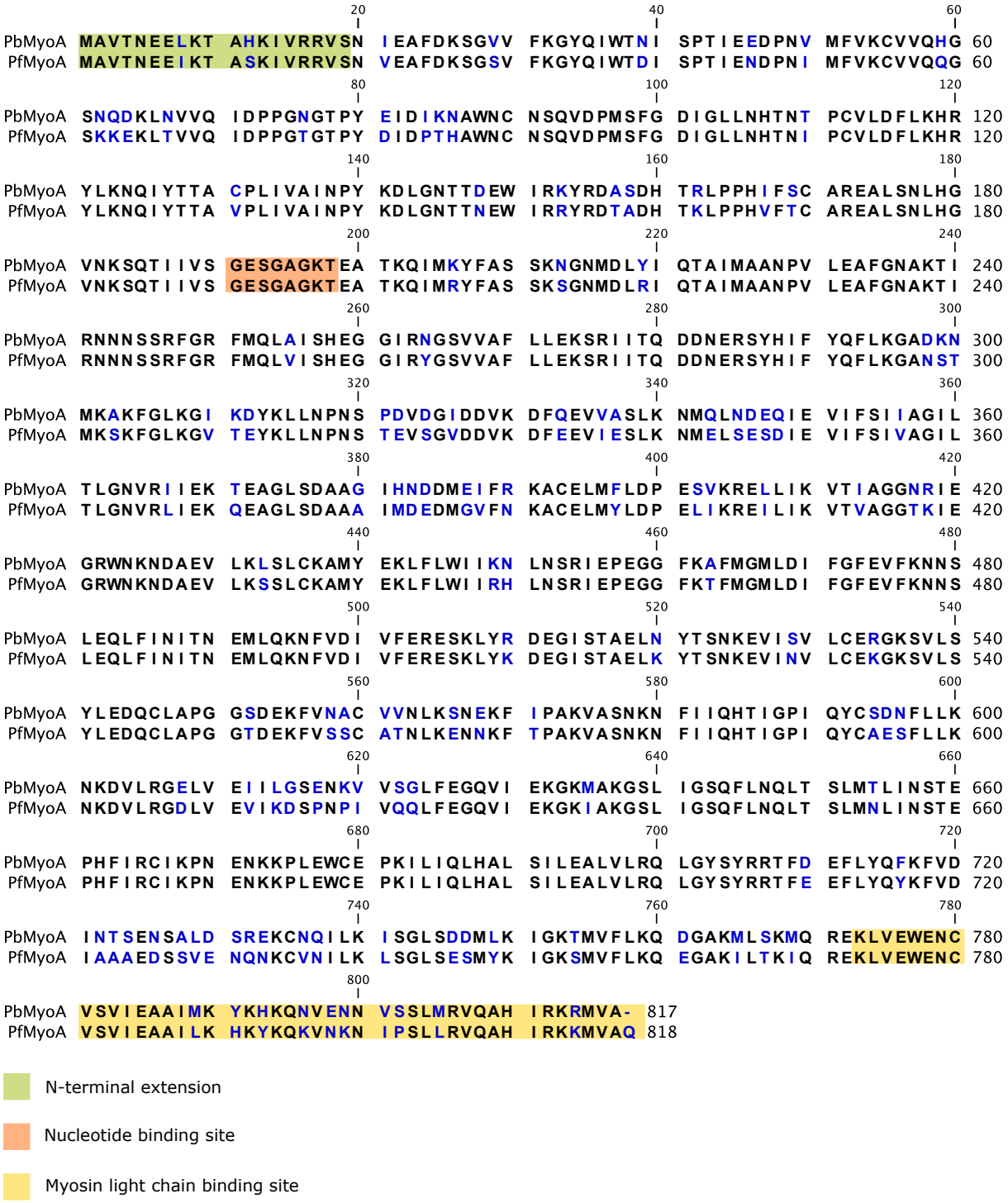

Figure 1.6: Sequence alignment of *P. berghei* and *P. falciparum* MyoA.
Divergent amino acid residues are depicted in blue. Important structural motifs are highlighted. Sequences were obtained from PlasmoDB (Bahl et al., 2003).

2015). Phosphomimetic mutants at residues S20/21/29 have been shown to be faster in motility assays *in vitro* (Powell et al., 2018). In PfMyoA there seems to be a single phosphorylation site at S19 (Lasonder et al., 2015). A phosphodeficient mutant at S19 transported actin filaments at a slower speed *in vitro* (Robert-Paganin et al., 2019).
Phosphorylation sites have also been characterized in the myosin light chains binding to MyoA. Phosphorylation of MTIP residue S108 is required for efficient binding to MyoA *in vitro* (Douse et al., 2012). Furthermore, MTIP is phosphorylated by CDPK1 at residues S47 and S51 (Green et al., 2008). The relevance of these phosphorylation sites *in vivo* needs to be further investigated.
In addition to the phosphorylation sites, TgELC has a calcium binding site (Williams et al., 2015). In contrast to TgELC, PfELC does not seem to possess a calcium binding site (Bookwalter et al., 2017; Green et al., 2017).

Many studies on the function and importance of MyoA in gliding motility have been performed in *Toxoplasma*. The advantage is that mutagenesis in *Toxoplasma* is much easier and faster. Everything can be done in cell culture and there is no need for animal experiments. However, the function of MyoA can be partially complemented by MyoC (Frenal et al., 2014), which is not expressed in *Plasmodium*. Furthermore, studying the function of MyoA throughout the *Plasmodium* life cycle can give us much more insight on the stage-specific regulation of MyoA as well as its role *in vivo*. Together with structural and biochemical data this allows to establish a structure-function relationship.

In *P. berghei* the *myoA* gene is located on chromosome 13 (Bahl et al., 2003). It consists of three exons and two small introns close to the start codon. The length of the transcript is 2454 base pairs and the length of the protein 817 amino acids. Usually, myosins contain a highly conserved glycine between SH1 and SH2 helix, which allows for flexibility of these helices and thereby enable structural changes of the proteins when it goes through the kinetic cycle (Kinose et al., 1996; Kad et al., 2007; Preller et al., 2011). However, apicomplexan myosin A contain a serine at this site. Robert-Paganin et al. (2019) suggest, that the N-terminal extension of MyoA is important for the motor function of the protein, since it compensates for the missing glycine (Fig 1.7). Two amino acids within the N-terminal extension seem to be especially important.

Structural analysis of PfMyoA showed that an interaction between phosphorylated S19 in the N-terminus and K764 in the converter domain in the rigor-like state is involved in the lever arm swing. This leads to fast ADP release which reduces the time of MyoA being strongly attached to F-actin. As a result the duty ratio is affected and the speed at which actin filaments are transported is enhanced. Indeed, phosphorylated PfMyoA at position S19 displaced actin filaments faster than a phosphodeficient S19A mutant or a mutant with reversed charge at position K764 in an *in vitro* motility assay.

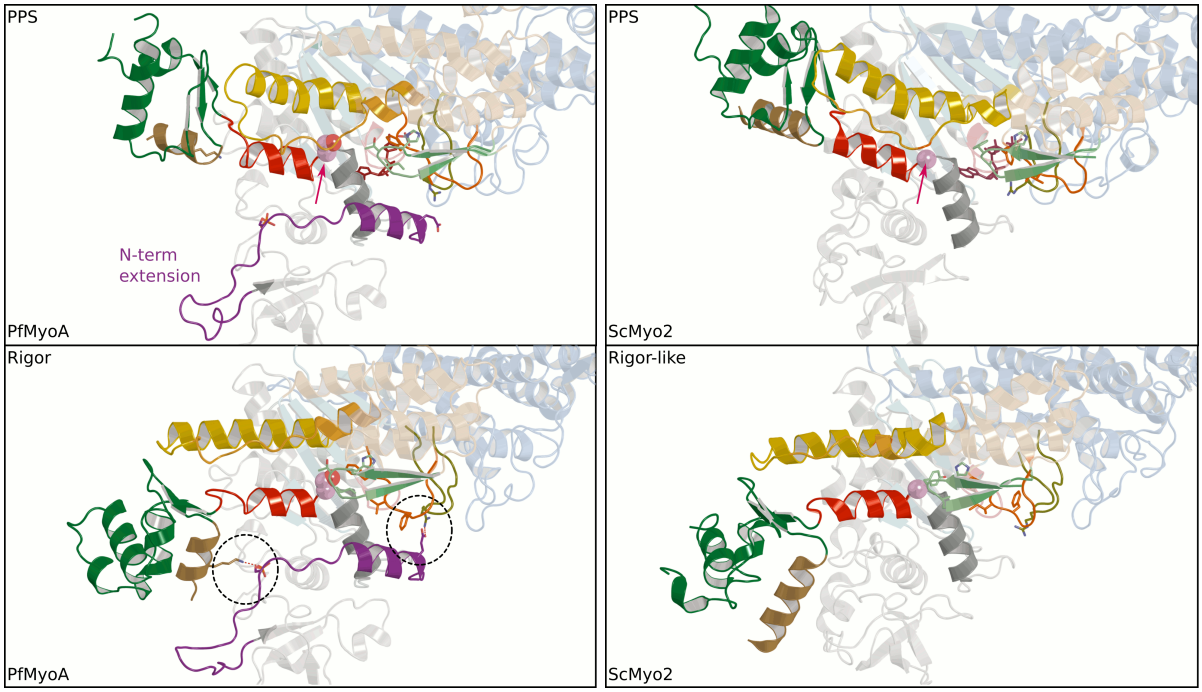

Figure 1.7: Important amino acid residues in MyoA compensating for the lack of flexibility of the SH1-helix as compared to classical myosins such as scallop myosin II (ScMyo2).
Shown are the conformational changes of PfMyoA (left) and ScMyo2 (right) before (upper part, PPS) and after (lower part, rigor/rigor-like) the powerstroke. Two residues in the N-terminal extension of MyoA (purple), E6 and phosphorylated S19, are thought to build important interactions with residues from Switch1/2 or the converter, respectively (highlighted by dashed black circles). This allows for a lever arm swing which is comparable to classical myosins although many canonical residues are not conserved in MyoA. The orange arrow points towards the conserved glycine which allows for the mobility of the SH1-helix in classical myosins but is replaced by a serine in MyoA. The converter is depicted in green, Relay in yellow, Switch II in orange and SH1 helix in red. Figure modified from Robert-Paganin et al. (2019). The images are published under a Creative Commons Attribution 4.0 International License (http://creativecommons.org/licenses/by/4.0/).

Another important interaction in the rigor-like state as predicted by structural analysis was found between residues E6 in the N-terminal extension, R241 and F476 (Robert-Paganin et al., 2019). However, it was not tested whether this interaction is important

for MyoA function *in vitro*. The authors suggest, that phosphorylation of residue S19 might switch between high speed and high force of the motor to allow for tuning the motor according to the requirements of different parasite stages. Sporozoites move fast but need less force while merozoites need a higher force to invade erythrocytes but do not need to be fast. Although this hypothesis is not in line with proteomic studies that found MyoA to be phosphorylated in sporozoites as well as merozoites (Lasonder et al., 2015), it might be that MyoA is not phosphorylated in merozoites that are in the process of invasion which cannot be seen in large scale proteomic studies.

1.5 Synthetic substrates to study cell migration

In their natural environment, cells migrate through a complex mixture of molecules. Cell migration is often studied on planar glass substrates as this allows for simple microscopy in a single plain. However, a variety of factors influence cell migration *in vivo*. To study the effect of single environmental parameters on cell migration or to mimic the complex three-dimensional (3D) environment that cells naturally move through, different assays are used (Ruprecht et al., 2017; Muthinja et al., 2018). Nano- or micropatterning allows for a defined arrangement of ligands that cells can bind to. This enables investigation of the effects of different ligands, ligand density or topography on cell migration. Microstructured environments, also called micropillar arrays, are utilized to study how cells move on top of these pillars and how forces are transmitted which results in bending of the pillars. If the pillars are designed in a way, that the spaces between pillars is large enough, cells can also be observed when moving between pillars. This allows for studying the effect of different topologies and the influence of confinement. Another assay to study these factors are microchannels which can be structured in different ways depending on the biological question that should be adressed. Hydrogels are hydrophilic polymer networks that absorb large amounts of water. They offer a wide variety of experimental setups to understand the influence of substrate elasticity on cell migration, to measure cellular forces (as described in Section 1.6) and to study the effect of a three-dimensional environment on cell migration. If assembled in a complex fashion, they can also be used for organotypic cultures/3D cell culture (Muthinja

et al., 2018). Natural or synthetic hydrogels can be used for these purposes (Liaw et al., 2018). Natural hydrogels are either polysaccharide-based (e.g. hyaluronic acid), decellularized ECM-based or peptide/protein-based such as collagen or matrigel. Collagen is the most abundant ECM protein and it can be crosslinked. Matrigel is a mixture of ECM-proteins, heparin sulfate proteoglycans and growth factors. The precise properties of natural hydrogels may vary from batch to batch. Synthetic hydrogels on the other hand are well-defined and biologically inert substrates with tunable biochemical as well as mechanical properties. They are typically composed of polyethylene glycol (PEG), polyvinyl alcohol or polyacrylamide (PA) and can be functionalized with ligands. Depending on the monomer to crosslinker ratio, PA hydrogels can be fabricated to have different elasticities and thereby mimic the mechanical properties of tissues (Engler et al., 2006; Tse and Engler, 2010). The elastic properties of these hydrogels are defined by the Young's modulus which determines the strain (deformation of the substrate) when stress (force per area) is applied. The Young's modulus is given in Pascal ($pN/\mu m^2$). Hydrogels with a small Young's modulus can be easily deformed when cells move over them, while hydrogels with an increasing Young's modulus are stiffer and the cell needs to apply higher forces to deform the substrate. Adjusting the crosslinker concentration also has an effect on the pore size of the hydrogel (Holmes and Stellwagen, 1991; Wen et al., 2014). For 3D hydrogel assays, cells can either be encapsulated into hydrogels or sandwiched between two-dimensional (2D) hydrogel substrates (Liaw et al., 2018). Stable hydrogels are crosslinked in a way, that cells cannot degrade the hydrogel, while other hydrogels allow for degradation via hydrolysis or proteolysis which usually promotes cell migration.

Using some of these assays, the impact of ligand-density, elasticity, hydrodynamic flow and substrate topography on sporozoite motility has been investigated (Hegge et al., 2010; Hellmann et al., 2011; Perschmann et al., 2011; Muthinja et al., 2017). This revealed that sporozoites move best on stiff substrates with intermediate ligand density, slow motility under flow and adapt to environmental constrains on their way through the skin. However, these studies were limited to 2D surfaces and were not suited to investigate ookinetes or compare the small but possibly important elasticity differences between different cell types encountered by sporozoites.

Both, sporozoites and ookinetes move in helical trajectories through natural hydrogels (Battista et al., 2014; Kan et al., 2014). However, sporozoites stop moving in matrigel after several minutes as polymerization proceeds. As the cells need to be encapsulated in collagen before polymerization takes place, the time which remains for imaging is also shortened and cell density is usually very low. A 3D assay with a synthetic hydrogel on the other hand allows for higher cell densities and longer periods of imaging which enables quantification of parameters such as speed of large numbers of cells in a confined environment. It has been shown for different motile cells, that a 3D environment can change morphology, speed or persistence of cell migration as compared to a planar substrate (Vu et al., 2015). In confined environments, specific receptor-ligand interactions become less important for cell migration (Lämmermann et al., 2008; Bergert et al., 2015; Liu et al., 2015; Ruprecht et al., 2015). Pore diameter can specifically affect cell migration of mammalian cells (Tayalia et al., 2011; Lang et al., 2015). The pore size of synthetic hydrogels is typically smaller than for collagen hydrogels (Holmes and Stellwagen, 1991; Wen et al., 2014; Lang et al., 2015). The pore size of polyacrylamide hydrogels depends on the amount of acrylamide (AA) and bis-acrylamide (BIS) used for the fabrication of these hydrogels (Holmes and Stellwagen, 1991; Wen et al., 2014). Increasing the AA concentration at constant BIS concentration or increasing the BIS concentration at constant AA concentration decreases the pore size. The same is true for hydrogel stiffness which also depends on AA and BIS concentration. Increasing the BIS concentration at constant AA concentration or increasing the AA concentration at constant BIS concentration increases the stiffness (Tse and Engler, 2010; Denisin and Pruitt, 2016). Tuning the elasticity of PA hydrogels allows for analyzing the effect of different physiologically relevant substrate stiffnesses on cell migration.

The speed and pattern of actin-myosin based motility depends on the extracellular microenvironment and differs between life cylce stages. Sporozoites move at 1-3 µm/s while ookinetes move at 0.05-0.2 µm/s (Vanderberg, 1974; Siden-Kiamos et al., 2006). It is not clear, what causes the speed differences on a molecular level. Reasons might be different actin dynamics for example due to a stage-specific set of actin-binding proteins. Alternatively, forces might be transmitted at different efficiencies because of stage-specific expression of adhesins. Another reason might be differences in myosin

kinetics due to posttranslational modifications of MyoA or its light chains.
Sporozoites move in circular trajectories on plane substrates and in helical trajectories in 3D (Battista et al., 2014). On 2D surfaces, some ookinetes display straight segment motility while others move in circles (Siden-Kiamos et al., 2006). In 3D they move in helical trajectories (Kan et al., 2014).

1.6 Traction force microscopy to study force transmission

Except for mimicking the mechanical properties of tissues, PA hydrogels can also be used to measure cellular forces exerted onto the substrate. As these flexible hydrogels deform when cells move over them, displacement maps of embedded fluorescent marker beads can be used to reconstruct the traction forces applied by the cells (Schwarz and Soiné, 2015). This method is called traction force microscopy (TFM). The displacements of marker beads can be determined by comparing an image of the deformed substrate with the cell on top with an image of the relaxed substrate when the cell is detached or moved out of the field of interest. Detection of bead displacements is restricted by the optical resolution limit and force measurements highly depend on the image quality. The major limitation of TFM studies with sporozoites is their small size as the cell-substrate interface at which forces can be transmitted is also very small resulting in low sensitivity of the method. Traction forces of sporozoites have been shown to be 100-200 Pa on average (Münter et al., 2009; Kratzer, 2016). Depletion of the adhesin TLP leads to reduced traction forces (Kratzer, 2016).

1.7 Aim of this thesis

The aim of this project was to get a better understanding of the role of myosin in force generation and motility of *Plasmodium*. Using an interdisciplinary approach, we aimed at establishing a structure-function relationship by combining molecular data from structural and biochemical analysis of myosin with *in vitro* and *in vivo* data from parasites expressing mutated versions of myosin. This would lead to a deeper under-

standing of the molecular motor.

Using the *P. falciparum* myosin structure, amino acid residues potentially important for the motor function of myosin were defined by the Houdusse group (Robert-Paganin et al., 2019). A reverse genetic approach should help to elucidate the function of these amino acid residues on a cellular level. Therefore, I planned to genetically manipulate *P. berghei* parasites to generate parasite lines with mutations of single amino acids. This allows for accession of the role of myosin throughout the whole life cycle including mosquito stages.

Cell migration assays are usually performed on glass. However, these experiments do not reflect properties of the physiological environment. *In vivo* experiments in the mosquito or mouse on the other hand are complicated to conduct and do not allow to study the effect of single parameters such as stiffness or confinement on force transmission and motility of the parasites. To be able to analyze forces and motility of native as well as mutant parasite lines, I planned to develop a set of assays, which should bridge the gap between simple *in vitro* experiments on glass and *in vivo* experiments. After validating these hydrogel assays with mutant parasite lines already characterized *in vivo*, I wanted to use these in order to characterize the myosin mutants in detail.

Additionally, I planned to use TFM to measure forces of mutant ookinetes and sporozoites and to analyze the contribution of certain amino acid residues to force generation.

2 Material and Methods

2.1 Material

Table 2.1: Technical Equipment

Apparatus	Supplier
Amaxa Nucleofector II	Lonza (Köln, Germany)
Analytic balance TE124S-OCE	Sartorius (Göttingen, Germany)
Axiostar Plus Transmitted-Light Microscope	Zeiss (Oberkochen, Germany)
Axiovert 200 M Inverted Microscope	Zeiss
Balance EW600-2M	Kern (Balingen, Germany)
CCD Camera EASY 400 K	Herolab (Wiesloch, Germany)
Centrifuge 5417 C	Eppendorf (Hamburg, Germany)
Centrifuge Galaxy Mini	VWR (Radnor, USA)
Centrifuge Labofuge 400e	Heraeus (Hanau, Germany)
Centrifuge Multifuge 1 S-R	Heraeus
Centrifuge Pico 17	Heraeus
Centrifuge Pico 21	Heraeus
Centrifuge Fresco 21	Heraeus
Desiccator	Glaswerk Wertheim (Wertheim, Germany)
Eclipse Ti Inverted Microscope	Nikon (Minato, Japan)
Eclipse E100 Microscope	Nikon
Excella E24 Incubator Shaker Series	New Brunswick Scientific (Edison, USA)
Freezer -80℃	New Brunswick Scientific
Freezer -20℃, Fridge 4℃	Liebherr (Ochsenhausen, Germany)

Gel electrophoresis system EV231	Consort (Turnhout, Germany)
Heating block AccuBlock Digital Dry Bath	Labnet (Edison, USA)
Heating block ThermoMixer C	Eppendorf
Hotplate stirrer CB162	Stuart (Staffordshire, UK)
Incubator CO_2 Ihnova CO-170	New Brunswick Scientific
Incubator CO_2 Lab C201	Labotect (Göttingen, Germany)
Incubator MIR253	Sanyo (Osaka, Japan)
Liquid Nitrogen Tank ARPEGE 170	Air Liquide (Düsseldorf, Germany)
Liquid Nitrogen Tank LS6000	Taylor-Wharton (Minnetonka, USA)
Microwave oven	Severin (Sundern, Germany)
Mosquito cages	BioQuip Products (Compton, USA)
NanoPhotometer	Implen (Munich, Germany)
Neubauer counting chamber	Marienfeld (Lauda Königshofen, Germany)
Pipette (P2, P10, P200, P1000)	Gilson (Middleton, USA)
Pipetus	Hirschmann Laborgeräte (Eberstadt, Germany)
Prime BSI (CMOS) Teledyne	Photometrics (Thousand Oaks, USA)
Safety cabinet Herasafe KS 15	Thermo Fisher Scientific (Waltham, USA)
Shaking incubator Multitron 2	Infors (Bottmingen, Switzerland)
SMZ1500 Stereomicroscope	Nikon
Thermocycler FlexCycler2	Analytik Jena (Jena, Germany)
Thermocycler Mastercycler EP Gradient	Eppendorf
UltraView spinning disk confocal unit	Perkin Elmer (Waltham, USA)
UV-table UVT-28 L	Herolab (Wiesloch, Germany)

Table 2.2: Chemicals and Reagents

Chemical/Reagent	Supplier
1 kb DNA ladder	New England Biolabs (Ipswich, USA)
3-Aminopropyltrimethoxysilane (APTMS)	Sigma-Aldrich (St. Louis, USA)
5-Fluorocytosine	Sigma-Aldrich (München, Germany)

Accudenz	Accurate Chemical & Scientific Corporation (New York, USA)
Acrylamide (AA) solution 40%	Bio-Rad Laboratories (Hercules, USA)
Agarose Serva research grade	Carl Roth (Karlsruhe, Germany)
Albumin fraction V	Carl Roth
Alsever's solution	Sigma-Aldrich
Ammonium persulfate (APS)	Bio-Rad Laboratories
Ampicillin sodium salt	Carl Roth
Bacto-Tryptone (peptone)	Fluka Honeywell (Seelze, Germany)
Bacto-Yeast extract	Sigma-Aldrich
Bis solution 2%	Bio-Rad Laboratories
Bovine serum albumine BSA Fraction V	Carl Roth
CutSmart buffer (10x)	New England Biolabs
di-Sodiumhydrogenphosphate (Na_2HPO_4)	AppliChem (Darmstadt, Germany)
Dimethyl sulfoxide (DMSO)	New England Biolabs
dNTP mix (10 mM)	Fermentas (Burlington, USA)
E. coli DH5α competent	New England Biolabs
Ethanol 99.8 %	Sigma-Aldrich
Fetal bovine serum (FBS) 1600	Gibco Thermo Fisher (Waltham, USA)
FluoSpheres carboxylate-modified Microspheres, 200 nm, (580/605)	Life Technologies (Carlsbad, USA)
Gentamycin (10 mg/mL)	PAA Laboratories (Pasching, Austria)
Giemsa staining solution	Merck (Darmstadt, Germany)
Glutaraldehyde solution 25%	Sigma-Aldrich
Glycerin	AppliChem
Glycerol 99% pure	Thermo Fisher Scientific (Waltham, USA)
Heparin-Sodium 25000 U	Ratiopharm (Ulm, Germany)
Hoechst 33342 (10 mg/mL)	Sigma-Aldrich
Hypoxanthine	Sigma-Aldrich
Immersol (518F, ne = 1.518)	Carl-Zeiss (Jena, Germany)
Isopropanol	Carl Roth

Ketamine	WDT (Garbsen, Germany)
Loading Dye Purple (6x)	New England Biolabs
Mercurochrome NF XII	Sigma-Aldrich
Methanol 100%	VWR (Radnor, USA)
Midori Green Advance	Nippon Genetics Europe (Düren, Gernamy)
Nonidet P40	AppliChem (Darmstadt, Germany)
Nycodenz	Axis-Shield Diagnostics (Dundee, UK)
Para-Aminobenzoic acid (PABA)	Sigma-Aldrich
PBS tablets	Gibco Thermo Fisher
PBS w/o $CaCl_2$ w/o $MgCl_2$	PAA Laboratories
Penicillin/Streptomycin (Pen/Strep) 100x	PAA Laboratories
Phusion GC Buffer (5x)	New England Biolabs
Phusion polymerase	New England Biolabs
Potassium chloride (KCl)	AppliChem
Potassium phosphate monobasic (KH_2PO_4)	Sigma-Aldrich
Pyrimethamine	Sigma-Aldrich
Restriction enzymes	New England Biolabs
RPMI 1640 + L-Glutamine - Phenol Red	Gibco Thermo Fisher
RPMI 1640 + HEPES + L-Glutamine	Gibco Thermo Fisher
Saponin	Sigma-Aldrich
Sodium acetate CH_3COONa	Carl Roth
Sodium bicarbonate	Sigma-Aldrich
Sodium chloride (NaCl)	Sigma-Aldrich
Sodium dihydrogen phosphate	J.T. Baker (Philippsburg, USA)
Sodium EDTA	Sigma-Aldrich
Sodium hydroxide (NaOH)	Merck
Sodium hypoxide	Sigma-Aldrich
T4 DNA ligase	Fermentas
T4 DNA ligase buffer	Fermentas
Taq Polymerase	New England Biolabs

Taq Standard Buffer (10x)	New England Biolabs
Tetramethylethylenediamine (TEMED)	Bio-Rad Laboratories
TRIS / HCl	Carl Roth
Triton X-100	Merck
Xanthurenic acid	Sigma-Aldrich
Xylazine	Ecuphar (Greifswald, Germany)

Table 2.3: Buffers and Solutions

Solution	Ingredient	Concentration
Freezing solution	Alsever's solution	90% (vol/vol)
	Glycerin	10% (vol/vol)
Giemsa staining buffer	KH_2PO_4	508 mg/l
	Na_2HPO_4	110 mg/l
Ketamine/Xylazine in PBS	Ketamin	105 mM
	Xylazine	11 mM
LB agar in LB medium	agarose	1.5% (w/vol)
LB medium, pH 7.0	NaCl	1% (w/vol)
	Bacto-Tryptone	1% (w/vol)
	Bacto-Yeast Extract	0.5% (w/vol)
Nycodenz solution, pH 7.5	Tris/HCl	5 mM
	KCl	3 mM
	Na_2EDTA	0.3 mM
	Nycodenz	276 g/l
Ookinete medium in RPMI 1640	Hypoxanthine	50 mg/l
supplemented with HEPES and	Pen/Strep	1%
Glutamine	$NaHCO_3$	2 g/l
	Xanthurenic acid	100 µM
Phosphate-buffered saline (PBS)	NaCl	137 mM
	KCl	3 mM
	Na_2HPO_4	10 mM

	KH_2PO_4	2 mM
PA gel	AA	5% (vol/vol)
	Bis-acrylamide	0.03 - 0.3% (vol/vol)
	APS	0.05% (vol/vol)
	TEMED	0.1% (vol/vol)
TRIS-acetate-EDTA (TAE) buffer	Tribase	242 g
	Acetic acid	57.1 ml
	0.5 M EDTA	100 ml
	ddH_2O	fill up to 1 L
Transfection medium in RPMI 1640	FCS	20% (vol/vol)
	Gentamycin	0.03%

Table 2.4: Consumables

Consumable	Supplier
96-well optical plate CBG nontreated	Nalge Nunc International (New York, USA)
Amaxa Human T Cell Nucleofector Kit	Lonza (Köln, Germany)
Cell culture flask Cellstar T75	Greiner Bio-One (Frickenhausen, Germany)
Cover slips 24x40 mm and 22x22 mm	Marienfeld (Lauda Königshofen, Germany)
Cryovials CRYO.S	Greiner Bio-One
DNeasy Blood and Tissue Kit	Qiagen (Hilden, Germany)
Eppendorf tubes (1.5 ml, 2 ml)	Eppendorf (Hamburg, Germany)
Falcon tubes (15 ml, 50 ml)	Greiner Bio-One
Gibson Assembly Master Mix	New England Biolabs (Ipswich, USA)
Gloves latex, powder-free	Semperit (Vienna, Austria)
Gloves nitrile	TouchNTuff (Richmond, Australia)
HiFi DNA Assembly Master Mix	New England Biolabs
High Pure PCR Purification Kit	Roche (Basel, Switzerland)
Microscopy slide 76x26 mm	Menzel (Braunschweig, Germany)
PCR tubes Quali, 8-strips	Kisker Biotech (Steinfurt, Germany)
Pipette Tips (10 µl, 200 µl, 1 ml)	Gilson (Middleton, USA)

Pipettes Plastic (5 ml, 10 ml, 25 ml)	Greiner Bio-One
Stericup Quick Release	Merck Millipore (Darmstadt, Germany)
Syringe cannula Microlance 3	BD (Heidelberg, Germany)
Syringe Micro-Fine+ U-100 Insulin 0.5 ml	BD
Syringe Plastipak 1 ml	BD
QIAprep Spin Miniprep Kit	Qiagen

Table 2.5: Parasite lines

Parasite line	Strain	Source
CS-GFP	NK65	Natarajan et al. (2001)
Coronin(-)	ANKA	Bane et al. (2016)
Hsp20(-)	ANKA	Montagna et al. (2012)
PbMyoA *3'dhfs*	ANKA	This project
PbMyoA GFP	ANKA	This project
PfMyoA	ANKA	This project
5'ama1 PbMyoA	ANKA	This project
PbMyoA E6R	ANKA	This project together with Xanthoula Smyrnakou
PbMyoA S19A	ANKA	Smyrnakou (2019)
PbMyoA S19D	ANKA	This project together with Xanthoula Smyrnakou

Table 2.6: Oligonucleotides (Numbers according to ID from primer list of Frischknecht group)

Promoter swap		
Name	Sequence (5' to 3')	Number
KpnI *5'myoA* F	CGGGGTACCTCATTTTTGAAGGGGGCGTCG GGGTACCTCATTTTTGAAGGGGGCGT	1762
HpaI *5'myoA* R	AAAGTTAACTTTTAAATAAAGAAATACAATAAA AAAACAAAAACA	1819
PstI EcoRI *myoA* F	AACTGCAGAAAGAATTCAAAATGGCTGTTAC AAATGAGGAATTAA	1825
SacII *myoA* ORF R	TCCCCGCGGGCATCGGATAAACCAGCT	1820

PstI *5'ama1* F	AACTGCAGTTCTATAAACTAATACAAACCCCG	1826
EcoRI *5'ama1* R	GCGAATTCTATATCGTTTTATTTTATTAATATTTT TAATTTACAA	1827
PstI *5'clag* F	AACTGCAGCTGATATTTATGAGTATTCCATG	1681
EcoRI *5'clag* R	GCGAATTCTTTTCCTAATTTTTAATATATATATTA TCTTTATCCT	1739
PstI NotI *5'clag9* F	AACTGCAGGCGGCCGCTGATATACACCTTAT TTACAATTTCGT	1641
EcoRI *5'clag9* R	CGGAATTCCTTCCAATATTTATGGCATTTTCT	1737
PstI *5'msp9* F	GTCTGCAGCTCGTACATTGATAAGGCC	1878
EcoRI *5'msp9* R	CTGAATTCTTCTTAATAAAGAATAGTAATTTGT TTTATATAGCT	1879
PstI *5'msp10* F	GACTGCAGGCAAATAAAGCTTACTATCGG	1876
EcoRI *5'msp10* R	CAGAATTCATTTTACTTAGCAAAGTCAGGTAA	1877
MyoA replacement		
HindIII *3'myoA* F	CCCAAGCTTGGGGAGAGCACACACTGA	1773
KpnI *3'myoA* long R	CGGGGTACCTGTAATTCCCCATTGCATTTATT CA	1774
SacII *5'myoA* F	TCCCCGCGGCCAAAAGCGCAATATTATCGGA	1775
EcoRI AatII *5'myoA* R	GCGAATTCGACGTCTTTTAAATAAAGAAATAC AATAAAAAAACAAAAACA	1776
SpeI Linker GFP F	GGACTAGTGCAGCAGCAGCAATGTCTGTGA GTAAAGGAGAAGA	1772
EcoRV *3'dhfs* R	CGGGATATCATATTTGTAATGATGCTTTTTCA CG	388
Spooki *myoA* Gibson F	GCACAAAACACATATGCATATGCACTAGTAAA ATGGCTGTTACAAATG	1844
Gfp myoA Gibson R	ATTGCTGCTGCTGCAGCAACCATTCTCTTTC TTATATGAGCTTG	1845
AatII *myoA* F	CGCGACGTCAAAATGGCTGTTACAAATGAG GAATTAA	1861
NotI *3'dhfs* R	ATAAGAATGCGGCCGCTTTTTCACGTATATTT TTTTGTTACATAAAAAG	1862

BamHI *myoA* R	CGCGGATCCTTAAGCAACCATTCTCTTTCTTATATGAGCT	1900
AatII *PfmyoA* cm F	CGCGACGTCATGGCTGTGACCAACGAGGAAA	1779
SpeI *PfmyoA* cm R	GGACTAGTTTATTGAGCGACCATCTTCTTGC	1780
CRISPR/Cas9		
EcoRI *5'hsp70* F	CCGGAATTCTTGTAATATTTTGTTGGTGAGCT	1943
AvrII *5'hsp70* R	CCGCCTAGGATTTAAATAATTGTAATTGTAATTTATTGGGA	1944
PstI sel R	CCGCTGCAGCAATTCTTTTCGAGCTCTTTATGC	1945
XhoI sel F	CCGCTCGAGTAGCTAAAAGGTGTGCAAGC	1946
BamHI PbU6 start Gibson F	TAGAATACTCAAGCTTGGGGGGATCCCACACACCTATATATCGAGAAC	1947
gRNA cassette PbU6 start Gibson R	CTCGAAGACCCAATAATATTGTATAACTCGAAGTATGC	1948
PbU6 start gRNA cassette Gibson F	ACAATATTATTGGGTCTTCGAGAAGACCTGTTTAAGAG	1949
3'dhfr gRNA cassette Gibson R	ATGGCGGCCGCAATCTGCAGAAAAAAGCACCGACTCGGTG	1950
gRNA cassette 3'dhfr Gibson F	GTGCTTTTTTCTGCAGATTGCGGCCGCCATCGA	1951
XhoI *3'dhfr* Gibson R	GAAGGTGGGAAGGGGGTAACTCGAGGCTAGCTTTGATCCCGTTTTTCTTACT	1952
PbU6 terminator F	GTTTTTAGTTTTTTTTTTCAAATATTATAAAATATACTGTGTATGTACATTGC	1959
NotI overhang PbU6 terminator PstI overhang R	GGCCGCAATGTACATACACAGTATATTTTATAATATTTGAAAAAAAAAACTAAAAACTGCA	1960
EcoRI S19 donor F	CGGGAATTCTGGCTTTTATTCCTATATATTTGTTTTGT	2074
AatII S19 donor R	CGCGACGTCCACAGGGTGTATTTGTGTGG	2075
MyoA K764 Gibson donor 1 F	CACCAACAAAATATTACAAGAATTCGAAACCATTAGAATGGTGTGAACCCAA	2010

MyoA K764 Gibson donor 1 R	CTCAACTAATTTTTCTCTTTGCATCTTTGACAA CATCTTTGCGCCATC	1977
MyoA K764 Gibson donor 2 F	GATGTTGTCAAAGATGCAAAGAGAAAAATTAG TTGAGTGGGAAAATTGTGTAAGTGT	1978
MyoA K764 Gibson donor 2 R	CGAAAAGTGCCACCTGACGTCATGTATTCAT CTATGTATTTGCTCTCGTGTGT	1979
MTIP S108 Gibson donor 1 F	CACCAACAAAATATTACAAGAATTCTGACGCT AAAACAACAATAGGTCCATATGATAATGA	2011
MTIP S108 Gibson donor 1 R	GATGATGGAGCTAAACCAAGTCTTCTAGCATT GTAAGAAGCA	1981
MTIP S108 Gibson donor 2 F	CTTGGTTTAGCTCCATCATCTAAGGATGAAGA AAAAATTAGAGATTTATATGGAGA	1982
MTIP S108 Gibson donor 2 R	CGAAAAGTGCCACCTGACGTCTCGATTTTGT CGTCATTTGAAAATGCA	1983
MyoA E6 gRNA F	TATTAAAAATGGCTGTTACAAATG	2054
MyoA E6 gRNA R	AAACCATTTGTAACAGCCATTTTT	2055
MyoA S19 gRNA F	TATTTAAAAGTGGAGTAGTCTTTA	1969
MyoA S19 gRNA R	AAACTAAAGACTACTCCACTTTTA	1970
MyoA K764 gRNA F	TATTAAAGAGAAAAACTTGTAGAA	2001
MyoA K764 gRNA R	AAACTTCTACAAGTTTTTCTCTTT	2002
MTIP S108 gRNA F	TATTCTTACAATGCTAGAAGATTA	2003
MTIP S108 gRNA R	AAACTAATCTTCTAGCATTGTAAG	2004
BamHI gRNA cassette F	GGGGGGATCCCTCACAAAATG	2012
NotI gRNA cassette R	ATGGCGGCCGCAATGTACA	2013
Gene Insertion/Marker Out		
AatII *myoA* E6R F	CGCGACGTCATGGCTGTTACAAATCGGGAA TTAAAAACAGCCCAT	2041
AatII *myoA* S19A F	CGCGACGTCATGGCTGTAACAAATGAAGAA TTGAAAACAGCCCATAAGATTGTTAGAA-GAGTTGCAAATATTGAAGCTTTTGATAAAAGT	2016
AatII *myoA* S19D F	CGCGACGTCATGGCTGTAACAAATGAAGAA TTGAAAACAGCCCATAAGATTGTTAGAA-GAGTTGACAATATTGAAGCTTTTGATAAAAGT	2039

BamHI myoA R	CGCGGATCCTTAAGCAACCATTCTCTTTCTT ATATGAGCT	1900
Genotyping *5'ama1* PbMyoA		
Locus F	TCTCGTTTCTCGTTTTTCGT	1870
Locus R	TGTATTTGCTCTCGTGTGT	1871
5'integration F	TTGGCTAGCCCAAAATTTA	1754
5'integration R	TAATTCAAAGGGACGAGG	960
3'integration F	TGAGGGGTGAGCATTTAAAG	1734
3'integration R	GATAATTTCAATACTTCTGCGTC	1711
Selection marker F	ATCCTCTGGTAATTTTTCG	961
Selection marker R	GGCCTGCAGCCCAGCTTAATTC	788
Genotyping PbMyoA *3'dhfs*		
Locus F	TCTCGTTTCTCGTTTTTCGT	1870
Locus R	TGTATTTGCTCTCGTGTGT	1871
5'integration F	TTGGCTAGCCCAAAATTTA	1754
5'integration R	ATAAGAATGCGGCCGCTTTTTCACGTATATTT TTTTGTTACATAAAAAG	1862
3'integration F	TGAGGGGTGAGCATTTAAAG	1734
3'integration R	ATGTATAATATATGGATGAAAGTTCAGT	1872
Selection marker F	CATACTAGCCATTTTATGTGTG	683
Selection marker R	GTACGTACCTAGGGGGCCCAATTCTTTTCG	325
Genotyping PbMyoA GFP		
Locus F	TCTCGTTTCTCGTTTTTCGT	1870
Locus R	TGTATTTGCTCTCGTGTGT	1871
5'integration F	TTGGCTAGCCCAAAATTTA	1754
5'integration R	TCCAGTGAAAAGTTCTTCTCCT	862
3'integration F	TGAGGGGTGAGCATTTAAAG	1734
3'integration R	ATGTATAATATATGGATGAAAGTTCAGT	1872
Selection marker F	GGCTATTCATACTAGCC	167
Selection marker R	GTACGTACCTAGGGGGCCCAATTCTTTTCG	325

Genotyping PfMyoA		
Locus F	TCTCGTTTCTCGTTTTTCGT	1870
Locus R	TGTATTTGCTCTCGTGTGT	1871
5'integration F	TTGGCTAGCCCAAAATTTA	1754
5'integration R	GACTTCCTTGTTGGAGGT	1873
3'integration F	TGAGGGGTGAGCATTTAAAG	1734
3'integration R	ATGTATAATATATGGATGAAAGTTCAGT	1872
Selection marker F	GGCTATTCATACTAGCC	167
Selection marker R	GTACGTACCTAGGGGGCCCAATTCTTTTCG	325
Genotyping PbMyoA point mutations		
Locus F	TCTCGTTTCTCGTTTTTCGT	1870
Locus R	TGTATTTGCTCTCGTGTGT	1871
Selection marker F	ATCCTCTGGTAATTTTTCG	961
Selection marker R	GGCCTGCAGCCCAGCTTAATTC	788

Table 2.7: Plasmids (Numbers according to ID from plasmid list of Johanna)

Name	Description	Source	Number
p32-*gfp-5'clag*	Vector to perform a promoter swap in *P. berghei*	Jessica Kehrer	-
p32-*5'ama1*	Ama1 promoter swap of *myoA*	This project	20
p32-*5'clag*	Clag promoter swap of *myoA*	This project	27
p32-*5'clag9*	Clag9 promoter swap of *myoA*	This project	28
p32-*5'msp9*	MSP9 promoter swap of *myoA*	This project	29
p32-*5'msp10*	MSP10 promoter swap of *myoA*	This project	30
p262-*coronin-mCh*	Tagging vector for coronin	Bane et al. (2016)	-
p262-*myoA*(-introns)-*gfp-3'dhfs*	Tagging vector for *myoA*	This project	25
p262-*myoA-3'dhfs*	Exchange of *3'myoA* and introduction of selection marker	This project	33

p262-*myoA*(-introns)-*3'dhfs*	Replacement of *myoA* by transcript	This project	32
p262-*PfmyoA-3'dhfs*	Replacement of *PbmyoA* by *PfmyoA*	This project	26
p262-*myoA*-E6R	Replacement of *5'ama1 myoA* by *myoA* E6R using GIMO	Smyrnakou (2019)	-
p262-*myoA*-S19A	Replacement of *5'ama1 myoA* by *myoA* S19A using GIMO	Smyrnakou (2019)	-
p262-*myoA*-S19D	Replacement of *5'ama1 myoA* by *myoA* S19D using GIMO	Smyrnakou (2019)	-

2.2 Biophysical methods

2.2.1 Functionalization of glass coverslips

To assure that polyacrylamide (PA) hydrogels form covalent bonds with the glass surface, 24*40 mm glass coverslips were activated as described in Pelham and Wang (1997). To this end, the glass coverslips were passed through the flame of a Bunsen burner to make them hydrophilic. Subsequently, the glass coverslips were covered with 0.1 M NaOH for at least 5 min and dried. Then, the glass coverslips were covered with APTMS for 4-5 min and washed extensively with distilled water. Next, the glass coverslips were incubated in 0.5% glutaraldehyde in PBS for 30 min, washed extensively with distilled water and dried. Functionalized glass coverslips were stored for several weeks.

2.2.2 Fabrication of elastic polyacrylamide hydrogels

PA hydrogels with an elastic modulus ranging from about 200 Pa to 40 kPa can be prepared by adjusting the relative concentrations of monomer and crosslinker (Tse and Engler, 2010). A scheme of the fabrication process is shown in Fig 2.1. In this study, AA, BIS, PBS and fluorescent beads were mixed as stated below (Table 2.8). Fluorescent beads were sonicated or vortexed for at least 5 min prior to preparation of the prepolymer solution to remove aggregates. As oxygen prevents polymerization of AA,

the mixture was degassed for at least 20 min before adding APS and TEMED to induce polymerization. Then, 30 µl of the prepolymer solution were pipetted onto a functionalized glass coverslip and covered with a 22*22 mm glass coverslip. Polymerization was allowed to proceed for at least 15 min. After incubation in PBS for 10 min, the 22*22 mm glass coverslip was carefully removed from the PA hydrogel using forceps. Since long-term storage can affect stiffness of PA hydrogels (Denisin and Pruitt, 2016), they were stored in PBS for a maximum of one week at 4℃.

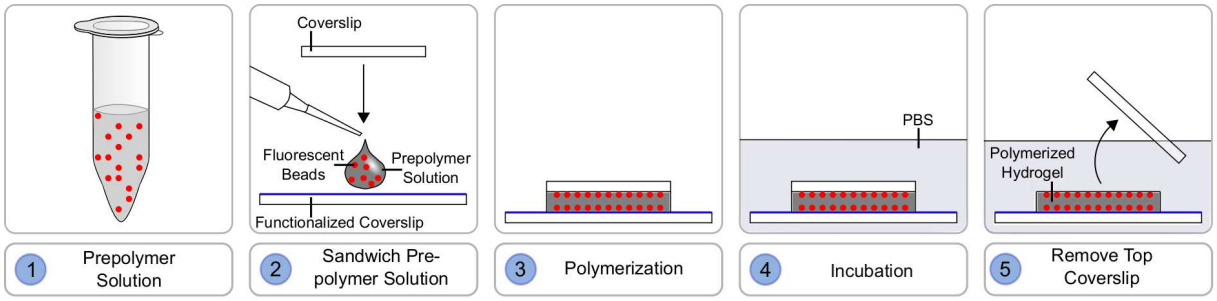

Figure 2.1: Schematic showing the fabrication of polyacrylamide hydrogels.
(1) AA, BIS, PBS and fluorescent marker beads are pipetted together and degassed.
(2) APS and TEMED are added to induce polymerization and a drop of prepolymer solution is immediately pipetted on top of a functionalized coverslip and covered with a second coverslip.
(3) Polymerization takes place in a wet chamber for about 15 min. Fluorescent beads collect at the interface between gel and glass.
(4) Incubation of the sandwich in PBS for about 10 min.
(5) The top coverslip is carefully removed using forceps. (Figure generated with Inkscape, adapted from Ribeiro et al. (2016)).

Table 2.8: PA hydrogel mixture (Young's modulus according to Tse and Engler (2010))

Formulation (AA[%]/BIS[%])	3/0.03	3/0.06	5/0.015	5/0.03	5/0.3	8/0.48
Young's modulus [kPa]	0.2	0.5	n.a.	1.0	8.7	40.4
AA (40% solution) [µl]	75	75	125	125	125	200
BIS (2% solution) [µl]	15	30	7.5	15	150	240
PBS [µl]	900	885	857	850	715	550
Beads	5					
APS (10% solution) [µl]	5					
TEMED [µl]	1					

2.2.3 Cell migration assays on elastic substrates

Before imaging, PA hydrogels were incubated in the appropriate medium for at least 10 min. The experimental setup differed depending on the aim of the experiment and the examined *Plasmodium* stage.

- Chamber setup: One well was removed from an 8 well silicone chamber (ibidi) using a scalpel. The silicone chamber was put onto the PA hydrogel and 15-30 µl of cells in the appropriate medium were pipetted into the chamber. The cells were allowed to settle for 7 min. Then, additional 100 µl of medium were carefully pipetted into the chamber to prevent the hydrogel from drying out due to evaporation of medium during imaging.
- Sandwich setup: 30 µl of cells in the appropriate medium were pipetted onto a PA hydrogel. Afterwards, the PA hydrogel was covered with a second hydrogel or a glass coverslip. To receive a constrained setting, medium was removed from the sides using a tissue paper 5 min after adding the cells to the PA hydrogel. For elongated periods of imaging, the sandwich was sealed with paraffin wax.
- 3D setup: Whole infected salivary glands were dissected into 30 µl of medium on a 22*22 mm glass coverslip placed on top of a glass slide. Then, the salivary glands were covered with a PA hydrogel. The sandwich was turned around and imaging was performed through the gel.

2.2.4 Image acquisition

For cell motility assays, fluorescent sporozoites were imaged with a 10x air objective (NA 0.5) or non-fluorescent sporozoites with a 25x water immersion objective (NA 0.8) on an inverted Axiovert Zeiss microscope using Axiovision or ZEN 2.6 software. Ookinetes were imaged with the same 25x water objective or with a 63x oil objective (NA 1.4). For sporozoites, images were recorded at 1 Hz or every 3 s for a total of 2 or 3 min. Ookinetes were imaged every 20 s or 1 min for a total of 5 or 10 min. Imaging of collective migration of sporozoites as well as Traction Force Microscopy was carried out on an Eclipse Ti inverted microscope (Nikon) with an UI-

traView spinning disk confocal unit (Perkin Elmer) with 60x (NA 1.49) or 100x (NA 1.4) magnification and a Hamamatsu Orca Flash camera.

2.2.5 Data analysis

Cell migration Motility patterns of sporozoites were categorized as shown in Fig 2.2. Sporozoites were considered as moving if they performed at least half a circle within 100 s. As *coronin(-)* and *hsp20(-)* sporozoites are much slower than wt sporozoites and do not necessarily move in circles, they were considered as moving if they moved for more than one parasite length within 3 min. Ookinetes were considered as moving if they moved for more than one parasite length within 10 min. Only those ookinetes that moved outside of aggregates were analyzed. Speed was analyzed using the Manual Tracking Plugin of Fiji (Schindelin et al., 2012) by tracking the parasite's apical end. Only those parasites continuously moving for at least 60 s without detachment were tracked. The direction of movement was defined as clockwise (CW) or counterclockwise (CCW) as seen under an inverted microscope.

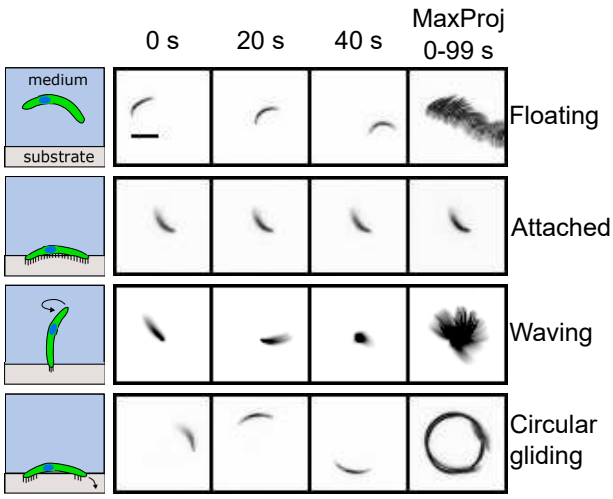

Figure 2.2: Motility patterns of salivary gland sporozoites.
(Left) Schematic showing the different motility patterns of sporozoites if pipetted onto a planar glass substrate. (Right) Image sequence and maximum projections of sporozoites that are floating, fully attached, waving (attached at one end and moving with the other end in the medium) or gliding in circles. Fully attached and waving sporozoites were combined into a single category as attached within this thesis. Scale bar, 10 µm.

Traction Force Microscopy Bead displacements were measured using PyTFM Software (provided by Dimitri Probst). Only those ookinetes moving out of the field of view were anlyzed in order to have a cell-free reference image. Traction forces could not be reconstructed for ookinetes moving between two hydrogels as a prerequisite of these calculations is that all forces are exerted on a single substrate.

2.2.6 Statistical analysis

Box-and-whisker plots depict the 25% quantile, median, 75% quantile and nearest observations within 1.5 times the interquartile range (whiskers). Outliers beyond this range are shown as black dots. GraphPad Prism version 5.0 was used to generate graphs and carry out statistical analyses. Non-parametric data was tested for significance using a Mann-Whitney test (if two groups were compared) or a Kruskal-Wallis test (for comparison of multiple groups).

2.3 Methods in Molecular Biology

2.3.1 Transformation of competent cells and plasmid amplification

DH5α competent *E. coli* cells (NEB) stored at -80℃ were thawed and mixed with appropriate amounts of plasmid DNA (35 µl of bacteria with 10-100 ng of plasmid DNA). The mixture was incubated for 10-30 min on ice, heat shocked at 42℃ for 90 s and incubated again for 5 min on ice. Then, the mixture was plated onto sometimes prewarmed LB agar-plates containing ampicillin and incubated at 37℃ over night.

For plasmid amplification 5 ml of LB medium containing 0.1 mg/ml ampicillin were inoculated with single colonies from LB agar-plates. Bacterial cultures were incubated on a shaker at 130 rpm over night at 37℃. Transformed bacteria were cryopreserved by mixing 750 µl of bacterial culture with 750 µl of 50% glycerol and stored at -80℃.

2.3.2 Plasmid DNA extraction

For plasmid DNA isolation, 4 ml of bacterial cultures were pelleted by centrifuging twice 2 ml of overnight culture at 13000 rpm for 3 min. DNA was extracted from the pellet using the QIAprep Spin Miniprep Kit (Quiagen) as described in the manufacturer's protocol.

2.3.3 Amplification of DNA fragments via PCR

DNA was amplified via polymerase chain reaction (PCR) run in a thermocycler FlexCycler 2 (Analytik Jena AG). PCR mixtures were pipetted according to Table 2.9. DNA fragments for molecular cloning were amplified using Phusion polymerase with the conditions shown in Table 2.10. Colony PCRs were performed with Taq polymerase and the according program. 10 µl of PCR mixture were inoculated with a single colony by picking the colony and pipetting up and down. Genotyping PCRs were run with Taq polymerase as well in a volume of 25 µl. Oligonucleotides were designed using the software Snapgene version 3.2.1 and ordered from Thermo Fisher Scientific.

Table 2.9: PCR mixture

	Phusion	Taq
Ingredient	Volume [µl]	Volume [µl]
Primer forward (100 µM)	0.5	0.5
Primer reverse (100 µM)	0.5	0.5
Buffer	10	2.5
dNTPs (2 mM)	5	2.5
Polymerase	0.5	0.5
Template (gDNA or plasmid DNA 1:1000)	2	2
H_2O_{dd}	31.5	16.5
Total	50	25

Table 2.10: PCR program

	Phusion		Taq	
	Temperature	Time	Temperature	Time
Initial Denaturation	98℃	30 s	95℃	30 s
30 cycles	98℃	10 s	95℃	30 s
	45-65℃	30 s	45-65℃	30 s
	72℃	30 s/kb	68℃	1 min/kb
Final Extension	72℃	5 min	68℃	5 min
Hold	4℃		4℃	

2.3.4 Molecular cloning

Vectors For the generation of mutant parasite lines different plasmids were used. Vector Pb262 (Deligianni, 2011) was used for conventional gene editing of *myoA*. Homology regions and different versions of *myoA* (with/without introns, GFP-tag and PfmyoA) were cloned into this vector. Vector p32 (kindly provided by Jessica Kehrer) was used to generate promoter swap mutants. To this end, homology regions and different blood stage specific promoters were cloned into this vector. For CRISPR/Cas9-mediated gene editing, vector pDC2 (Lee and Fidock, 2014), which was originally generated for *P. falciparum* was modified to contain regulatory elements (promoters and 3'UTRs) of *P. berghei*.

Conventional cloning via restriction digest 1-2 µg of plasmid DNA were digested with the appropriate restriction enzymes for 1.5-2 h. If necessary, 1 µl of calf intestine phosphatase was added after an hour to dephosphorylate incompletely cut plasmid. The fragment with the right size was purified from an agarose gel by dissolving it for about 15 min at 60℃ in binding buffer of the High Pure PCR Purification Kit and further purification was carried out according to the manufacturers' instructions. In case of non-compatible restriction sites, sticky ends were filled up by adding 1 µl of 10 mM dNTPs and 1 µl of T4 DNA polymerase to the restriction digest and incubating the mixture for 20 min at room temperature. Backbone and insert DNA were mixed at a ratio of 1:7 or 3:5 (vol/vol) and ligated at room temperature for at least 30 min using T4 DNA ligase. 10 µl of ligation solution were then transformed into 35 µl competent bacteria as described before (Section 2.3.1).

Cloning of small fragments DNA fragments smaller than 100 bp were ordered as complementary oligonucleotides with overhangs compatible to the restriction sites which were used to clone in the DNA fragment. Oligonucleotides (100 µM) were phosphorylated with T4 polynucleotide kinase in T4 DNA Ligase Buffer and annealed in a thermocycler for 30 min at 37℃. The temperature was then increased to 94℃ for 5 min. Decreasing the temperature by 1℃ every 10 s, the mixture was slowly cooled down to 25℃. Then, the oligonucleotide mixture was diluted 1:200. Backbone and diluted

annealed oligonucleotides were mixed at a ratio of 1:1 (vol/vol) and ligated at room temperature for at least 30 min using T4 DNA ligase. 10 µl of ligation solution were then transformed into 35 µl competent bacteria as described before (Section 2.3.1).

Gibson Assembly To generate the backbone, 1-2 µg of plasmid DNA were linearized with one or two restriction enzymes, dephosphorylated using calf intestinal phosphatase (CIP) (in the case of linearization with only one restriction enzyme) and purified as described above. The insert was amplified via PCR using primers automatically generated in SnapGene containing 15-25 bp overlaps. DNA concentrations were determined using a Nanophotometer NP80 (Implen). About 100 ng of vector were mixed with at least 3-fold insert and an equal volume of Gibson Assembly Master Mix and incubated for 15-60 min as written in the manufacturer's protocol. Then, 2 µl of the mixture were transformed into 35 µl competent bacteria as described before. Alternatively, vector and insert were assembled using HiFi DNA Assembly Master Mix according to the manufacturer's protocol and 5 µl of the mixture were transformed.

Verification Introduction of the insert was tested using restriction enzymes that give different patterns for original vector or vector containing the integrated insert. After confirmation of insert integration, the sequence of the insert was verified by sequencing at GATC Biotech or Eurofins.

2.3.5 Genomic DNA extraction

Whole blood from infected mice was mixed with 1 ml PBS and 150 µl 1% saponin to lyse erythrocyte membranes. The mixture was centrifuged at maximum speed for 1 min and washed with PBS. Then the pellet was resuspended in 200 µl PBS and either directly further processed for DNA extraction or stored at -20 °C. Genomic DNA from parasites was extracted using the DNeasy Blood and Tissue Kit according to the manufacturer's protocol.

2.3.6 gRNA design

gRNAs were designed using the web tool EuPaGDT (Peng and Tarleton, 2015). The gRNAs closest to the mutation site (maximum 100 bp from mutation site to prevent alternative recombination events), with a high efficiency score (Doench et al., 2014) and no off-targets within the *P. berghei* genome were chosen to be tested. It has been shown, that the *P. falciparum* U6 snRNA promoter does not require an initial guanosine nucleotide as opposed to the mammalian U6 snRNA promoter (Ghorbal et al., 2014). Assuming that the same holds true for the *P. berghei* U6 snRNA promoter, no initial guanosine nucleotide was incorporated into the gRNAs.

2.3.7 Donor design

Donor templates were amplified with Gibson primers and carried the mutation which should be incorporated as well as a recodonized region to prevent the Cas9 from cutting again. Either the PAM-motif was replaced or if that was not possible without changing the amino acid sequence the gene encodes, two to three silent mutations were incorporated into the seed region of the gRNA (12 nucleotides upstream of the PAM-motif). As AAG can be recognized by Cas9 as an alternative PAM motif, additional mutations were introduced in the seed region, if this sequence was used as mutated PAM site. If possible, a BbsI site was introduced into the mutation site, which allowed for testing successful mutagenesis via amplification of the gene of interest and subsequent restriction digest. Otherwise successful mutagenesis was verified by sequencing.

2.4 Methods in Parasitology

2.4.1 *Plasmodium* transfection and generation of clonal lines

DNA preparation For transfections, plasmid DNA extracted from 4 ml of bacterial culture was linearized by restriction digest left and right to the homology regions. To do promoter swaps or *myoA* replacements, vectors were cut with KpnI and SacII, while they were linearized with BamHI and SacII for the GIMO strategy. Linearization of the

plasmid DNA was verified using gel electrophoresis. To precipitate the DNA, the solution was mixed with 15 µl of 3 M sodium acetate and 250 µl of ice-cold pure ethanol. The solution was incubated at -20°C for at least 30 min and centrifuged at 14000 rpm, 4°C for 15-30 min. The supernatant was completely removed and the pellet resuspended in 35 µl H_2O_{dd}.

Preparation and isolation of schizonts One day prior transfection, whole blood from a mouse with at least 2% parasitaemia was added to a cell culture flask containing 20 ml of prewarmed transfection medium and kept at 37°C and 5% CO_2 overnight. To check whether schizonts were fully developed the next day, a blood smear was made from the schizont culture, shortly fixed in methanol and stained in Giemsa solution. If schizonts were visible in the blood smear, the overnight culture was transferred into a 50 ml tube and underlaid using 10 ml of a 55% Nycodenz solution. To separate schizonts from other blood cells, the solution was centrifuged at 1500 rpm for 20 min without break. The ring containing schizonts that formed between Nycodenz and medium during centrifugation was transferred into a 10 ml tube using a Pasteur pipette. The solution was centrifuged at 1500 rpm for 10 min. Then, the supernatant was removed and the pellet was resuspended in 1 ml transfection medium per transfection. For each transfection, 1 ml medium containing schizonts was transferred into a tube, shortly centrifuged at maximum speed and the supernatant was removed.

Electroporation and transfer of transfected parasites into mice Electroporation was carried out using the Amaxa Human T Cell Nucleofector Kit (Lonza). To this end, 100 µl of Nucleofector solution were added to the DNA and the mixture was used to resuspend the schizont pellet. The mixture was pipetted into a cuvette and electroporation was carried out using program U33. After electroporation, 50 µl transfection medium were added to the mixture which was injected i.v. into a mouse. The following day, pyrimethamine was added to the drinking water of the mice to a final concentration of 70 mg/l to select for parasites that introduced the DNA via homologous recombination and therefore contained the selection cassette. Alternatively, 1.5 mg/ml 5-FC were added to the drinking water to select for parasites that replaced the selection cassette by a linearized construct. When the mice reached a parasitaemia of at least 1%, their

blood was collected via cardiac puncture.

Generation of clonal parasite lines To separate successfully transfected parasites from resistant wt parasites, limiting dilutions were carried out. To this end, a stabilate from the transfection was injected into a mouse. The next day, pyrimethamine was added to the drinking water. When parasitaemia reached 0.5–1% (to have less multiple infected erythrocytes), blood was collected via cardiac puncture and diluted down to have 18 parasites in 2 ml PBS. 100 µl of the solution were injected i.v. into a mouse to inject statistically less than one parasite per mouse. The blood of mice that became positive was analysed for parasites with the correct integration of the construct using genotyping PCR as described above.

2.4.2 Preservation of parasite lines

For long-term storage of parasite lines, 100 µl blood from an infected mouse containing blood-stage parasites were mixed with 200 µl of freezing solution (Table 2.3) in cryopreservation vials. These were stored in liquid nitrogen.

2.4.3 Mouse infection

To infect new mice, either frozen parasites were thawed and injected i.p. or the mice were anaesthetized with 100 µl Ketamine/Xylazine (Table 2.3) per 35 g weight and infected mosquitoes were allowed to feed on the mice.

2.4.4 Mosquito infection

Blood from an infected mouse was collected via cardiac puncture and a volume containing 20 mio parasites as estimated from the parasitaemia and the amount of erythrocytes per µl blood was injected into each of 2-3 naïve mice. After 3 d a drop of tail blood was collected, covered with a glass coverslip and left at room temperature for 10-15 min. If exflagellation was observed under the Axiostar plus microscope (Zeiss), the mice were anaesthetized with 100 µl Ketamine/Xylazine (Table 2.3) per 35 g weight and put on top of a mosquito cage containing 60-200 female mosquitoes. The mosquitoes

were allowed to suck blood for 20 min. Then the mice were removed from the mosquito cage and euthanized via cervical dislocation.

2.4.5 Parasite isolation from mosquitoes

Mosquito midguts were dissected for oocysts or midgut sporozoites from day 12 after infection onwards. Salivary glands were dissected from day 17 after infection onwards. Midguts and salivary glands were dissected into 50-100 µl PBS and kept on ice. Sporozoites were isolated mechanically from midguts or salivary glands using a plastic pestle. In case of low salivary gland infections, sporozoites were purified for cell migration assays. To this end, the medium containing salivary glands was filled up to 1 ml with RPMI and overlaid with 3 ml 17% Accudenz solution. Centrifugation was carried out at 2500 g for 20 min. The interphase containing sporozoites that formed between Accudenz and medium during centrifugation was transferred into a 2 ml tube and centrifuged for another minute at maximum speed. The supernatant was removed and the pellet resuspended in medium.
For isolation of hemolymph sporozoites, the mosquitoes were cut at the abdomen, the thorax was punctured using a very thin glass needle and flushed with PBS. The drop of PBS and hemolymph appearing at the abdomen was then collected and transferred into a tube. The solution was centrifuged for 1 min at maximum speed and the pellet resuspended in a defined volume of PBS. In case of fluorescent parasite lines, only those mosquitoes showing a fluorescent signal in the midgut were dissected to count sporozoites. For non-fluorescent parasite lines with point mutations in *myoA*, only those mosquitoes having oocysts as judged by eye were dissected to count sporozoites.

2.4.6 Ookinete cultures

For ookinete culture, an infected mouse with exflagellating parasites is needed. 10 ml of ookinete medium were supplemented with 2 ml of FBS and put into a cell culture flask. The medium was warmed up to 19℃ and up to 1 ml of blood collected from the mouse by cardiac puncture was added to the medium. The culture was incubated at 19℃ with gentle shaking for at least 21 hours. If ookinetes were observed in a

drop of concentrated culture, they were purified. To this end, the whole culture was transferred into a 50 ml tube and underlaid with 10 ml of a 63% Nycodenz solution. The solution was centrifuged for 25 min at 1000 rpm without brake to separate the parasites from uninfected erythrocytes and other blood cells. The ring containing ookinetes that formed between Nycodenz and medium during centrifugation was transferred into a 2 ml or 10 ml tube using a Pasteur pipette. Then, the cells were pelleted at maximum speed for 1 min or at 1000 rpm for 10 min. The pellet was resuspended in a small volume of medium.

2.4.7 Analysis of life cycle progression

Calculation of asexual growth rate Blood stage growth rates were calculated 7-9 days post limiting dilution assuming a single parasite was injected i.v. into a mouse. The number of parasites was estimated by counting the percentage of infected erythrocytes in a blood smear when the parasitemia was between 0.5 and 2%. The number of erythrocytes in mouse blood was assumed to be 7 million erythrocytes/µl and the total amount of blood 2 ml. The multiplication rate per day was calculated as described in Klug et al. (2016) using the formula

$$\text{Growth rate} = \text{Number of parasites}^{1/\text{day post injection}}$$

Staining of oocysts 12 to 14 days post infection, mosquito midguts were permeabilized in 100 µl 1% Nonidet P40 in PBS. After about 20 min the supernatant was taken off and oocysts were stained in 200 µl 0.1% mercurochrome solution for 30 min to two hours. Again, the supernatant was taken off and the midguts were washed with PBS for three to four times. Oocysts were counted at an inverted Axiovert Zeiss microscope using a 10x objective with transmission light and a GFP filter set (excitation BP 450/50, emission BP 510/50).

Analysis of infectivity The percentage of infected mosquitoes was calculated from the number of midguts positively stained for oocysts divided by the total number of midguts dissected.

Counting sporozoites Sporozoites were counted using a Neubauer hemocytometer. The total number of sporozoites was then divided by the number of dissected mosquitoes to get the number of sporozoites per infected mosquito. In case of non-fluorescent parasite lines the number was divided by the percentage of infected mosquitoes to account for non-infected mosquitoes in the sample. Alternatively, only infected mosquitoes were dissected for sporozoite countings.

3 Results

Plasmodium parasites face different environments and get in contact with a range of tissues on their way from the mosquito vector to the mammalian host. There are four motile stages of the parasite, three of them use an actin/myosin-based type of locomotion. Depending on where they are, these parasite stages need to adapt their migratory behavior to their environment in order to progress through the life cycle and survive.

3.1 Elastic PA hydrogels to study *Plasmodium* motility

It is of general interest how physical properties of the extracellular environment affect cell migration (Charras and Sahai, 2014). Trying to understand how environmental factors influence parasite motility, I developed a range of different hydrogel assays (Fig 3.1). These hydrogels have defined characteristics which allows for tuning of different parameters and dissecting their contribution to cell migration (Tse and Engler, 2010). I manufactured the hydrogels to mimic the physiological range of tissue stiffnesses by mixing monomer and crosslinker at various concentrations (Fig 3.1 A). Cells were either pipetted on top of 2D PA hydrogels in order to dissect how they move on planar substrates of different stiffnesses (Fig 3.1 B). In a different setup, the cells were sandwiched between two hydrogels to induce a confined environment while still being able to image in two dimensions. Alternatively, 3D motility was investigated by allowing the cells to move into the hydrogel. Sporozoites moved in circular trajectories in counterclockwise direction at a speed of 1-3 µm/s on 2D hydrogels (Fig 3.1 C). Ookinetes attach to but do not move continuously on uncoated 2D PA hydrogels. Therefore, their motility was observed in the sandwich setup, where they moved in circular or meandering fashion at a speed of 0.05-0.2 µm/s (Fig 3.1 D). Migration paths of manually tracked sporozoites and ookinetes are depicted in Fig 3.1 E-G. In 3D hydrogels, sporozoites

move in irregular helical trajectories. Using the established cell migration assays, I next analyzed how substrate stiffness, confinement and pore size affect *Plasmodium* motility.

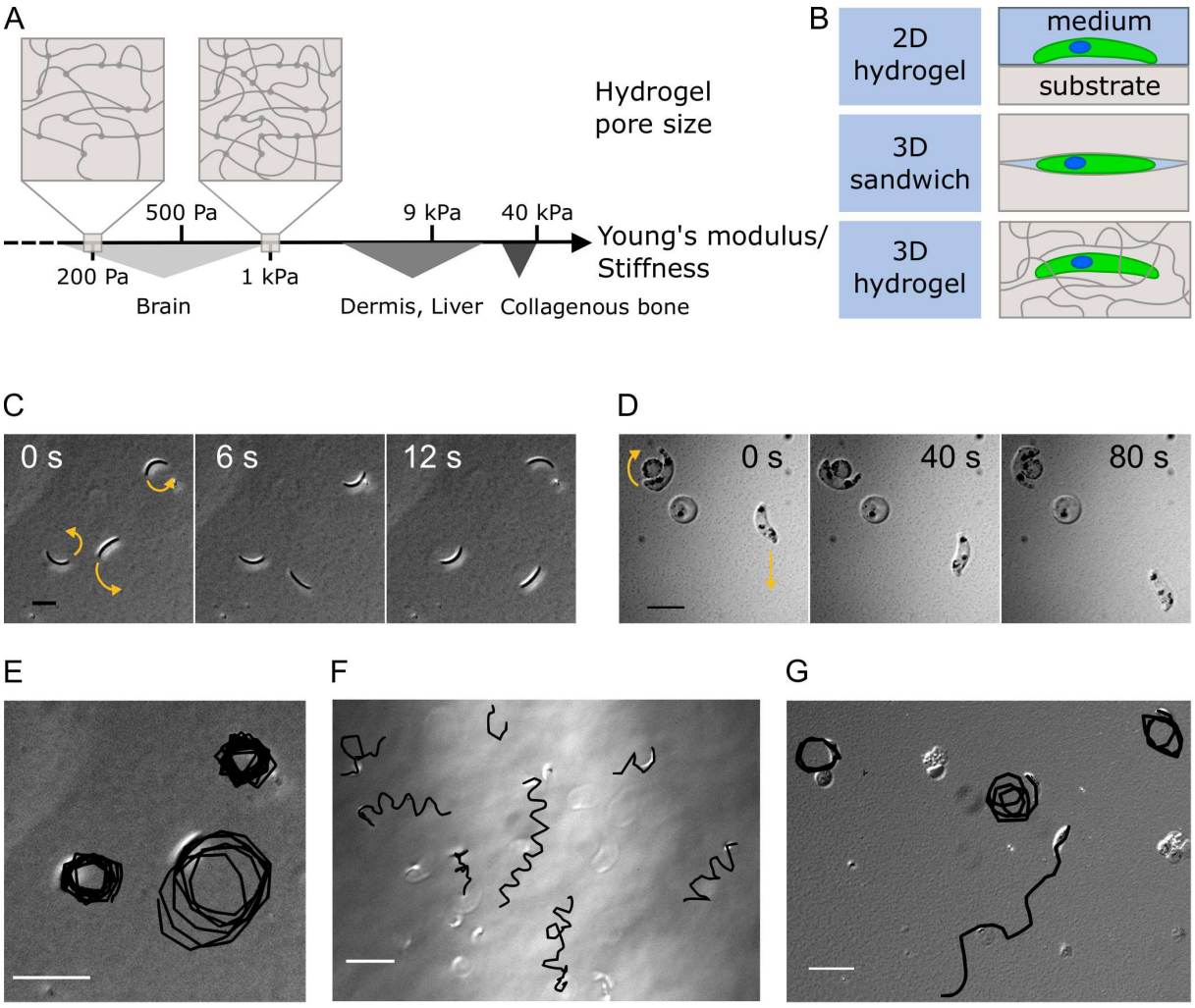

Figure 3.1: Hydrogel assays developed to investigate the effect of substrate stiffness, confinement and pore size on *Plasmodium* motility.
(**A**) PA hydrogels can be manufactured to mimic the range of tissue stiffnesses encountered by cells. Brain tissue is very soft with an elasticity of less than 1 kPa, while collagenous bone is much stiffer with an elastic modulus of 20-40 kPa (Engler et al., 2006). Dermis and liver tissues that are encountered by *Plasmodium* parasites exhibit an intermediate stiffness of around 9 kPa (Nyström and Bruckner-Tuderman, 2019; Zahouani et al., 2009). With increasing stiffness, the pore size of the hydrogels becomes smaller. Figure modified from Kratzer (2016). (**B**) In the 2D setup, parasite (indicated in green with the nucleus depicted in blue) motility is monitored on planar substrates of different stiffnesses. In the 3D sandwich, parasites are confined between two hydrogels. In the 3D hydrogel, the parasites move inside the synthetic substrates. (**C**) DIC images of sporozoites moving on planar 2D hydrogels at indicated timepoints. Yellow arrows indicate the direction of movement. Scale bar, 10 µm. (**D**) Ookinetes confined between hydrogels at indicated timepoints. (**E**) Migration paths (indicated in black) of sporozoites on a 2D hydrogel or in a 3D hydrogel (**F**) over a time course of 3 min. Scale bar, 20 µm. (**G**) Migration paths of ookinetes sandwiched between two hydrogels over a period of 10 min.

3.1.1 Confinement of ookinetes between uncoated PA hydrogels induces fast and persistent motility

To investigate whether substrate stiffness affects the gliding behavior of ookinetes, I analyzed these parasite stages in the hydrogel assays described above. Three different hydrogel formulations were fabricated mimicking soft, medium and stiff tissues (1, 9 and 40 kPa according to Tse and Engler (2010)). If sandwiched between two hydrogels, the migratory capacity of ookinetes increases substantially as compared to glass (Fig 3.2 A). While less than 50% of the ookinetes move on glass, 80%-100% move on elastic hydrogels. However, there is no significant difference in the fraction of motile ookinetes between hydrogels of different stiffnesses. Additionally, they move faster than on glass (Fig 3.2 B). On soft and medium hydrogels, their average speed is with about 0.15 µm/s twice as high as on glass. On stiff hydrogels the average speed increases even more to about 0.2 µm/s. These observations indicate that confinement can induce ookinete motility even in the absence of specific receptors or insect cells (Siden-Kiamos et al., 2006). However, motility is not influenced by substrate stiffness in these confined environments. As I observed ongoing motility after several hours of imaging, I incubated the ookinetes confined between hydrogels at 21℃ in a wet chamber overnight. Although no oxygen exchange was possible with the experimental setting, ookinetes could move for hours on hydrogels and a large fraction was still motile after 20-26 hours (Fig 3.2 C). While 40-130% of the ookinetes moved on elastic hydrogels as normalized to the percentage of moving ookinetes directly after induction of motility, less than 10% moved on glass after this period of time. After 20-26 hours their speed decreased to 0.12 µm/s on soft hydrogels, 0.07 µm/s on medium hydrogels and 0.15 µm/s on stiff hydrogels (Fig 3.2 D). On glass, their speed was not analyzed after 20-26 hours due to the low fraction of motile ookinetes.

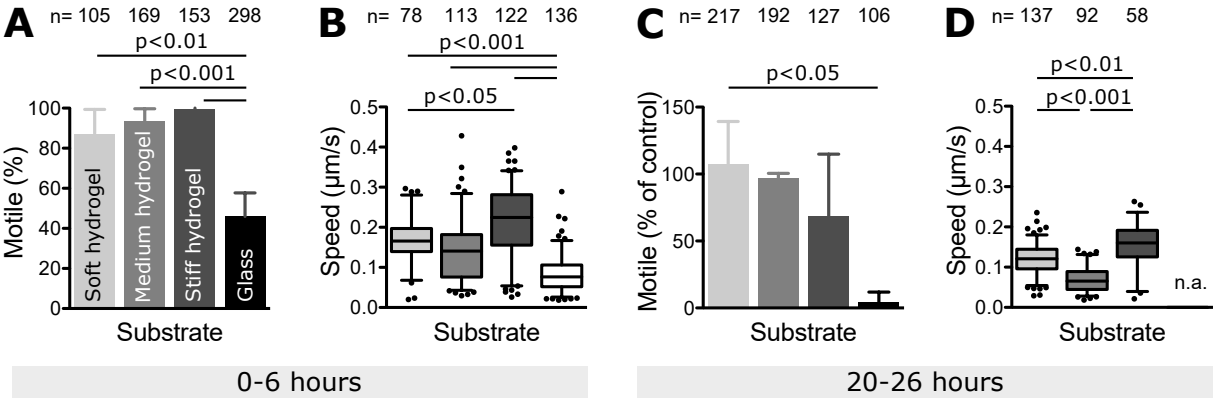

Figure 3.2: Confinement of ookinetes between uncoated PA hydrogels induces fast motility. (**A**) Fraction of motile ookinetes within 6 hours after inducing motility by confining the cells between two planar substrates. Bars represent the mean and error bars the standard deviation of at least three independent experiments. (**B**) Speed of ookinetes as determined by manually tracking. (**C**) Fraction of motile ookinetes 20-26 hours after inducing motility by confining the cells between two planar substrates and normalized to the fraction of motile ookinetes after 0-6 hours. At least two independent experiments were carried out. (**D**) Speed of ookinetes as determined by manually tracking. Speed on glass after 20-26 hours was not analyzed (n.a.) due to the low fraction of motile ookinetes at this timepoint. Numbers above indicate the number of ookinetes that were analyzed. Significance for **A** and **C** determined by One-way analysis of variance with Bonferroni's Multiple Comparison test. Significance for **B** and **D** determined by Kruskal-Wallis test with Dunn's Multiple Comparison test.

3.1.2 Sporozoite ability to move depends on substrate elasticity on planar substrates

Next, I was interested in the role that substrate stiffness plays for sporozoite motility. Sporozoites get in touch with a wide range of cells and tissues and need to cross different barriers. It has been shown before using PEG hydrogels, that sporozoite motility depends on substrate stiffness and ligand spacing (Perschmann et al., 2011). Here, I used the uncoated PA hydrogels with a narrow range of stiffnesses reflecting the mechanical properties of tissues to get a better understanding of the environmental impact on sporozoite motility. The following results have been partially obtained during my master thesis (Kratzer, 2016). Sporozoites were able to attach and move on uncoated 2D hydrogels with embedded marker beads. The fraction of motile sporozoites that moved for at least half a circle within 100 s increased with increasing stiffness being highest on glass (Fig 3.3 A). While only 5-15% of sporozoites moved on soft hydrogels, the fraction of motile sporozoites increased to 30-40% on medium and stiff hydrogels. On glass 50-70% of sporozoites were motile. The persistence of movement increased as well with increasing stiffness as measured by the number of circles they performed

within 100 s (Fig 3.3 B). On soft hydrogels, sporozoites were only moving for one circle on average, while the number of circles per 100 s increased to 2 on medium hydrogels and 4 on stiff hydrogels and glass. However, substrate stiffness had no obvious effect on the speed at which the sporozoites moved which was about 2 µm/s on average (Fig 3.3 C). Only those parasites that moved for at least 60 s without detachment were tracked. On soft hydrogels sporozoites did not move continuously for this period of time. Instead, they detached or stopped moving. Note that also the pore size varies between PA hydrogels of different stiffnesses. Therefore, we cannot exclude that the observed effects on motility were not exclusively due to stiffness differences but also because of differences in pore size that might affect surface texture. Importantly, sporozoites only attached to and moved on planar hydrogels if fluorescent beads were embedded into the hydrogel. This might indicate, that the beads serve as adhesion sites.

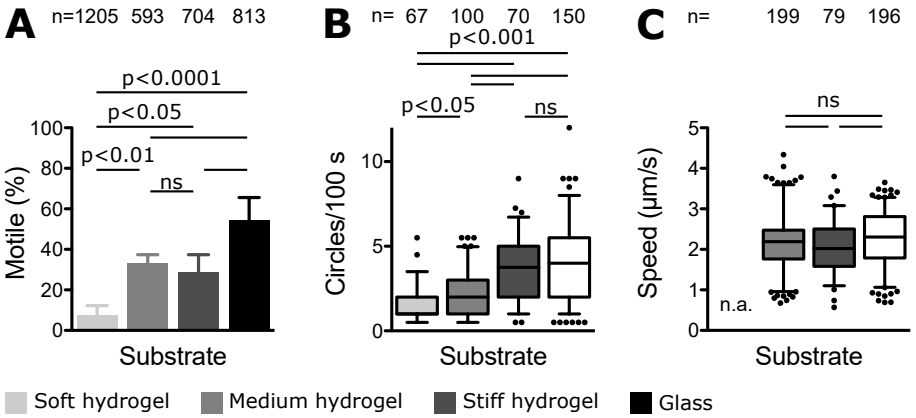

Figure 3.3: Sporozoite motility depends on substrate stiffness.
(**A**) Fraction of motile sporozoites 30 min after activation. Bars represent the mean and error bars the standard deviation of at least three independent experiments. Significance determined by One-way analysis of variance with Bonferroni's Multiple Comparison test. (**B**) Number of circles performed within 100 s as recorded 30 min after activation. (**C**) Speed of sporozoites within 45 min after activation as determined by manually tracking. Speed on soft hydrogels was not analyzed (n.a.) as sporozoites moving on these hydrogels did not meet the tracking requirements. Significance of (**B**) and (**C**) determined by Kruskal-Wallis test with Dunn's Multiple Comparison test. Numbers above indicate the number of sporozoites that were analyzed.

3.1.3 Sporozoite speed depends on pore size in 3D environments

Sporozoites could not be sandwiched between two hydrogels, as they are only about 1 µm wide and it is not possible to reduce the distance between the hydrogel sandwich

to this width. However, I sandwiched infected salivary glands between a hydrogel and a coverslip. Upon disintegration of the salivary glands this setup allowed the sporozoites to move into the hydrogel if the pores were large enough (Fig 3.4 A). This is the case for soft hydrogels but not for intermediate or stiff hydrogels. While sporozoites did not move continuously on soft 2D hydrogels (5/0.03 gel formulation), they moved well within these hydrogels, suggesting that confinement can compensate for the gliding defect on soft planar substrates. The speed distribution of sporozoites in the skin ranges from 0.04-2.16 µm/s (Douglas et al., 2018b). Inside hydrogels with small pores (5/0.03 gel formulation), the sporozoites were moving between 0.11 and 0.70 µm/s (Fig 3.4 B). Further decreasing acrylamide or bisacrylamide concentration (which decreases stiffness and increases pore size) resulted in higher speeds of sporozoites within these hydrogels. In the hydrogels with the largest pore size tested (5/0.015 gel formulation), the sporozoites revealed speeds up to 2.21 µm/s and thus a comparable speed as the fastest sporozoites *in vivo*. All experiments were carried out with BSA containing medium to activate sporozoite motility. However, sporozoites did also enter the hydrogels if there was no BSA added to the medium. Yet, they did not move any further when imaged inside the hydrogels without BSA. As opposed to the 2D assays, sporozoites also moved if no beads were embedded into the hydrogels suggesting that due to confinement in these 3D assays no additional anchoring points are required.

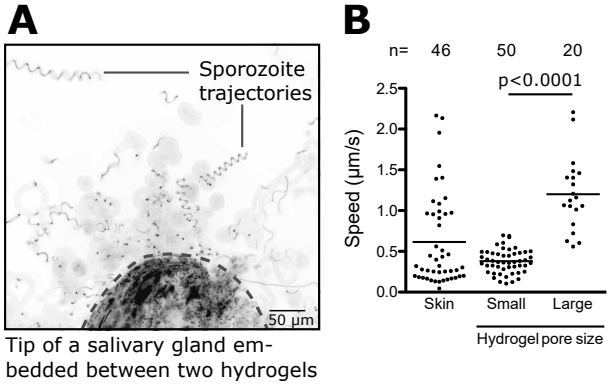

Tip of a salivary gland embedded between two hydrogels

Figure 3.4: PA hydrogels as a skin mimic to study 3D motility of sporozoites.
(**A**) Maximum projection of an infected salivary gland embedded between a hydrogel and a glass coverslip with sporozoites moving into the hydrogel. Images were recorded in the GFP channel. (**B**) Speed of sporozoites moving in the skin (Douglas et al., 2018b) and in hydrogels with small or large pores. Individual data points show the average speed of manually tracked sporozoites and black lines indicate the mean. Significance determined by Mann-Whitney test.

3.1.4 Effect of substrate stiffness and confinement on genetically modified parasites

Next, I wanted to test whether the hydrogels better reflect the *in vivo* environment of sporozoites as compared to conventional cell migration assays on glass. To this end, a mutant lacking the actin-filament binding protein coronin which is moving well in the skin, but moves slowly and in abnormal trajectories on glass (Bane et al., 2016), as well as a mutant lacking heat shock protein 20 (HSP20) with a cell migration defect both on glass and in the skin (Montagna et al., 2012) were analyzed. I aimed at reducing the influence of environmental factors other than substrate stiffness, such as temperature or batch-to-batch differences between hydrogels. Mutant and control sporozoites were imaged on the same batch of hydrogels within the same week or even on the same hydrogel by using fluorescent and non-fluorescent sporozoites to distinguish between mutant and control. Wt parasites of the ANKA strain or parasites expressing GFP of the NK65 strain (Natarajan et al., 2001) were used as control parasites. I fabricated hydrogels with defined stiffnesses and kept the AA concentrations constant while adjusting the BIS concentration to achieve different pore sizes (Tse and Engler, 2010; Wen et al., 2014). I used 3/0.03 (0.2 kPa) and 3/0.06 (0.48 kPa) gel formulations, which are for simplicity called large pore and small pore hydrogels in the following sections. The experiments with *coronin(-)* and *hsp20(-)* sporozoites were partially carried out by Xanthoula Smyrnakou (Smyrnakou, 2019) and Maren Nattermann under my supervision.

Soft hydrogels and confinement rescue the gliding defect of sporozoites lacking the actin modulator coronin

The mutant phenotype of *coronin(-)* sporozoites suggests that motility is differently regulated when the parasite has to transition from a circulatory system to penetrate an organ or whether it moves inside a tissue providing a confined environment as it is the case in the dermis. To analyze the effect of substrate stiffness and confinement on *coronin(-)* sporozoites, these parasites were examined on planar hydrogels of different stiffnesses as well as inside hydrogels of different pore sizes. Investigation of *coronin(-)* sporozoites on soft hydrogels revealed that only a fraction of 0-60% was able to move as normalized to control parasites (Fig 3.5 A). On intermediate substrates

however, similar numbers of mutant and control sporozoites were moving leading to a motile fraction of 40-120% normalized to the control. Next, we measured the speed of *coronin(-)* sporozoites on the different substrates and found that 40 kPa hydrogels could partially compensate the reduced migration ability observed on glass (Fig 3.5 B). The parasites moved more than twice as fast on these hydrogels than on glass (on average 1.2 versus 0.5 µm/s). Soft and intermediate hydrogels on the other hand did not have the same effect on sporozoites lacking coronin, although the mutant sporozoites were still faster on intermediate hydrogels as compared to glass. On 9 kPa hydrogels they moved at 0.7 µm/s, while they revealed speeds of 1 µm/s on 40 kPa hydrogels. In addition, the trajectories became more similar to the ones of wt parasites on intermediate and stiff hydrogels (Fig 3.5 C).

To test whether confined environments can completely rescue the gliding defect of *coronin(-)* sporozoites, we monitored their motility in hydrogels with smaller or larger pores. The mutant sporozoites moved in helical trajectories in small pore hydrogels, similar to control parasites (Fig 3.6 A). The collection of trajectories shows that radius and pitch of the helices differs among sporozoites. Interestingly, *coronin(-)* sporozoites moved at the same speed as control parasites within these dense hydrogels (Fig 3.6 B). Thus, confinement could completely compensate the motility defect of *coronin(-)* sporozoites. In hydrogels with larger pores, the trajectories of *coronin(-)* sporozoites still looked similar to control parasites (Fig 3.6 C). Although their speed was higher than in dense hydrogels, it was significantly reduced from an average of about 0.7 µm/s to about 0.5 µm/s as compared to control parasites (Fig 3.6 D).

Sporozoites lacking HSP20 have a defect in moving through confined environments

Next, we probed *hsp20(-)* sporozoites on PA hydrogels. Interestingly, the fraction of motile sporozoites was enhanced on all hydrogels with 100-250% of sporozoites being motile normalized to control parasites (Fig 3.5 A). We found a reduction in speed on elastic hydrogels, indicating that a lack of HSP20 results in a cell migration defect irrespective of substrate elasticity (Fig 3.5 B). The speed was on average 0.3 µm/s on 1 kPa and 40 kPa hydrogels, while it was 0.5 µm/s on 9 kPa hydrogels. Furthermore,

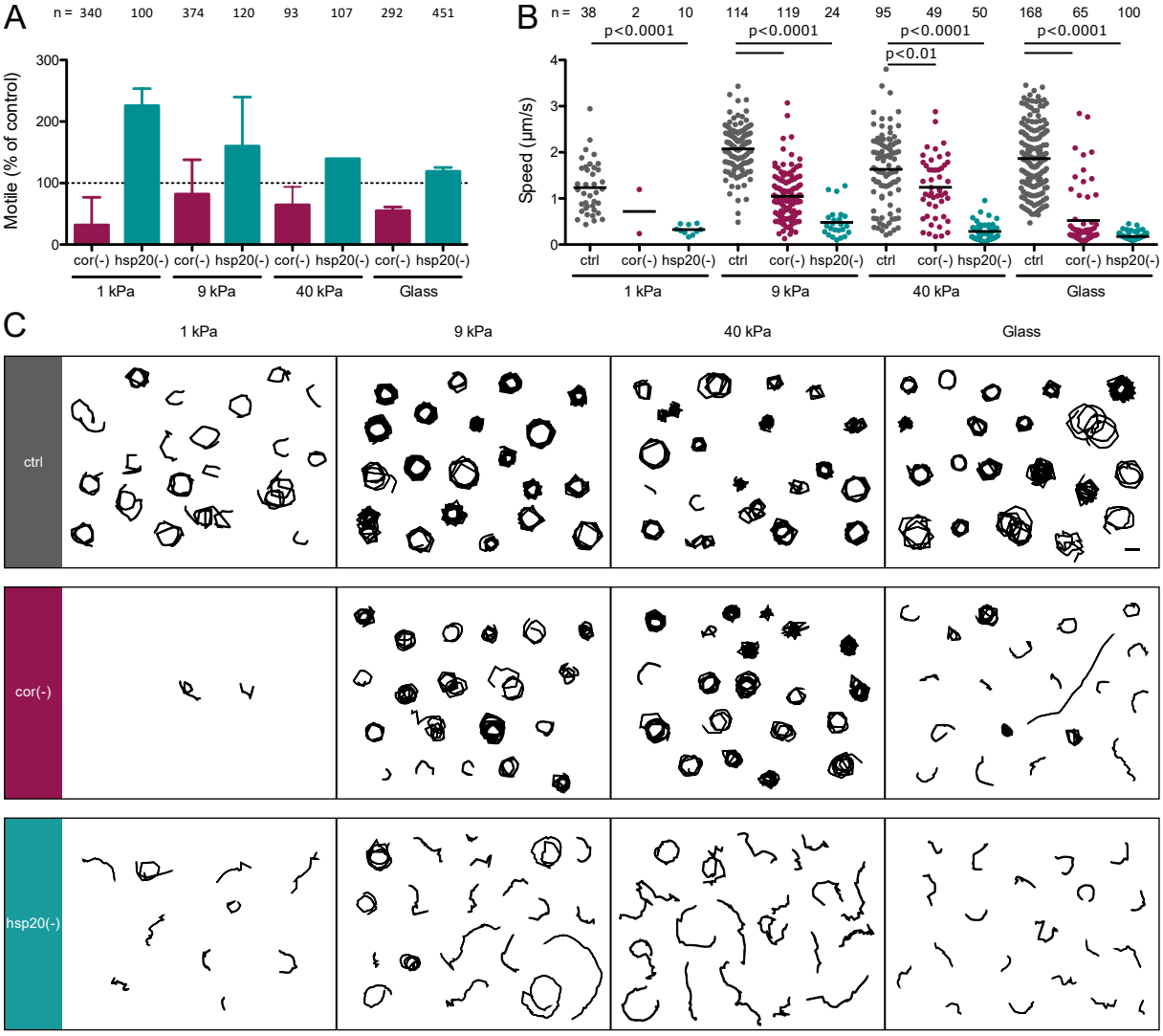

Figure 3.5: The cell migration defect of *coronin(-)* sporozoites but not *hsp20(-)* sporozoites is partially rescued on 40 kPa hydrogels.
(**A**) Fraction of motile sporozoites normalized to control parasites. Bars represent the mean and error bars the standard deviation. (**B**) Individual data points show the average speed of manually tracked sporozoites and black lines indicate the mean. Note that on soft hydrogels only low numbers of parasites met the tracking requirements as most observed parasites did not move continuously. Data from at least two biological replicates except preliminary data from a single experiment for *hsp20(-)* sporozoites on 40 kPa hydrogels. P-values have been calculated using the Mann-Whitney test. (**C**) Progressive lines of manually tracked sporozoites are shown. Scale bar, 10 µm.

we observed atypical trajectories of *hsp20(-)* sporozoites on all substrates (Fig 3.5 C).

Hsp20(-) sporozoites have similar movement patterns in the skin as wt parasites but move at lower speed (Montagna et al., 2012). Thus, we expected them to behave similarly in 3D hydrogels. Indeed, the sporozoite tracks looked similar to the ones of control parasites, albeit shorter (Fig 3.6 A). Their speed was significantly reduced to

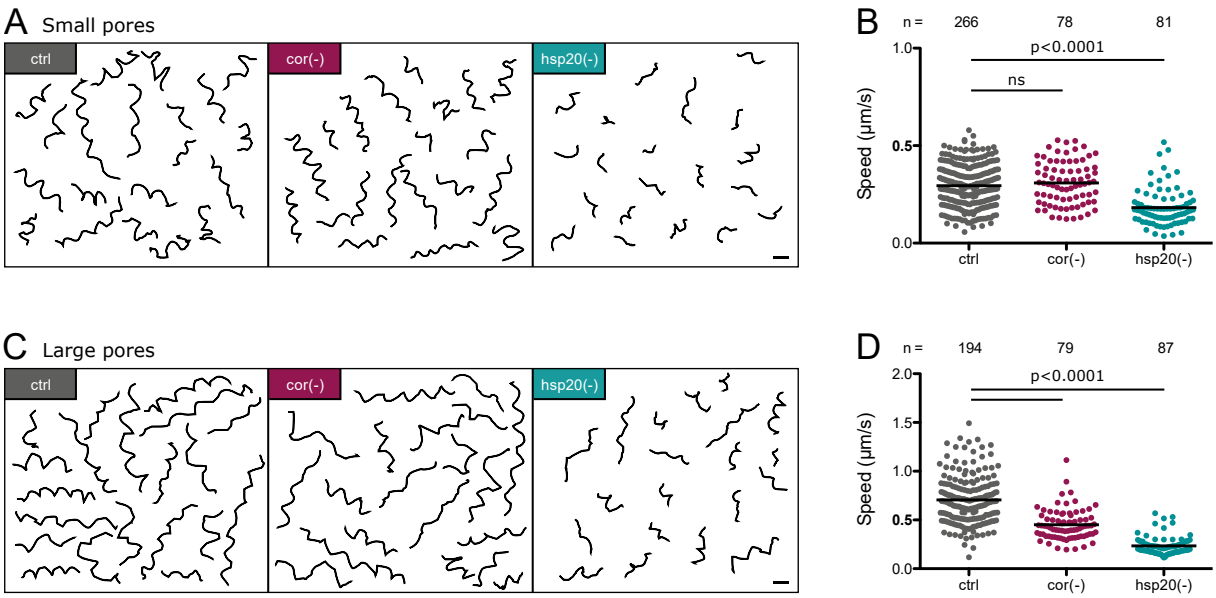

Figure 3.6: Dense synthetic 3D environments can rescue the cell migration defect of *coronin(-)* sporozoites but not *hsp20(-)* sporozoites.
(**A**) Collection of trajectories of manually tracked sporozoites moving in hydrogels with small pores. Scale bar, 10 µm. (**B**) Individual data points show the average speed of manually tracked sporozoites moving in hydrogels with small pores and black lines indicate the mean. P-values have been calculated using the Mann-Whitney test. Note that sporozoites were tracked in xy dimension only, which underestimates the original speed. (**C**) Trajectories of sporozoites moving in hydrogels with large pores. Note that sporozoites often moved quickly in and out of focus meaning that they usually could not be tracked for the same amount of time as those shown in (**A**). Scale bar, 10 µm. (**D**) Speed of sporozoites moving in hydrogels with large pores.

about half the speed of control parasites (Fig 3.6 B). In the hydrogels with larger pores, the trajectories of *hsp20(-)* parasites looked similar as in hydrogels with smaller pores and their speed was nearly identical (Fig 3.6 C, D). Compared to control parasites, the speed was drastically reduced from an average of about 0.7 µm/s to about 0.2 µm/s.

3.1.5 T cells on elastic PA hydrogels

For a broader application of the hydrogel assays, I wanted to test whether mammalian cells are able to move on uncoated PA hydrogels as well. To this end, cell migration assays with T cells using the different experimental setups shown in Fig 3.1 were carried out. The T cells were isolated from mice and kindly provided by Sheetal Kaw (Fackler Lab). Like ookinetes, T cells did not adhere to uncoated 2D PA substrates, but they moved well in the sandwich setup. In a 10 min movie, 20-40% of cells left their starting point (Fig 3.7). The other cells probed their environment without moving away. Motile

cells were moving at an average of 10 µm/min. The fraction of motile cells and speed did not depend on substrate stiffness. As elastic PA hydrogels can be used to perform TFM, these results show that force measurements of moving T cells are possible. However, due to their reduced speed as compared to sporozoites, longer periods of imaging are necessary which resulted in focus drift during this study. To allow for high quality imaging data, refocusing during imaging is therefore required.

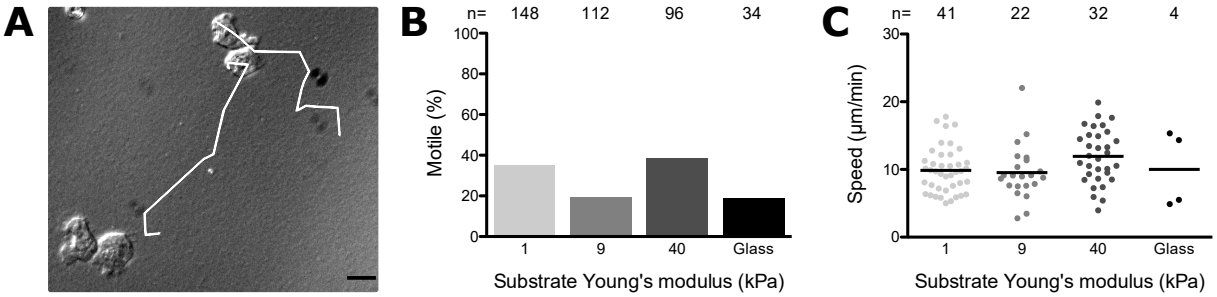

Figure 3.7: T cell migration in 3D hydrogel sandwiches.
(**A**) DIC image showing motile and stationary T cells confined between two hydrogel substrates. White trajectories indicate the migration path of motile T cells over a period of 10 min. Scale bar, 10 µm. Percentage (**B**) and speed (**C**) of motile T cells. Numbers above indicate the number of analyzed T cells. Preliminary data.

3.2 *Plasmodium* force transmission

To measure forces exerted onto the substrate during migration, I performed TFM of sporozoites and ookinetes on 9 kPa PA hydrogels. Sporozoites moved and transmitted forces on 2D PA hydrogels (Kratzer, 2016), whereas ookinetes only moved if sandwiched between two PA hydrogels. Bead displacements were by about an order of magnitude larger for ookinetes as compared to sporozoites (Fig 3.8). While maximum bead displacements were around 0.04 µm when sporozoites were moving over the hydrogels, ookinete caused deformations of up to 0.24 µm. Ookinetes moving in circles could not be analyzed, as a reference image is needed to calculate bead displacements (for sporozoites the average intensity over time or the parasite being at the opposite side of the circle was used as reference image). Therefore, ookinetes moving straight are shown here. Traction forces could only be calculated for sporozoites, since the software we used is not capable of calculating traction forces from cells moving within a 3D

environment (Probst, 2018). To allow for TFM measurements of ookinetes moving in circular trajectories as well, I tried to establish reference free TFM (Bergert et al., 2016). This method does not require a reference image as quantum dot nanodiscs are printed onto the silicone substrate in a regular pattern. The substrates with an elastic modulus of about 12.6 kPa were kindly provided by Tobias Lendenmann. Ookinetes moved well if sandwiched between the substrate and a glass coverslip. However, I could not observe any displacements of the quantum dot nanodiscs when the ookinetes moved over the substrate.

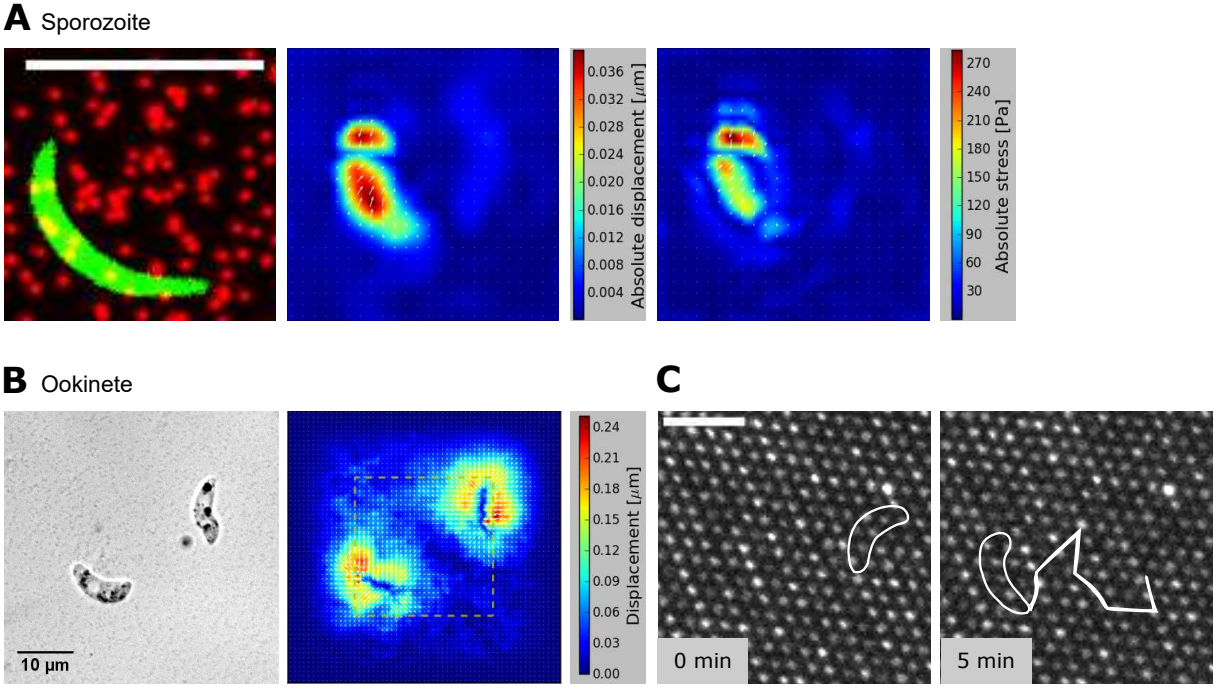

Figure 3.8: Traction force microscopy of motile *Plasmodium* parasites.
(**A**) Left: A sporozoite (depicted in green) on a PA hydrogel with embedded marker beads (shown in red). Scale bar, 10 µm. Middle: Displacement map of marker beads. Right: Traction forces calculated from bead displacements using a software developed by Probst (2018). Modified from Kratzer (2016). (**B**) Left: DIC image showing ookinetes confined between two PA hydrogels. Right: Displacement map of marker beads. (**C**) An ookinete (white outline) moving on an rfTFM substrate at indicated timepoints. A regular pattern of quantum dot nanodiscs can be seen as white dots. This pattern does not change upon movement of the ookinete (white track seen in the right image represents the migration path of the ookinete within 5 min). Scale bar, 10 µm.

3.3 The role of myosin A in gliding motility and force transmission

To understand how single amino acid residues contribute to the function of the molecular motor MyoA, I aimed at generating parasite lines expressing mutated versions of the protein. As MyoA is essential in blood stages (Bushell et al., 2017; Robert-Paganin et al., 2019), the stages which are used to perform gene editing in *P. berghei*, mutagenesis of *myoA* might affect the fitness of the parasites. In case the mutations have a severe impact on merozoite invasion, this might result in difficulties to obtain mutant parasites. However, conditional mutagenesis of *myoA* would prevent these difficulties.

3.3.1 Expression of *myoA* under blood stage-specific promoters is lethal for *P. berghei* parasites

I first aimed at setting up a system which allows for stage-specific mutagenesis of *myoA*. This would allow to study the effect of point mutations in MyoA in mosquito stages but not interfere with MyoA function in blood stages. The idea was to express wt MyoA in blood stages and insert a second copy of *myoA* containing the mutation and being expressed in ookinetes and sporozoites (Fig 3.9 A). Blood stage-specific promoters were needed to express wt MyoA in blood stages but not in ookinetes and sporozoites. To find a suitable promoter, I compared RNA sequencing data of candidate genes in different stages (Otto et al., 2014). As there is no RNA sequencing data for *P. berghei* sporozoites, I analyzed the expression of the *P. falciparum* orthologues of these proteins (Hoffmann, PlasmoDB). Promising candidates were CLAG, CLAG9, MSP9 and MSP10 (Fig 3.9 B). All of these proteins are expressed in schizonts, the blood stage in which merozoites are formed and thus MyoA is needed but RNA levels are very low in ookinetes and sporozoites. The ama1 promoter was used as a positive control since a conditional knockout of MyoA expressed under this promoter has already been published (Siden-Kiamos et al., 2011). However, the ama1 promoter was not suitable for our studies as AMA1 is expressed in sporozoites. As we do not know, which genomic region exactly contains the regulatory elements necessary for gene transcription defined as promoter, we amplified about 1.6 kb upstream of the

clag, *clag9*, *msp9* and *msp10* gene using the primers listed in Table 2.6.

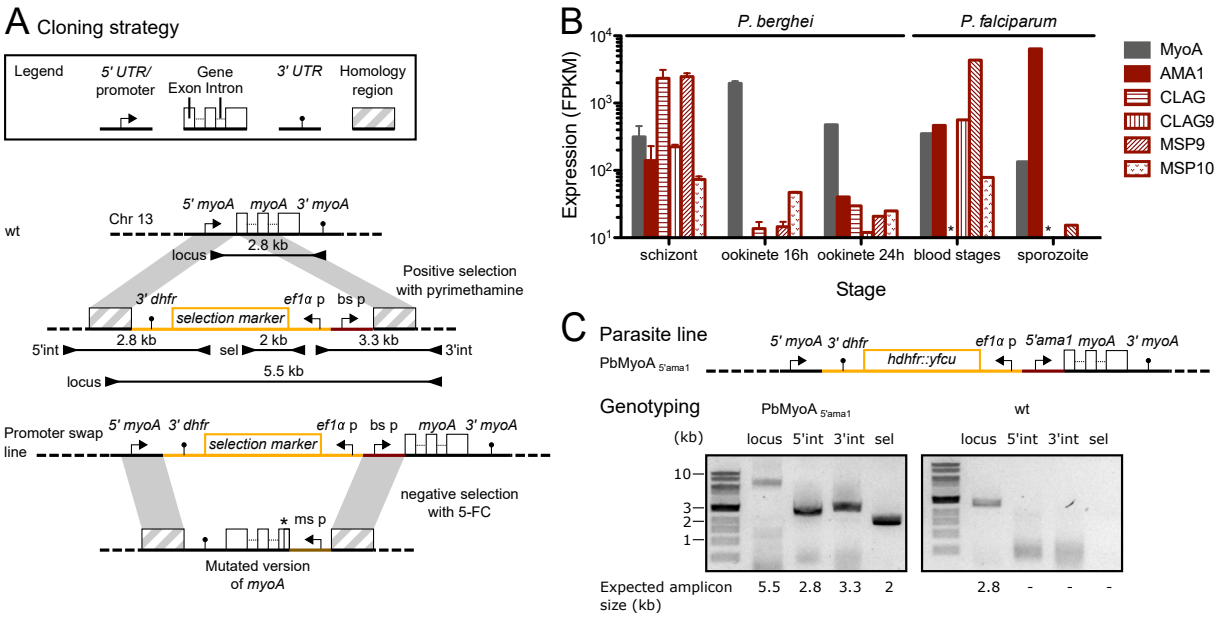

Figure 3.9: Generation of MyoA promoter swap parasite lines.
(**A**) Scheme of cloning strategy to generate parasite lines that express wt MyoA in blood stages and mutated MyoA in mosquito stages. In a first step, a selection cassette and a blood stage specific promoter (bs p) is inserted upstream of *myoA* via double-crossover recombination using pyrimethamine for selection of transfected parasites. Shown below are the PCR fragments amplified via PCR to test for successful integration, the primer binding site and the amplicon size. Indicated in grey are the homology regions. In a second step, the clonal promoter swap line should be used to replace the selection marker by a mutated version of *myoA* expressed under a mosquito stage specific promoter (ms p) using 5-FC for selection. Note that the scheme is not drawn to scale. (**B**) Expression profile of candidate genes that are expressed in blood stages but not mosquito stages (Otto et al., 2014). Sporozoite data is from *P. falciparum* orthologues of these proteins, as there is no *P. berghei* data available for this stage (Hoffmann, PlasmoDB). Stars indicate that there is no orthologue in *P. falciparum* for the respective gene. The 5'UTRs of these genes might serve as blood stage specific promoters to generate the promoter swap parasite lines depicted in (**A**). The ama1 promoter is used as a positive control, as it has been used before to perform a promoter swap in the *myoA* locus (Siden-Kiamos et al., 2011). (**C**) *MyoA* locus of the only promoter swap parasite line that was successfully transfected. Correct integration was shown via genotyping PCR. Given below are the expected sizes of the amplicons.

Generation of promoter swap mutants In order to generate parasites expressing *myoA* under a blood stage-specific promoter, I tried to integrate the 5'UTRs of *clag*, *clag9*, *msp9* and *msp10* upstream of *myoA* via double crossover homologous recombination (Fig 3.9 A). The region upstream of *myoA* and the myoA open reading frame (ORF) served as homology regions. Cloning was performed using the primers and restriction enzymes listed in Table 2.6. To be able to integrate a second mutated copy of *myoA* in a next cloning step, I used a selection marker which also allows for negative selection. After transfection, I tested for parasites that integrated the construct

via genotyping PCR using the primers depicted in Fig 3.9 A. I amplified the whole locus, which should give us a small fragment for wt parasites and a large fragment for successfully transfected parasites. Integration of the construct into the correct position was tested using primers binding upstream of the modified locus as well as within the construct (5' integration) and primers binding downstream of the modified locus as well as within the construct (3' integration). I amplified the selection marker as well to test whether the parasites had taken up the DNA in case there was no integration indicating that the transfection was successful but integration of the DNA is lethal for the parasites.

Parasites expressing *myoa* under the ama1 promoter were successfully generated. (Fig 3.9 C). However, none of the other promoter swaps yielded viable parasites. Either the mice stayed negative after transfection, or there was only a PCR product for the wt locus and the selection marker, suggesting uptake of the DNA by the parasites but not integration. As I was not able to get viable parasites expressing wt MyoA only in blood stages, I next tried to use conventional cloning strategies to replace *myoA* by a mutated version.

3.3.2 Exchange of *3'myoA* leads to a defect in salivary gland invasion of *P. berghei* sporozoites

To establish a system that allows for site-directed mutagenesis of *myoA* (Gene ID: PBANKA_1355700) using conventional editing techniques, I had to insert a selection marker into the *myoA* locus. *MyoA* contains two short introns at the beginning. It shares its 3'UTR with the neighboring gene, a putative DNA-directed RNA polymerase I, II, and III subunit RPABC4 (Gene ID: PBANKA_1355800), which is essential in blood stages (PlasmoGEM database, Schwach et al. (2015); Gomes et al. (2015)). The distance between both genes is about 600 bp. For conventional gene editing, the 3'UTR of *myoA* was replaced by *3'dhfs* to allow for integration of the selection marker (Fig 3.10 A).

Generation of mutant parasite lines using conventional gene editing To generate parsite lines carrying mutations in *myoA*, I aimed at replacing the endogenous *myoA*

by a mutated version of *myoA*. However, if there is only a single point mutation in the gene, alternative recombination events might lead to mutant parasites that integrated the selection cassette but do not carry the mutation (Section 1.2.2). To prevent this, a codon modified version of *myoA* which is composed of a different DNA sequence but still encodes the same amino acid sequence can be used for integration. To exclude a phenotype due to the codon modification or integration of the construct, I first generated control parasite lines. I used double crossover homologous recombination to generate mutant parasites lines (Fig 3.10 A). The genomic regions upstream and downstream of *myoA* were used as homology region. To increase the transfection efficiency, I used long homology regions of about 1.5 kb (upstream of *myoA*) and 0.9 kb (downstream of *myoA*). First, I made parasite lines still containing the original *myoA* gene but *3'dhfs* instead of *3'myoA* and the selection cassette downstream (parasite line PbMyoA$_{3'dhfs}^{+i}$). Additionally, I wanted to test, whether deletion of the introns has any effect on the parasites. Therefore, I used the same cloning strategy to replace *myoA* by its transcript that lacks the introns (parasite line PbMyoA$_{3'dhfs}^{-i}$). I amplified the transcript from cDNA kindly provided by Benjamin Spreng. Furthermore, I GFP-tagged the protein C-terminally to have the possibility to test an effect of the mutations on the localization of the protein.

MyoA has been c-terminally tagged with GFP using single crossover homologous recombination before (Green et al., 2017). Here I used the same cloning strategy as with the PbMyoA$_{3'dhfs}$ parasite lines. With this strategy alternative recombination events might lead to parasites still containing introns (Fig 3.10 A, depicted in light grey). To find out whether the introns were missing in the clonal lines, I amplified the *myoA* gene and sequenced the PCR product. The sequencing results showed that three out of four clonal lines lacked the introns (parasite line PbMyoA$_{3'dhfs}^{-i}$ GFP), while one clonal line still contained the introns within the *myoA* gene (parasite line PbMyoA$_{3'dhfs}^{+i}$ GFP).

To also investigate whether PfMyoA can complement the function of PbMyoA, I replaced the endogenous *myoA* with a codon-modified version of PfmyoA that has been used to recombinantly express the protein (Bookwalter et al., 2017). This yielded the parasite line PfMyoA$_{3'dhfs\ cm}^{-i}$.

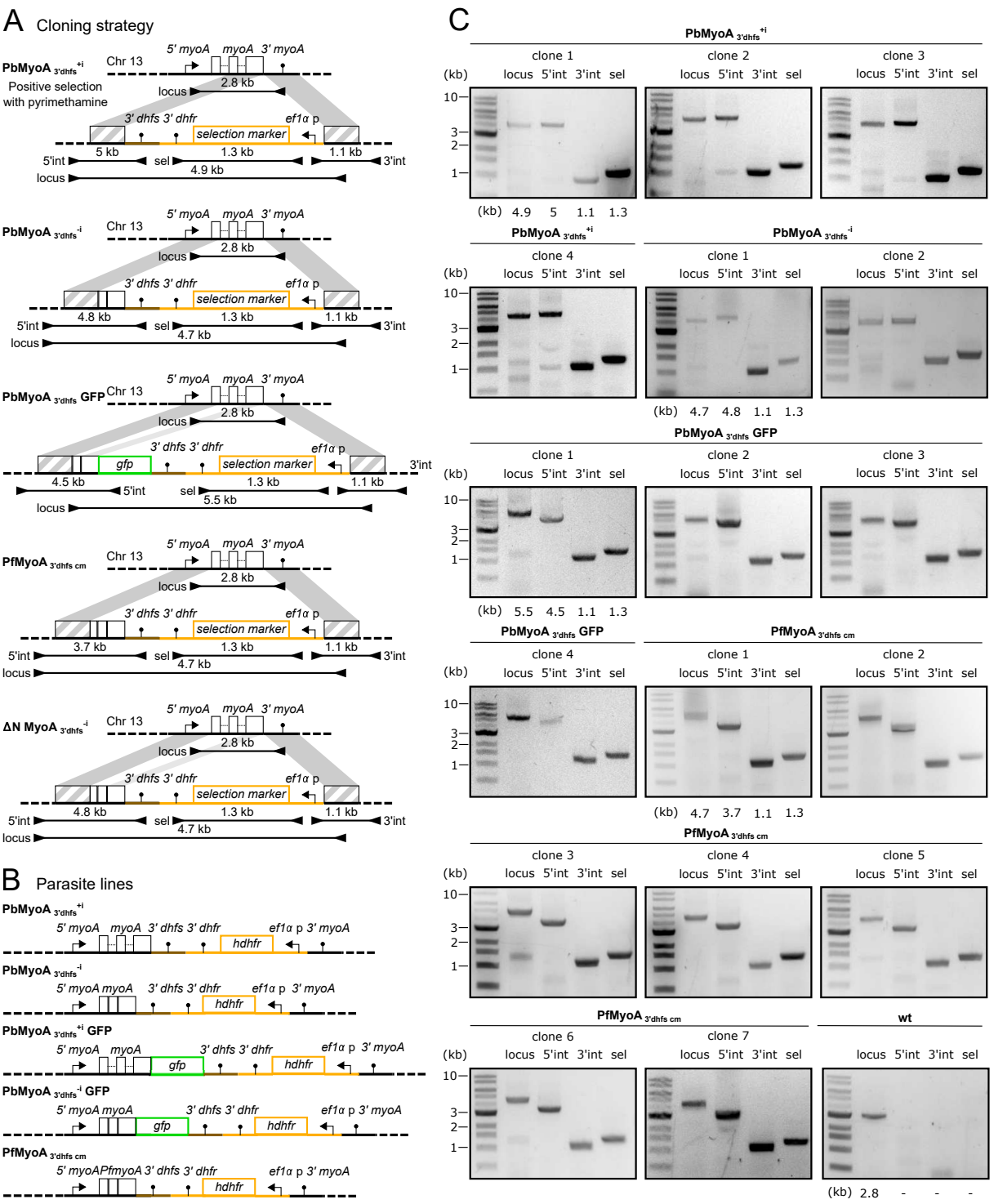

Figure 3.10: Generation of PbMyoA$_{3'dhfs}^{+i}$, PbMyoA$_{3'dhfs}^{-i}$, PbMyoA$_{3'dhfs}^{+i}$ GFP, PbMyoA$_{3'dhfs}^{-i}$ GFP and PfMyoA$_{3'dhfs\ cm}^{-i}$ parasite lines.
(**A**) Scheme of cloning strategy to test whether *myoA* can be mutated by conventional gene editing. Either, a selection cassette is integrated downstream of *myoA* and *3'myoA* replaced by *3'dhfs* or *myoA* is additionally replaced by its transcript which leads to deletion of the introns. Additionally, *myoA* is replaced by a GFP-tagged version of its transcript. Alternative recombination events that occured are depicted in light grey. Furthermore, *myoA* is replaced by a codon-modified (cm) version of PfmyoA. Using the same replacement strategy, the N-terminus of MyoA should be deleted. Shown below are the amplified PCR fragments to test for successful integration, the primer binding site and the amplicon size. Indicated in grey are the homology regions. All parasite lines should be obtained by positive selection using pyrimethamine. Note that the scheme is not drawn to scale. (**B**) *MyoA* locus of all parasite lines that were generated successfully using the cloning strategy depicted in (**A**). (**C**) Correct integration was shown via genotyping PCR. Given below are the expected sizes of the amplicons.

To test, whether the parasites integrated the construct into the *myoA* locus after transfection and to exclude that there were still wt parasites in the population, I performed a genotyping PCR on all transfected parasite lines. To this end, I used primers flanking the modified *myoA* locus as indicated in Fig 3.10 A. This should yield larger fragments for successfully modified parasite lines than for wt parasites. To verify that the construct was integrated into the *myoA* locus and not anywhere else in the genome, I used primers binding upstream (5' integration) or downstream (3' integration) of the modified locus together with primers binding in the construct, which should be integrated by the parasites. The presence of the selection marker was tested as well using the appropriate primer pair. I successfully transfected *P. berghei* parasites and received clonal lines that lacked the wt locus for all constructs after limiting dilutions as confirmed by PCR (Fig 3.10 B, C).

Phenotypic analysis of mutant parasite lines Imaging of PbMyoA$_{3'dhfs}$ GFP parasites revealed that the localization of MyoA was peripheral as expected in the motile stages (Fig 3.11). The results are in line with previous findings (Green et al., 2017).

To test, whether the clonal lines proceed through the life cycle, a prerequisite if the cloning strategy depicted in Fig 3.10 A should be used for site-directed mutagenesis, I analyzed all life cycle stages (Fig 3.12, Table 3.1).

Table 3.1: Life cycle progression of generated parasite lines (shown is the mean of at least two independent cage feeds ±standard deviation (except preliminary data from only one experiment for line PbMyoA$_{3'dhfs}^{+i}$ GFP), n indicates the number of mosquitoes that were investigated, the number of sporozoites were determined in the mosquitoes midgut (MG), hemolymph (HL) and salivary glands (SG) and normalized to one infected (inf) mosquito)

Parasite line	Infection rate [%] (n)	MG sporozoites/ inf mosquito (n)	HL sporozoites/ inf mosquito (n)	SG sporozoites/ inf mosquito (n)
wt	80 ± 10 (85)	76000 ± 42000 (90)	3000 ± 100 (37)	20000 ± 14000 (50)
PbMyoA$_{3'dhfs}^{+i}$	70 ± 20 (65)	76000 ± 45000 (66)	5000 ± 700 (36)	1100 ± 1200 (30)
PbMyoA$_{3'dhfs}^{-i}$	50 ± 20 (62)	91000 ± 25000 (57)	7700 ± 5200 (25)	400 ± 300 (29)
PbMyoA$_{3'dhfs}^{+i}$ GFP	90 (16)	180000 (11)	8600 (22)	100 (10)
PbMyoA$_{3'dhfs}^{-i}$ GFP	80 ± 20 (99)	65000 ± 28000 (48)	not determined	100 ± 100 (47)
PfMyoA$_{3'dhfs}^{-i}$ cm	50 ± 20 (58)	7500 ± 6400 (60)	not determined	600 ± 300 (56)

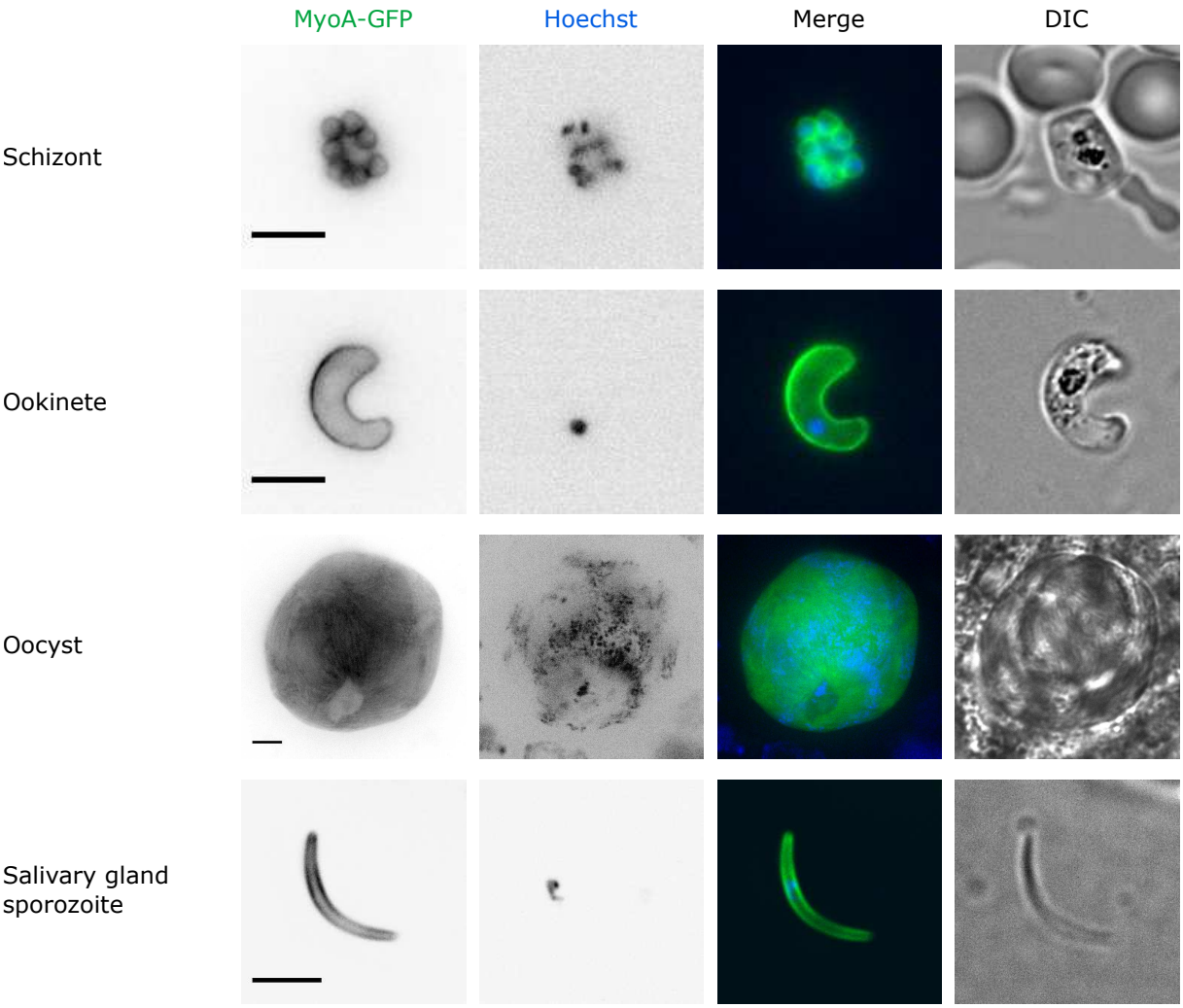

Figure 3.11: Localization of MyoA in motile *Plasmodium* stages.
Life cell imaging of PbMyoA$_{3'dhfs}$ GFP parasites reveals peripheral localization of MyoA in schizonts, ookinetes, day 11 oocyst containing developing sporozoites and salivary gland sporozoites. Nuclei were stained with Hoechst. Scale bar, 5 µm.

The mutant parasite lines formed normal numbers of oocysts. Sporozoite numbers within these oocysts were similar to wt. However, sporozoite numbers were largely reduced in the mosquito salivary glands to less than 1000, whereas the number of hemolymph sporozoites was enhanced compared to wt, suggesting a defect in salivary gland invasion. PbMyoA$_{3'dhfs}^{-i}$, PbMyoA$_{3'dhfs}^{+i}$ GFP and PbMyoA$_{3'dhfs}^{-i}$ GFP parasites showed the same phenotype, implicating that the integration of a different 3'UTR and the selection marker downstream of *myoA* might be the cause for the mutant phenotype.

The fitness of PfMyoA parasites on the other hand was reduced in all stages of the life cycle where motility is important. Growth rate in blood stages was reduced drastically

from 9 fold per day in wt to 6 fold per day in the transgenic parasite line. Oocyst numbers were reduced as well from an average of about 100 to less than 20. Midgut and salivary gland sporozoites were also much lower compared to wt. Yet it was surprising, that the ratio of salivary gland to midgut sporozoites was similar to wt and much higher than in the mutant lines described before although the same 3'UTR and selection marker was integrated downstream of *myoA* in the PfMyoA parasites.

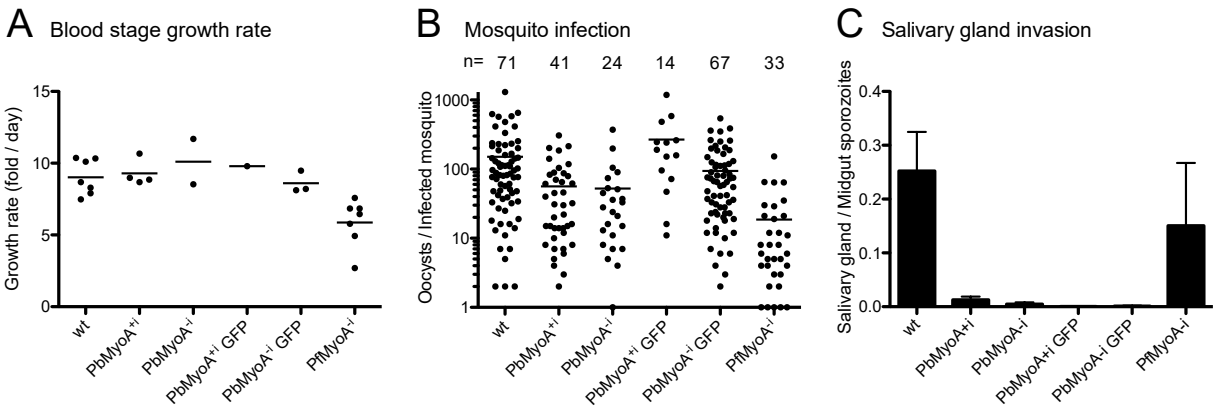

Figure 3.12: Exchange of *3'myoA* by *3'dhfs* results in a salivary gland invasion defect.
(**A**) Blood stage growth rate of clonal parasite lines. A single parasite was injected i.v. into a mouse and the growth rate calculated from parasitemia at day 7-9. The growth rate of wt parasites is taken from Douglas et al. (2018a) as I only received correct clones with conventional gene editing. (**B**) Number of oocysts per infected mosquito. Numbers above indicate the number of mosquitoes that were analyzed. (**C**) Ratio of salivary gland to midgut sporozoites.

A possible explanation for the defect in salivary gland invasion of the generated parasite lines might be reduced motility of hemolymph sporozoites. To find out, whether gliding is impaired in hemolymph sporozoites of these parasite lines, I performed cell migration assays with isolated sporozoites on glass. Indeed, the number of motile hemolymph sporozoites was reduced in the investigated parasite lines (Fig 3.13 A). I hypothesized, that a difference in RNA levels of *myoA* or its neighbor gene might affect protein abundance and lead to the motility defect of hemolymph sporozoites in the PbMyoA$_{3'dhfs}^{+i}$, PbMyoA$_{3'dhfs}^{-i}$, PbMyoA$_{3'dhfs}^{+i}$ GFP and PbMyoA$_{3'dhfs}^{-i}$ GFP parasite lines. To test, whether stabilization of actin filaments by Jas and thus elongation of actin filaments can compensate for reduced *myoA* expression and thus rescue the gliding defect of hemolymph sporozoites, I treated PbMyoA$_{3'dhfs}$ sporozoites with a low concentration of Jas and analyzed their movement on glass. However, 50 nM Jas did not

improve gliding of PbMyoA$_{3'dhfs}$ hemolymph sporozoites (Fig 3.13 B).

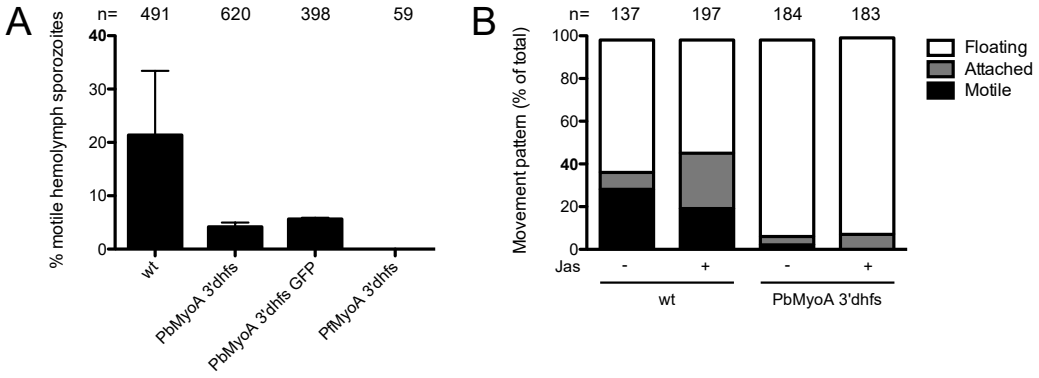

Figure 3.13: Exchange of *3'myoA* by *3'dhfs* leads to reduced migration capacity of hemolymph sporozoites.
(**A**) Fraction of motile hemolymph sporozoites. Bars represent the mean and error bars the standard deviation of at least two independent biological replicates. Numbers above indicate the number of sporozoites that were analyzed. Note that the number of analyzed sporozoites in the PfMyoA$_{3'dhfs}$ parasite line was low due to generally low numbers of hemolymph sporozoites within this line. (**B**) Movement patterns of hemolymph sporozoites in the absence (-) or presence (+) of 50 nM Jas. Preliminary data from a single experiment.

The role of the N-terminal extension of MyoA Although the integration of a selection marker which is required for conventional gene editing of *Plasmodium* parasites results in a block of salivary gland invasion, I aimed at deleting the N-terminal extension of MyoA to examine whether it plays a role in merozoite invasion of erythrocytes or ookinete gliding. I used the construct shown before (Fig 3.10 A) to replace the gene by a version lacking the N-terminal extension ($\triangle$N MyoA). In two attempts (with or without introns), I was not able to receive $\triangle$N MyoA parasites. Instead, I only yielded parasites that used alternative recombination to integrate only the selection marker. This suggests, that deletion of the N-terminus is lethal for the parasites.

Next, I tried to use genetic engineering methods that do not lead to genetic alterations except the modification of interest to study an effect of site-directed mutagenesis on MyoA function in sporozoites. I decided to adapt CRISPR/Cas9-mediated gene editing for *P. berghei*. Alternatively, I tried to use the Gene Insertion/ Marker Out approach (Lin et al., 2011) to delete the N-terminus of MyoA or mutate single amino acid residues without changing any gene regulatory elements. To this end, I used the ama1 promoter swap mutant described in Section 3.3.1 as a recipient line.

3.3.3 Site-directed mutagenesis of *myoA*

CRISPR/Cas9-mediated mutagenesis of *myoA* The CRISPR/Cas9 system allows for site-directed mutagenesis of a target gene without altering gene regulatory elements. However, the method is published for *P. falciparum* and *P. yoelli* but not *P. berghei* (Ghorbal et al., 2014; Lee and Fidock, 2014; Wagner et al., 2014; Zhang et al., 2014, 2017; Lee et al., 2019)). To introduce mutations into MyoA or its light chain MTIP, I used the plasmid designed for *P. falciparum* (Lee and Fidock, 2014) and exchanged all promoters as well as 3'UTRs by *P. berghei* sequences. The plasmid contains the Cas9 from *Streptococcus pyogenes*, a gRNA expression cassette under the U6 small nuclear RNA (snRNA) promoter and a donor template which is used by the parasites to repair the double strand break introduced by Cas9 (Fig 3.14).

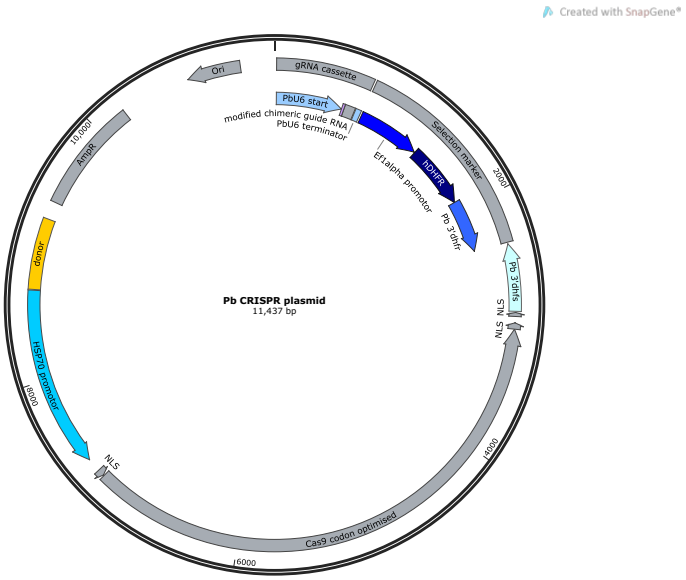

Figure 3.14: Vector map for CRISPR/Cas9-mediated site-directed mutagenesis in *P. berghei*. The plasmid was taken from Lee and Fidock (2014) and modified to contain gene regulatory elements of *P. berghei*. It contains a gRNA expression cassette, positive selection marker, Cas9 and donor template. Arrows indicate the direction of promoter activity and gene orientation. The vector map was created using SnapGene.

As a proof of principle, I planned the mutagenesis of the amino acids shown in Table 3.2 via CRISPR/Cas9. I designed gRNAs with a length of 20 bp binding in close proximity to the desired mutation sites (Table 3.3). The efficiency score is a value between 0 and 1 which predicts gRNA activity (Doench et al., 2014). The higher the value, the bigger the chance that the gRNA is active. To establish the CRISPR/Cas9 system, silent mutations were tried to be introduced first as these should not have an effect on parasite fitness. Since the efficiency of different gRNAs varies a lot and can still not be perfectly predicted (Doench et al., 2014), four gRNAs targeting different regions in the *myoA* or

mtip gene were tested. With the help of Jessica Kehrer, I transfected all plasmids but we did not receive parasites with mutations in *myoA* or *mtip*. Reasons might be that gRNAs or Cas9 were not expressed successfully or that the gRNAs were not active. Therefore, further work is required to establish the CRISPR/Cas9 technology in our lab.

Table 3.2: Mutations

Mutation site	Original codon	Mutation	Mutated codon	Silent mutation
MyoA E6	GAG	Arginine	AGA	GAA
MyoA S19	TCA	Alanine (phosphodeficient)	GCA	TCT
		Aspartic acid or		
		Glutamic acid (phosphomimetic)		
MyoA K764	AAA	Glutamic acid	GAA	AAG
MTIP S108	AGT	Glutamic acid	GAA	TCT

Table 3.3: gRNA design

Mutation site	gRNA sequence with PAM	Efficiency score	Distance from mutation site
MyoA E6	AAAAATGGCTGTTACAAATGAGG	0.45	0 bp
MyoA S19	TAAAAGTGGAGTAGTCTTTAAGG	0.45	19 bp
MyoA K764	AAAGAGAAAAACTTGTAGAATGG	0.4	18 bp
MTIP S108	CTTACAATGCTAGAAGATTAGGG	0.45	12 bp

Mutagenesis of *myoA* using the Gene Insertion/Marker Out strategy Another cloning strategy which allows for gene editing without interfering with regulatory elements is the Gene Insertion/Marker Out (GIMO) strategy (Lin et al., 2011). I planned to use the ama1 promoter swap line (clone 2) described in Section 3.3.1 to replace the selection marker and ama1 promoter by a mutated version of *myoA* (Fig 3.15 A). As homology regions I used the region upstream of *myoA* and the *myoA* ORF. To prevent alternative recombination events, the region between the left homology arm and the mutation site was codon modified. This cloning strategy results in selection marker free parasite lines.

All constructs for site-directed mutagenesis of *myoA* using the GIMO strategy were

cloned by Xanthoula Smyrnakou under my supervision (Smyrnakou, 2019). Transfections and generation of clonal lines were partially carried out by Xanthoula Smyrnakou as well. Parasite lines carrying point mutations in the N-terminal extension were generated successfully, however the efficiency with the GIMO strategy was low (Fig 3.15 B). As with conventional gene editing, no ∆N MyoA parasites appeared after transfection, supporting an essential role of the MyoA N-terminus in merozoites. Proper integration and successful mutation of *myoA* was verified via PCR and sequencing (Fig 3.15 C).

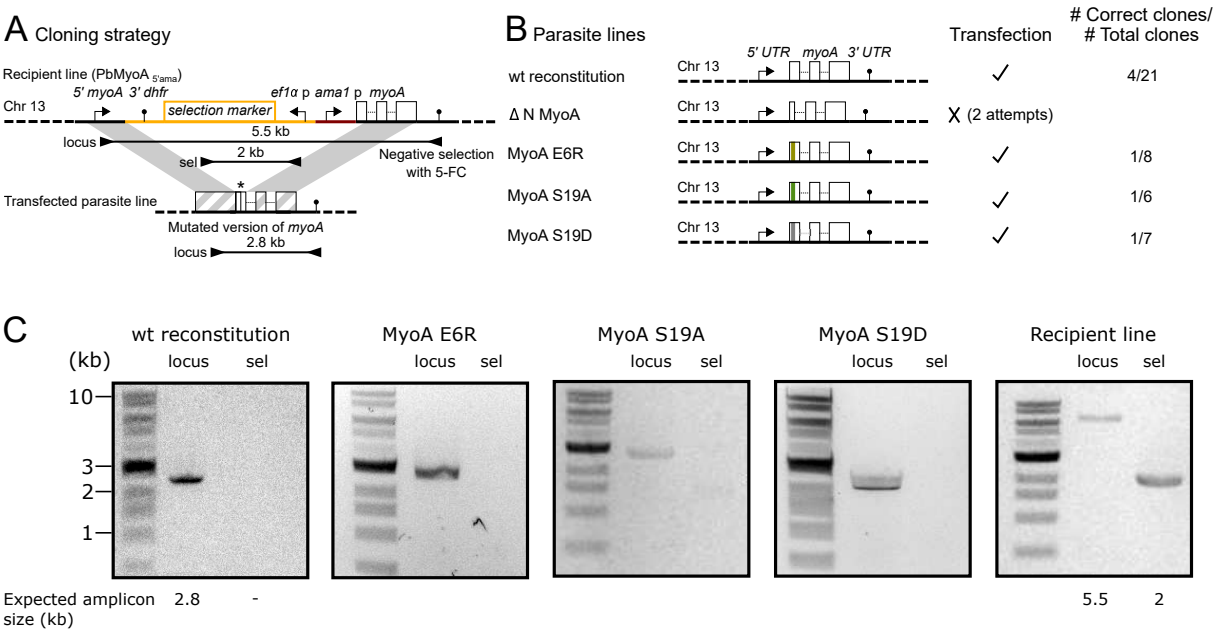

Figure 3.15: Generation of mutant MyoA parasite lines.
(**A**) Scheme of cloning strategy to introduce point mutations into MyoA while not interfering with gene regulatory elements. Shown below are the PCR fragments amplified via PCR to test for successful integration, the primer binding site and the amplicon size. Indicated in grey are the homology regions. All parasite lines should be obtained by negative selection using 5-FC. Note that the scheme is not drawn to scale. (**B**) Parasite lines that I tried to generate using the cloning strategy shown in (**A**) and cloning efficiency. (**C**) Correct integration was shown via genotyping PCR. Given below are the expected sizes of the amplicons.

3.3.4 Modulation of the myosin motor affects sporozoite motility

Structural studies showed that the N-terminal extension of MyoA is important for force production of the motor as it harbors amino acid residues that form stabilizing interactions to allow for the transition into the rigor-like state (Robert-Paganin et al., 2019). We therefore hypothesized, that disruption of these interactions via mutagenesis would

affect the kinetic properties of MyoA and thereby influence its function in the parasite. Glutamic acid 6 interacts with arginine 241 and phenylalanine 476 from switch I and II, while phosphorylated serine 19 interacts with lysine 764 in the converter (Fig 3.16 A). I introduced a reverse charge at position 6 by changing glutamic acid into arginine (Fig 3.16 B). Furthermore, I changed serine 19 into alanine to prevent phosphorylation of this residue. Additionally, I tried to mimic the phosphorylated state of S19 by changing it into aspartic acid. The resulting MyoA versions are depicted in Fig 3.16 C.

To test the importance of the respective amino acid residues for the living organism, the parasite lines expressing mutated versions of MyoA were analysed for life cycle progression (Fig 3.16, Table 3.4). The asexual growth rate was similar to the recipient line for all mutants except the MyoA S19D parasite line indicating that erythrocyte invasion was not affected by the E6R or S19A mutation (Fig 3.16 D). The phosphomimetic mutation might have a slightly reduced growth rate, however the mice were 5-FC treated (the mice infected with the other parasite lines received drinking water not containing the drug) which might result in slower parasite growth. Therefore, a possible effect of this mutation on parasite growth needs to be further confirmed by injecting a defined number of parasites i.v. and monitoring parasitemia. As expected from previously published results (Siden-Kiamos et al., 2011), depletion of *myoA* in the ookinete stage by a promoter swap resulted in a complete block of mosquito infection in the recipient line (Table 3.4). With an average of 100-200 oocysts per mosquito, the parasite lines possessing point mutations in MyoA on the other hand were similar infectious to mosquitoes as wt parasites indicating that there was no effect on ookinete midgut traversal (Fig 3.16 E). In order to find a possible effect of the point mutations on sporozoite egress from oocysts, hemolymph sporozoites were counted and normalized to the number of midgut sporozoites. The ratio of hemolymph to midgut sporozoites was on average between 0.05 and 0.07 in wt and all mutants except the phosphodeficient mutant MyoA S19A which showed a ratio of 0.1 meaning it had elevated numbers of hemolymph sporozoites (Fig 3.16 F). To test for salivary gland invasion, salivary gland derived sporozoites were counted and normalized to the number of midgut sporozoites. Salivary gland sporozoites were reduced ten-fold to a ratio of about 0.03 in the MyoA S19A parasite line, while the number of salivary gland sporozoites was comparable to

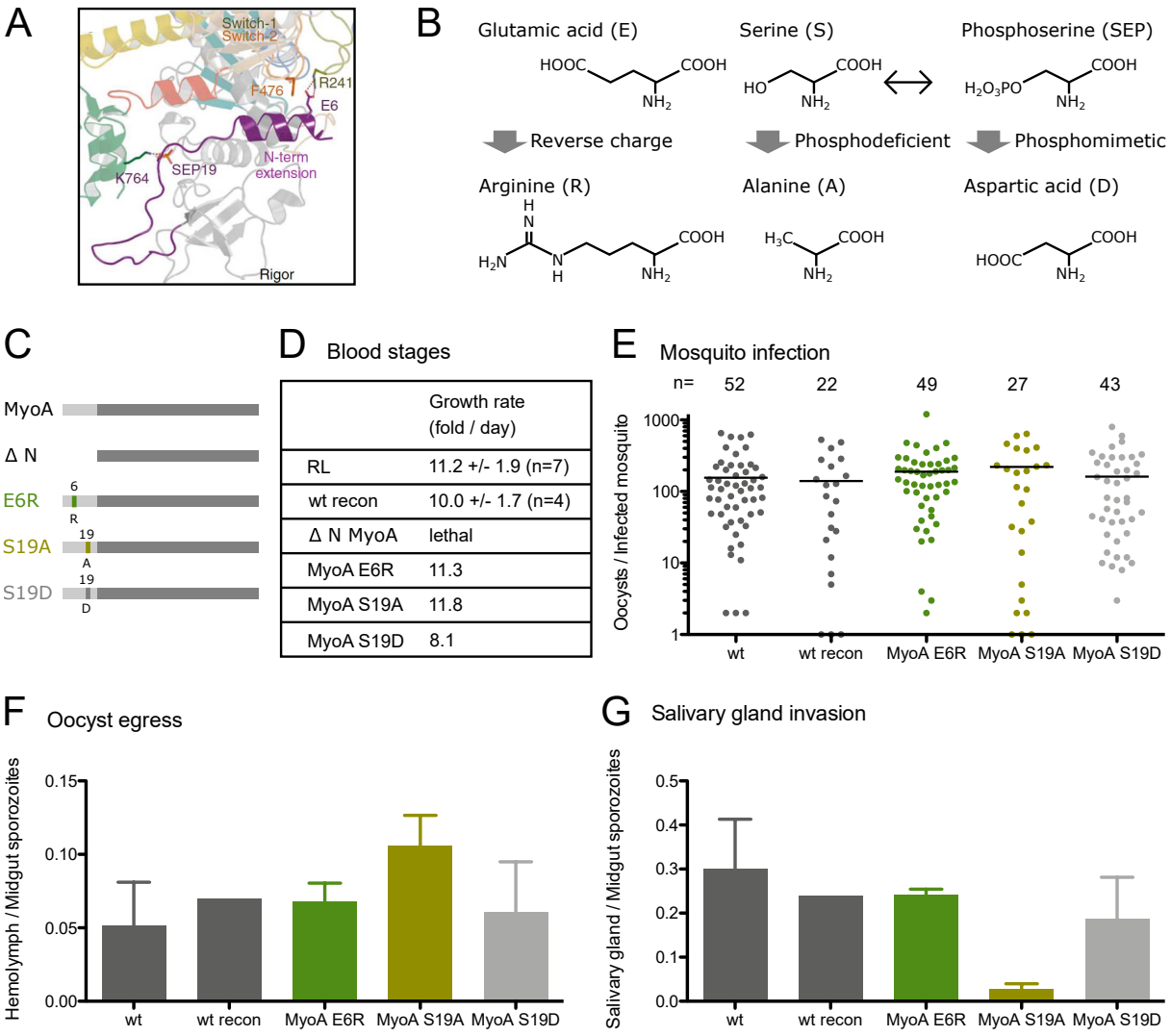

Figure 3.16: Phosphorylation of MyoA at serine 19 is important for salivary gland invasion of sporozoites.
(**A**) Zoom of the PfMyoA structure showing important amino acid interactions for stabilization of the rigor-like state that are thought to influence the kinetic properties of MyoA. The N-terminal extension is depicted in purple. It is located in proximity to Switch I (green) and the connectors Switch II (orange) and Relay (yellow). Phosphorylated serine 19 (SEP19) in the N-terminal extension interacts with lysine 764 (K764) in the converter and glutamic acid 6 (E6) in the N-terminal extension interacts with arginine 241 (R241) as well as phenylalanine 476 (F476) from switch I and II. Image taken from Robert-Paganin et al. (2019). The image is published under a Creative Commons Attribution 4.0 International License (http://creativecommons.org/licenses/by/4.0/). (**B**) Mutations to interrupt the interactions shown in (**A**). Glutamic acid 6 is exchanged by arginine to introduce a reverse charge. Serine 19 is either replaced by alanine to ablate phosphorylation or by aspartic acid to mimic the phosphorylated state. (**C**) Scheme of mutated MyoA versions that are expressed in clonal parasite lines. Either the complete N-terminal extension is depleted (19 amino acids) or point mutations within amino acids that are located in the N-terminal extension are introduced. (**D**) Blood stage growth rate of clonal parasite lines. A single parasite was injected i.v. into a mouse and the growth rate calculated from parasitemia at day 7-9. Note that MyoA S19D parasites were 5-FC selected which might have a negative impact on growth rate. (**E**) Number of oocysts per infected mosquito. Numbers above indicate the number of mosquitoes that were analyzed. Data from two independent cage feeds except preliminary data from a single cage feed for the wt reconstitution (recon). (**F**) Ratio of hemolymph to midgut sporozoites. (**G**) Ratio of salivary gland to midgut sporozoites.

Table 3.4: Life cycle progression of generated parasite lines (shown is the mean of at least two independent cage feeds ±standard deviation except for recipient line (RL) and wt reconstitution (recon) which were only analyzed once, n indicates the number of mosquitoes that were investigated, only infected mosquitoes were dissected to count sporozoites, the number of sporozoites were determined in the mosquitoes midgut (MG), hemolymph (HL) and salivary glands (SG) and normalized to one infected (inf) mosquito, n.a. not applicable)

Parasite line	Infection rate [%] (n)	MG sporozoites/ inf mosquito (n)	HL sporozoites/ inf mosquito (n)	SG sporozoites/ inf mosquito (n)
wt	80 ± 10 (85)	76000 ± 42000 (90)	3000 ± 100 (37)	20000 ± 14000 (50)
RL	0 (40)	n.a.	n.a.	n.a.
wt recon	60 (39)	56000 (38)	3600 (20)	14000 (18)
MyoA E6R	70 ± 20 (72)	76000 ± 12000 (66)	4600 ± 1400 (33)	21000 ± 1000 (33)
MyoA S19A	50 ± 20 (63)	130000 ± 90000 (54)	7400 ± 4600 (23)	5400 ± 500 (30)
MyoA S19D	90 ± 10 (50)	78000 ± 64000 (64)	4100 ± 2500 (29)	9400 ± 3300 (34)

wt in the other mutants (Fig 3.16 G).

I was further interested in the effect of the mutations on parasite motility. As we only saw an *in vivo* effect for sporozoites, we only used this stage for further characterization. Therefore, I isolated sporozoites of all generated parasite lines from hemolymph as well as salivary glands and analyzed their migratory capacity, speed and movement trajectories *in vitro*. The fraction of motile hemolymph sporozoites was drastically reduced from 30% to 3% in the MyoA S19A mutant (Fig 3.17 A). The MyoA S19D mutant showed a defect as well, albeit to a lower extent than the phosphodeficient mutant. The speed of hemolymph sporozoites for the wt reconstitution was reduced as compared to wt. This might be a clonal effect. However, only a single experiment was conducted for this line and differences could also be due to experimental variations. There was no obvious speed difference between the MyoA E6R mutant and the wt reconstitution. However, the speed of the phosphodeficient and phosphomimetic mutant were reduced from an average of about 1.1 µm/s to about 0.8 µm/s. Note that the low number of MyoA S19A sporozoites that were analyzed for speed is due to the reduced percentage of motile parasites. Next, I determined the migration capacity and speed of sporozoites derived from salivary glands. In line with former studies (Hegge et al., 2010; Sato et al., 2014), the gliding capacity generally increased in salivary gland sporozoites as compared to hemolymph sporozoites (Fig 3.17 B). The fraction of motile

salivary gland sporozoites was slightly reduced to an average of 50% for the MyoA E6R and MyoA S19A mutants whereas it was similar to wt for the MyoA S19D mutant with an average of 80%. The speed of MyoA E6R sporozoites was reduced from an average of about 1.9 µm/s to about 1.3 µm/s, while the speed of the phosphodeficient and phosphomimetic S19 mutant was reduced to about 1 µm/s. The trajectories were similar for all parasite lines (Fig 3.17).

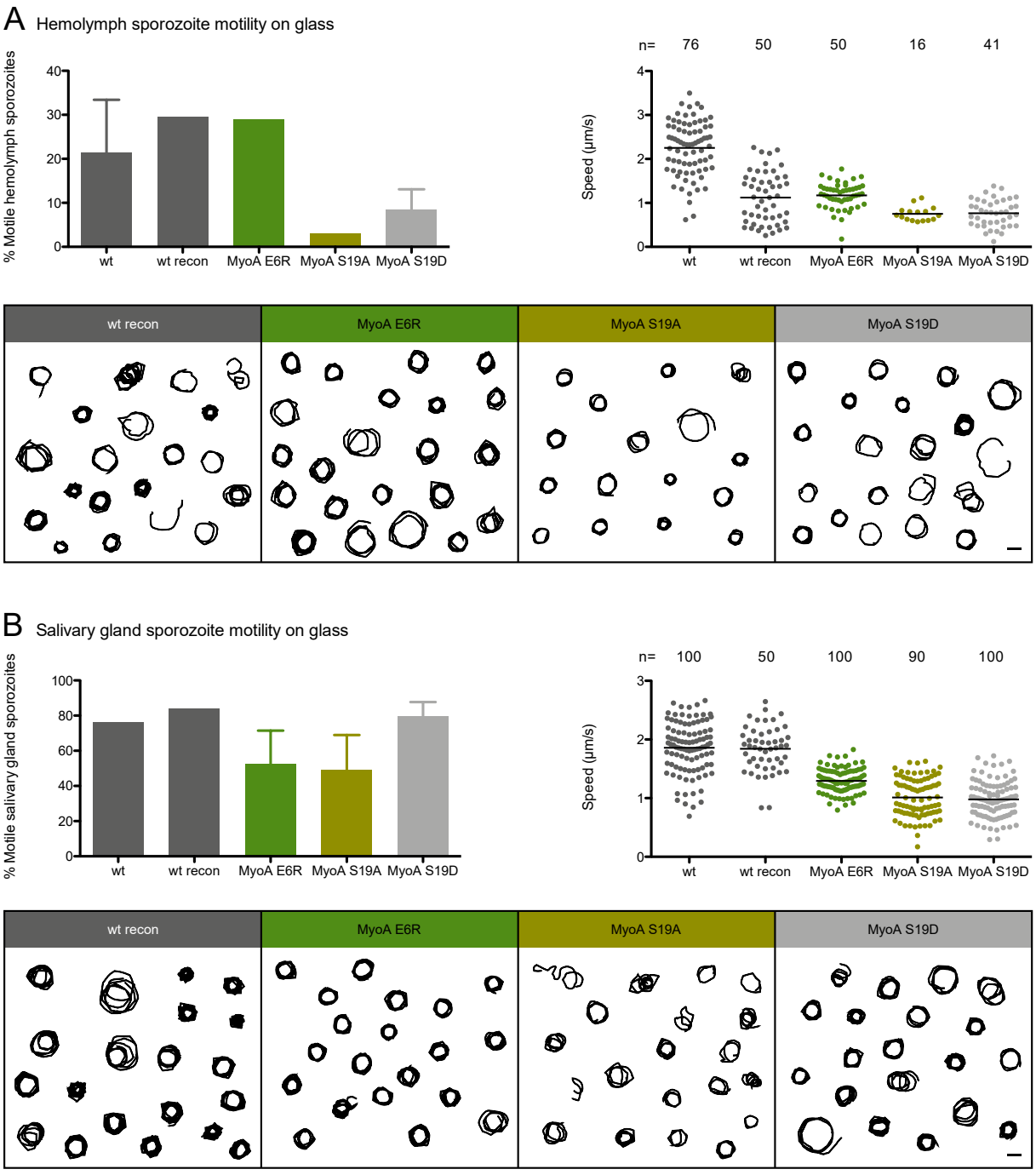

Figure 3.17: Changing MyoA kinetics affects sporozoite motility.
(**A**) Upper lane: Fraction of motile hemolymph sporozoites and their speed. Preliminary data. Lower lane: Trajectories of manually tracked hemolymph sporozoites. Scale bar, 10 µm. (**B**) Upper lane: Fraction of motile salivary gland sporozoites and their speed. Data from two independent experiments except preliminary data from a single experiment for wt and wt reconstitution (recon). Lower lane: Trajectories of manually tracked salivary gland sporozoites. Scale bar, 10 µm.

4 Discussion

Plasmodium parasites need to invade host cells and migrate across tissues at different stages throughout their life cycle to survive and establish an infection (Fig 4.1). In the process of evolution, diverse selective pressures act on the parasites. These involve immunological pressures as well as environmental conditions, for instance physical properties such as tissue elasticity and density. It is of great interest, which environmental cues allow the parasite to sense and respond to their environment. In this study, I used uncoated PA hydrogels to assess the role of substrate stiffness, confinement and pore size for ookinete and sporozoite adhesion and migration.

4.1 *Plasmodium* motility on elastic substrates

Former studies analyzed sporozoite motility on PEG gels of different stiffnesses as a function of ligand density (Perschmann et al., 2011; Hellmann et al., 2013). These experiments revealed that sporozoites move best on stiff substrates with intermediate ligand density. Here, I investigated the effect of small but possibly important elasticity differences which might be relevant as sporozoites encounter cells and tissues of different stiffnesses on their journey from the mosquito vector to the mammalian host. According to Tse and Engler (2010), hydrogels with elasticities of 1, 9 and 40 kPa were fabricated in order to mimic soft, medium and stiff tissues. In contrast to previous experiments (Hellmann et al., 2013), sporozoite speed on intermediate and stiff PA hydrogels was similar to glass and only decreased on soft 1 kPa hydrogels. Importantly, almost no sporozoites were moving consistently on soft hydrogels while the migratory capacity and consistency was significantly higher on hydrogels of intermediate and high stiffness. Interestingly, unpublished results of Jessica Kehrer reveal that sporozoites move well on confluent fibroblast monolayers, whereas there is reduced motility

on endothelial cell layers. Endothelial cells that line the interior of blood vessels are softer than dermal fibroblasts (Grady et al., 2016). We hypothesized, that the softness of endothelial cells limit the capacity of sporozoites to move (Fig 4.1). This mechanism might be relevant to avoid adhesion to blood vessels and ensure that the sporozoites reach the liver, where they are arrested by a combination of slower blood flow and highly sulphated proteoglycans that serve as receptors where the sporozoites can bind to (Pradel et al., 2002; Coppi et al., 2007; Tavares et al., 2013). To test, whether elasticity or the presence of different cell surface receptors cause the difference, one could treat the cultured cells with a compound that reduces the elastic modulus of fibroblasts or enhances the elastic modulus of endothelial cells and analyze whether this affects sporozoite motility. Latrunculin A is a cytoskeletal destabilizer which reduces the elastic modulus of fibroblasts (Rotsch and Radmacher, 2000) while not affecting sporozoite motility (Smyrnakou, 2019). Yet, we could not use this compound for the proposed experiments as it also affects the confluence of fibroblasts which has an impact on the capability of sporozoites to move on these cells. A possibility to enhance the elastic modulus of cells would be to treat them with paraformaldehyde (PFA) (Codan et al., 2013). However, this compound affects sporozoite adhesion and motility and even with multiple washing steps between treatment of cultured cells and cell migration assay we could not completely remove residual PFA. Therefore, we currently lack an experimental setup which allows us to study whether the elasticity differences between fibroblasts and endothelial cells account for the reduced migration capacity of sporozoites on the latter.

Mechanotransduction is the process by which cells convert mechanical stimuli into biochemical signals resulting in adaptation of cellular functions (Schwarz and Gardel, 2012; Humphrey et al., 2014; Iskratsch et al., 2014; Chen et al., 2017; Elosegui-Artola et al., 2018; Seetharaman and Etienne-Manneville, 2018; Kechagia et al., 2019). This regulation is mediated by transmembrane proteins such as integrins, adaptor proteins (e.g. vinculin, talin) and the actin cytoskeleton in mammalian cells. Mechanical signals can for example be integrated by conformational changes of integrins upon mechanical force acting on them through ligands or clustering of integrins leading to reduced forces acting on a single protein. It remains an open question, whether sporozoites

actively sense and respond to mechanical cues of their environment or which mechanism restricts their reduced capacity to move on soft substrates. To elucidate whether mechanotransduction occurs in sporozoites, investigation of proteins potentially acting as tension sensors would be necessary.

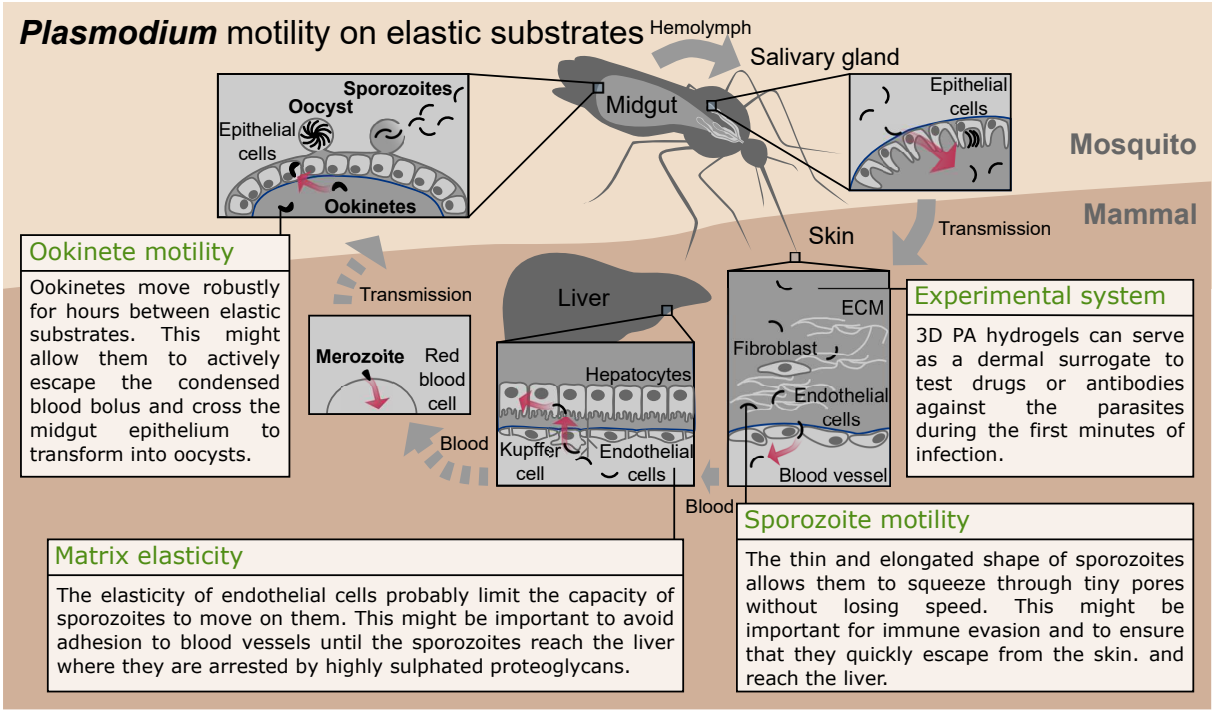

Figure 4.1: Graphical summary of results obtained in this study.
The life cycle of *Plasmodium* parasites is illustrated with a focus on those motile stages that use an actomyosin motor to move across tissues or invade host cells. Red arrows depict active parasite movement. Discontinuous arrows indicate that there are further parasite stages not shown in the scheme. Barriers that the parasites need to overcome are depicted in blue. Brown boxes explain the main findings of this project.

4.1.1 Synthetic hydrogels to study 3D motility of sporozoites

To bridge the gap between artificial planar glass substrates and complex *in vivo* environments for the study of sporozoite migration, I developed a 3D hydrogel assay. Natural hydrogels have served for the examination of sporozoite motility before (Amino et al., 2008; Battista et al., 2014) but their use is limited as sporozoites only move for short periods of time within these hydrogels and few sporozoites can be observed simultaneously. Confinement of infected salivary glands between a PA hydrogel and a

glass coverslip on the other hand resulted in hundreds of sporozoites that move into the hydrogel within a single experiment. The PA hydrogels have an estimated pore size of less than 200 nm (Wen et al., 2014). Possibly due to steric hindrance imposed by the polymeric network, sporozoites slowed down with decreasing pore size and a higher fraction of sporozoites seemed to get stuck until they eventually failed to enter the hydrogels. Larger mammalian cells do not enter into these synthetic hydrogels as they cannot degrade the matrix or squeeze through the tiny pores. Our findings suggest that the thin and elongated shape of sporozoites might have evolved to fit through dense environments such as the salivary duct of the mosquito and move through small pores in the skin at high speed (Fig 4.1). This might be relevant for the parasites to evade the host's immune system and to quickly escape the skin and reach the liver.

Sporozoites move through PA hydrogels in helical trajectories as in matrigel (Amino et al., 2008; Battista et al., 2014), however their trajectories are more regular than in natural hydrogels. Importantly, sporozoite speed in PA hydrogels is similar to the speed distribution observed in the skin *in vivo*. The established experimental system enables us to investigate higher numbers of mutant parasites than would have been possible *in vivo*. Even parasites with a slight salivary gland invasion defect, as it is the case for *coronin(-)* sporozoites, could be quantitatively analyzed. Another advantage as compared to *in vivo* experiments is the reduced number of mice necessary for the experiments and the saving of time.

We currently lack an experimental system to understand why some mutant parasite lines are not capable to invade salivary glands. In principle, this could be due to a lack of tissue recognition, reduced adhesion to salivary glands, diminished capacity to get across the basal lamina or a defect in migration or force exertion to propel the parasites through the epithelial cell layer and reach the lumen where they await transmission. A limitation of the 3D hydrogel assay is that it can only be used with salivary gland sporozoites although it would also be interesting to investigate hemolymph sporozoites in confined environments. Mutants which do not enter the mosquitoes' salivary glands can thus not be examined in this assay.

Using genetically modified sporozoites, I could show that the *in vitro* setting of this new assay is similar to what has been observed *in vivo*. Therefore, quantitative analysis of small differences in motility between mutant parasite lines is possible in the future. We could also show that small compounds, such as CytoD, can diffuse into the hydrogels and act on the parasites (Smyrnakou, 2019). Together, these data suggest that 3D PA hydrogels can be used to mimic sporozoite migration in the skin and serve as model system to easily test drugs or antibodies targeting the parasite directly after it is transmitted (Fig 4.1).

4.1.2 Migratory differences between planar substrates and confined environments

There is increasing evidence that cell motility on planar substrates and movement through 3D environments are differently regulated (Charras and Sahai, 2014; Katakai and Kinashi, 2016; Patteson et al., 2019). Previous studies on mammalian cells have shown that integrin-dependent adhesions required for cell migration on 2D substrates were less important for motility in confined environments (Lämmermann et al., 2008; Liu et al., 2015; Ruprecht et al., 2015). Analyzing *coronin(-)* sporozoites in 2D and 3D hydrogel assays led us to the conclusion that coronin is required for efficient movement on planar substrates but is dispensable for motility in confined environments indicating that the protein is important for adhesion regulation if the cell is in contact with a flat surface. This might be the reason, why *coronin(-)* sporozoites invade salivary glands less effectively but move through the skin like wt sporozoites. It has been shown, that the migration defect of *coronin(-)* sporozoites on glass is partially rescued if they move on basal lamina (Beyer, 2017). The finding that elastic hydrogels can compensate for the mutant phenotype to a similar extent, suggests that the loss of coronin restricts migration in a way that depends on substrate stiffness. However, mechanistic insights into how elastic substrates can rescue the motility defect of *coronin(-)* sporozoites on glass are missing. The migratory capacity of *hsp20(-)* sporozoites on the other hand was enhanced on planar elastic hydrogels when compared to wt while their speed was largely reduced which might be explained by the enlarged but non-dynamic adhesion site shown for these mutant parasites (Montagna et al., 2012). This mutant, which

moves slowly in the skin, also showed reduced speed in 3D hydrogels. Together, these results might indicate that adhesion to planar substrates is important for the parasites to go from a circulatory system (hemolymph or blood) into an organ. Dense environments such as the skin might compensate for reduced adhesion whereas efficient force production and transmission are required there to squeeze through small pores.

Ookinetes, the parasite stages which need to traverse the midgut epithelium to establish oocysts at the outer side of the midgut, but do not require to go from a circulatory system into an organ, do not adhere to soft planar hydrogels but migrate well through confined hydrogel systems that do not harbor any ligands. This again suggests, that receptor-ligand-mediated adhesions are less important for migration through dense environments. I found a significant increase in speed for ookinetes confined between uncoated PA hydrogels as compared to glass. It has been shown for mammalian cells, that confinement and low adhesion can induce fast motility (Liu et al., 2015). While the morphology of mammalian cells changed under these conditions, ookinetes did not show an obvious change in migration mode under high confinement and low adhesion. The finding that ookinetes can move robustly for extended periods of time if confined between elastic substrates suggest that these parasite stages can actively escape the condensed blood meal and traverse the midgut epithelium to transform into oocysts at the basal lamina lining the mosquito midgut (Fig 4.1). Studies of ookinete movement in their *in vivo* environment are required to test, whether the parasites already start moving in the blood bolus. So far, their movement has only been observed in explanted mosquito midguts due to the opaque nature of the cuticle (Vlachou et al., 2004; Volohonsky et al., 2020). In these explanted midguts, only passive movement has been observed for ookinetes located in the blood meal, however the constriction imposed by the cuticle is missing in this experimental setting.

The actomyosin system has been shown to be essential for 3D motility in *Toxoplasma* (Whitelaw et al., 2017). CytoD treatment of sporozoites moving in 3D hydrogels had a drastic impact on their migration leading to non-motile sporozoites already at low concentrations of the drug (Smyrnakou, 2019). The effect of the actin modulating drug on sporozoites moving through hydrogels was even more pronounced as on sporozoites

moving on planar glass substrates. These results suggest that actin polymerization is especially important for 3D motility of sporozoites.

While substrate stiffness influenced parasite motility on flat substrates, there was no such effect on 3D motility. Under confined conditions, ookinetes and sporozoites were highly motile even if the hydrogels were extremely soft.

4.1.3 Conclusion

It is not entirely clear how the parasites sense their environment, which factors trigger stage transitions such as ookinete-to-oocyst-transformation or how target tissues that the parasites need to invade, such as the mosquitoes' salivary glands or the liver of the mammalian host, are recognized. The findings of the first part of this study suggest that important processes that allow the parasites to progress efficiently through the life cycle may not necessarily or not exclusively be mediated by receptor-ligand interactions but also by physical and mechanical properties of the cellular microenvironment such as stiffness.

4.2 *Plasmodium* force transmission

Using traction force microscopy the forces exerted onto a substrate by moving sporozoites were shown to be in the range of 100-200 Pa (Münter et al., 2009; Kratzer, 2016). A major limitation of these measurements is the low sensitivity of the method due to the optical resolution limit. Optical tweezers on the other hand have proven to be more sensitive but have the disadvantage of measuring forces only on the dorsal side of the cell (Quadt et al., 2016). In this study, I extended TFM to the ookinete stage, which is slightly larger and much slower than the sporozoite stage. Force measurements of ookinetes have not been possible so far because they only move in confined settings which resulted in difficulties to perform force measurements using optical tweezers. In contrast to sporozoites, the ookinetes did not move on uncoated flat hydrogels. Therefore, I monitored their movement and bead displacements in a sandwich assay. I observed higher bead displacements than for sporozoites. I did not succeed in

adapting reference free TFM for ookinetes which would allow to analyze traction forces of all ookinetes without the requirement of a reference image. Reasons that we did not observe deformations of the silicone substrate by moving ookinetes might be the elasticity of the substrate (12.6 kPa) or a lower sensitivity of the method as compared to conventional TFM.

4.3 The role of myosin A in gliding motility and force transmission

Myosin A has been identified as the motor protein powering cell migration of apicomplexan parasites. The role of this protein has mainly been studied in *Toxoplasma*. In this organism, MyoA is needed for host cell egress and important but not essential for invasion and gliding (Meissner et al., 2002; Andenmatten et al., 2013; Egarter et al., 2014). In *Plasmodium* on the other hand MyoA is dispensable for egress but required for erythrocyte invasion (Perrin et al., 2018; Robert-Paganin et al., 2019) and ookinete gliding (Siden-Kiamos et al., 2011). While there might be functional redundancies with other myosins in *Toxoplasma*, this is less likely in *Plasmodium* which possesses a reduced set of myosin isoforms (Chaparro-Olaya et al., 2005; Foth et al., 2006). Together, this hints at differences in the role of the actomyosin motor between different Apicomplexa. The importance of MyoA for *Plasmodium* sporozoite motility has not been addressed before. In this thesis, I used reverse genetic approaches to elucidate the function of this protein throughout the whole *Plasmodium* life cycle. By site-directed mutagenesis of MyoA, the role of amino acid residues within the unusual N-terminal extension of MyoA for parasite motility *in vivo* as well as *in vitro* was investigated. A summary of life cycle progression for all parasite lines generated during this project to better understand the role of MyoA in *Plasmodium* gliding motility is depicted in Fig 4.2.

4.3.1 Transcriptional regulation is crucial for MyoA function *in vivo*

Exchanging *5'myoA* by four different promoters that showed similar temporal expression in blood stages did not yield viable parasites (Fig 4.2). Furthermore, replacing *3'myoA* by *3'dhfs* resulted in parasites that showed enhanced numbers of hemolymph sporozoites, while the number of salivary gland sporozoites was reduced. These results indicate, that exchanging *3'myoA* by *3'dhfs* affects the parasites ability to infect mosquito salivary glands which is important for parasite transmission. This might be due to a reduced migratory capacity of hemolymph sporozoites. Indeed, their ability to move was largely reduced *in vitro*. I further speculated, that the exchange of *3'myoA* might have effects on RNA levels of *myoA* or its neighboring gene which encodes DNA-directed RNA polymerase I, II, and III subunit RPABC4. This gene is located on the complementary DNA strand meaning that its UTRs could reach into the coding region of *myoA* (van Lin et al., 2001). A change in RNA levels might in turn result in an alteration of protein levels. RT-PCR results by Xanthoula Smyrnakou suggest, that in early oocysts RNA levels of *myoA* but not its neighboring gene are reduced in the PbMyoA$_{3'dhfs}$ line which might explain the mutant *in vivo* phenotype (Smyrnakou, 2019). It has been estimated that nine myosin proteins are needed to transport actin filaments at maximum speed in *Plasmodium* (Bookwalter et al., 2017). Assuming a filament length of approximately 100 nm (Schmitz et al., 2005) and taking into account that myosins can only bind actin filaments at the junction between two adjacent actin monomers in the long pitch helix (Robert-Paganin et al., 2020) this would mean that bundling or crosslinking of filaments is necessary to ensure even rearward translocation of actin filaments and thus retrograde flow. An explanation for the observed mutant phenotype of the PbMyoA$_{3'dhfs}$ line might be that the number of MyoA proteins is too low to transport the short actin filaments rearwards. Analysis of MyoA protein levels, for example via Western Blotting or Mass Spectrometry, would reveal the extent of MyoA reduction in the mutant parasite line. Reasons that we only detected an effect on the sporozoite stage might be stage-specific regulation of MyoA expression. Alternatively, merozoites and ookinetes might be less sensitive to changes in MyoA levels. While we had difficulties in exchanging 5'UTR and 3'UTR of *myoA*, deletion of the introns did not

have a detectable effect on life cycle progression of *Plasmodium* parasites.

The PbMyoA$_{3'dhfs}$ GFP parasite line grew at the same rate as wt parasites in the blood and formed normal numbers of oocysts, indicating that tagging does not have an effect on merozoites and ookinetes. However, it had the same salivary gland invasion defect as the PbMyoA$_{3'dhfs}$ line. Therefore, we cannot be sure, whether there is an additional effect on the sporozoite stage which is masked by the strong effect caused by the exchange of *3'myoA* by *3'dhfs*. In a previous publication, tagging of MyoA with GFP did not have an effect on life cycle progression (Green et al., 2017). In this study, the authors used single crossover homologous recombination for tagging, resulting in an exchanged 3'UTR as well. Still, the authors state that they did not detect an abnormal phenotype for this parasite line. One reason might be, that they characterized a polyclonal parasite population, which possibly led to cross-fertilization of mutant and wt gametocytes resulting in a rescue of the phenotype due to protein inheritance from heterozygous oocysts to sporozoites (Rathnapala et al., 2017; Stanway et al., 2019). Another possibility could be that they used a different 3'UTR which better mimics the properties of *3'myoA* resulting in MyoA expression levels closer to wt parasites. To test whether GFP-tagging affects MyoA function in sporozoites, a GFP-tagged parasite line should be generated using the CRISPR/Cas9 system or GIMO method.
The importance of the regulatory elements upstream and downstream of *myoA* clearly show how important transcriptional regulation of this gene is at different life cycle stages. An exchange of the actin 3'UTR also had a drastic effect on salivary gland invasion (Ross Douglas, unpublished), suggesting that the regulatory elements downstream of a gene are generally important for proper expression levels of essential proteins in *Plasmodium*. The 3'UTR could be specifically important in sporozoites as these are the longest living stages that encounter different environments.

4.3.2 *P. falciparum* MyoA cannot functionally complement *P. berghei* MyoA

Replacement of a *P. berghei* gene by its *P. falciparum* ortholog allows for straightforward mutational analysis of a protein that has been biochemically analyzed before if

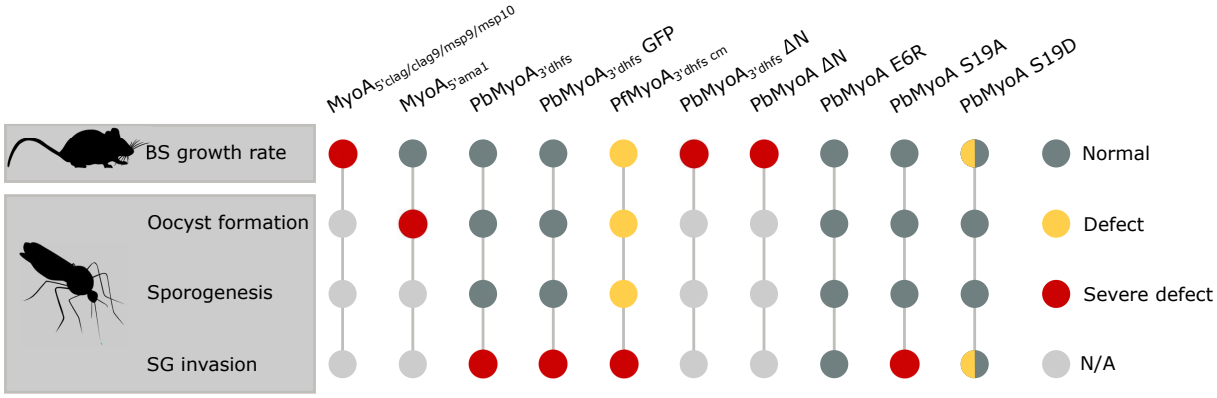

Figure 4.2: Summary of life cycle progression for all parasite lines generated in this project. Shown is the phenotypic effect of MyoA mutagenesis. No asexual blood stage (BS) parasites were obtained for clag/clag9/msp9 and msp10 promoter swaps as well as N-terminal deletion of MyoA suggesting that these genetic manipulations were lethal for the parasites and preventing the analysis of other life cycle stages for these parasite lines. Exchange of *3'myoA* by *3'dhfs* led to severely reduced salivary gland (SG) invasion of sporozoites, while the replacement of PbMyoA by PfMyoA resulted in a reduced fitness of all motile parasite stages. Mutation of glutamic acid 6 to arginine did not have a detectable effect on any of the examined life cycle stages, while mutating serine 19 to alanine lead to a severe defect in salivary gland invasion of sporozoites. Exchanging serine 19 by aspartic acid might have a slight effect on merozoites and sporozoites.

the orthologs can complement each other (Moreau et al., 2017). Importantly, PbMyoA shares 80% sequence identity with PfMyoA. However, replacing PbMyoA by a codon-modified version of PfMyoA resulted in severe defects in blood stage growth and oocyst formation as compared to wt parasites (Fig 4.2). Reasons for the defect in life cycle progression of the transgenic parasite line might be structural differences of the protein that could lead to different localization, kinetics or protein binding. Alternatively, differences in protein levels might occur due to codon modification of *myoA* as has been shown for tubulin (Spreng et al., 2019). Consequently, this parasite line could not be used for mutational studies of MyoA.

4.3.3 Implementation of a system for site-directed mutagenesis of MyoA

MyoA is thought to play an essential role in *Plasmodium* blood stages (Zhang et al., 2018; Schwach et al., 2015) as it is required for merozoite invasion of erythrocytes (Robert-Paganin et al., 2019). Gene editing of the *myoA* locus would therefore benefit from a system for stage-specific mutagenesis which could be achieved via a promoter swap strategy in combination with a synthetic promoter (Siden-Kiamos et al., 2011;

Bantuchai et al., 2019; Klug et al., 2018). However, exchanging *5'myoA* by blood stage specific promoters did not yield viable parasites in several attempts while it was possible to replace *5'myoA* by the ama1 promoter, which is active in blood stages and sporozoites and has already been shown to work (Siden-Kiamos et al., 2011). This suggests, that the precise timing of MyoA expression in blood stages did not work out for the chosen promoters, indicating that it is difficult to predict promoter activity from high-throughput RNA sequencing data (Otto et al., 2014). To study genes that are essential in blood stages, *P. berghei* research would greatly benefit from the development of a more advantageous system for stage-specific mutagenesis of genes. This could for example be achieved by using the auxin-inducible degron system (Philip and Waters, 2015) in combination with stage-specific expression of a second mutated copy of the GOI.

As I did not succeed to implement a system for stage-specific mutagenesis of MyoA, conventional gene editing served as an alternative strategy. It allows for introducing mutations into the *myoA* locus but it is restricted to mutations that do not affect merozoite survival. This method has been used for several gene loci to better understand the function of different proteins in *P. berghei* (Bane et al., 2016; Moreau et al., 2017; Douglas et al., 2018b). However, conventional gene editing requires to integrate a selection cassette upstream or downstream of the gene of interest. Furthermore, integration of the selection marker goes along with a change of regulatory elements of the gene of interest. As these changes resulted in parasites, that were not able to invade the mosquitoes' salivary glands any longer, another strategy was needed.

A first attempt in establishing the CRISPR/Cas9 system for *P. berghei* failed within this study. As the community would largely benefit from this system, which allows for fast and straightforward site-directed mutagenesis, tagging or deletion of any GOI, further effort to adapt it to *P. berghei* is important.

Using the GIMO strategy, it was finally possible to edit the *myoA* locus while leaving all gene regulatory elements intact. In contrast to published results (Lin et al., 2011; Orr et al., 2012), this strategy revealed very low efficiency in my hands. Yet, this ap-

proach allowed me to generate mutant parasite lines with substitutions in single amino acids of MyoA (Fig 4.3). To exclude clonal effects, a wt reconstitution served as control.

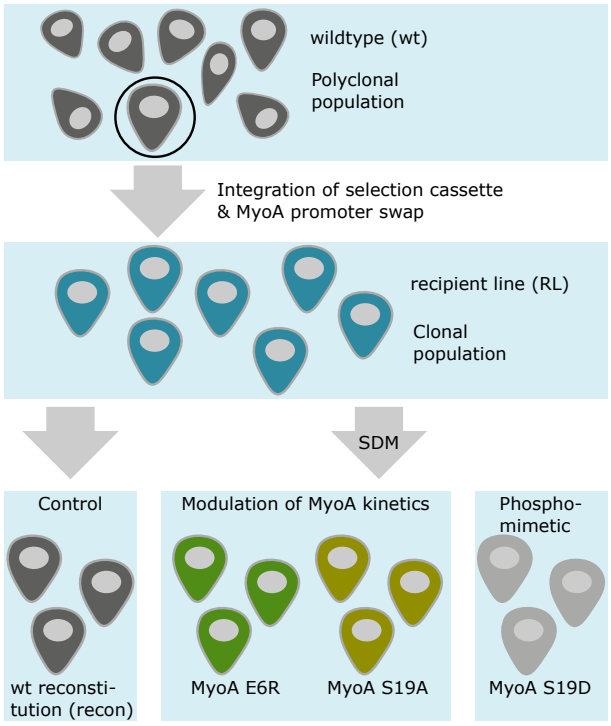

Figure 4.3: Overview of MyoA mutants generated to study how stabilizing interactions of N-terminal residues in the rigor state affect MyoA function *in vivo*.
First, a recipient line was generated harboring a selection marker. The wt reconstitution served as a control to account for clonal effects. MyoA kinetics were modulated by ablating stabilizing interactions in the rigor state using site-directed mutagenesis (SDM). Either a reverse charge was introduced at residue E6 or a phosphodeficient mutant of S19 was generated. To mimic the phosphorylated state of wt MyoA, a phosphomimetic mutant of S19 was generated as well.

4.3.4 MyoA phosphorylation modulates myosin motor properties to allow for efficient salivary gland invasion of sporozoites

Force generation of MyoA happens by an atypical mechanism (Robert-Paganin et al., 2019). The absence of a glycine between helices SH1 and SH2, which is conserved among canonical myosins (Preller et al., 2011), is compensated by an unusual N-terminal extension (Robert-Paganin et al., 2019). By interacting with switch II and converter, the N-terminal extension stabilizes the rigor state and thus determines the kinetic properties of MyoA as it affects the amount of time that MyoA is bound to actin and thereby the duty ratio. Phosphorylation of S19 tunes motor activity by switching between higher speed (phosporylated state) or higher force (unphosphorylated state). To test, how changing the kinetic properties of MyoA affects parasite motility *in vitro* and life cycle progression *in vivo*, the mutant parasite lines (Fig 4.3) were characterized.

Deletion of the N-terminal extension (19 amino acids) failed in several attempts, suggesting that it might be crucial for merozoite invasion of erythrocytes (Fig 4.2). Although biochemical experiments with purified ΔN MyoA show, that the protein is still able to carry out its function *in vitro* (Robert-Paganin et al., 2019), we cannot completely rule out, that deletion of 19 amino acids might affect proper folding of the protein. However, the reduction of speed at which this mutant transports actin filaments rearwards (Robert-Paganin et al., 2019), might also lead to merozoites that do not invade erythrocytes properly anymore and therefore explain why we were not able to get viable ΔN MyoA parasites. To test the effect of deleting the whole N-terminal region of MyoA on ookinete and sporozoite motility, conditional or stage-specific gene editing would be necessary.

Two amino acid residues within the N-terminal extension which were predicted to be important for MyoA kinetics (Robert-Paganin et al., 2019), were further investigated within this study. To understand their role in forming stabilizing interactions in the rigor state of MyoA, these interactions were abolished by introducing a reverse charge (E6R) or by mimicking the phosphorylated (S19D) or unphosphorylated (S19A) state. We assumed from structural and biochemical studies (Robert-Paganin et al., 2019), that the latter would affect kinetic properties of MyoA leading to lower speed and higher force (S19A) or higher speed and lower force (S19D) by changing the duty ratio. A possible effect of the E6R mutation on the motor properties of MyoA has not been investigated so far.

The MyoA E6R line behaved like wt *in vivo*, suggesting that the interaction between E6 and two amino acids of switch I and II is not required for proper MyoA function *in vivo* (Fig 4.2). However, migration capacity and speed of isolated salivary gland sporozoites, but not hemolymph sporozoites, was slightly reduced in this parasite line (Table 4.1). This suggests that motility of salivary gland sporozoites is more prone to changes in MyoA function. Transmission experiments will reveal whether the effect of the mutation on *in vitro* cell migration also has an impact *in vivo* on either skin traversal or liver infection.

Table 4.1: Summary of *in vitro* motility of MyoA mutants (compared to wt reconstitution, + indicates an increase; = indicates no apparent difference; - indicates a slight decrease; – indicates a strong decrease)

	Hemolymph sporozoites		Salivary gland sporozoites	
	Migration capacity [%]	Speed	Migration capacity [%]	Speed
E6R	=	=	-	-
S19A	–	-	-	–
S19D	-	-	=	–

The phosphodeficient MyoA S19A line grew normally in the blood and infected mosquito midguts at wt levels (Fig 4.2). This indicates, that phosphorylation of serine 19 is not important for merozoite invasion of erythrocytes as well as ookinete motility *in vivo*. However, sporozoite levels in the mosquito hemolymph were enhanced, while sporozoite numbers in the mosquito salivary gland were reduced. This phenotype has been observed for other mutants as well, e.g. for sporozoites lacking TRAP as this protein is important for sporozoites to attach to the salivary glands (Sultan et al., 1997). The sporozoites, that cannot enter the salivary glands, probably circulate in the hemolymph for enhanced time periods until they finally die due to the lacking signal to mature or they might be killed by the mosquitoes' immune system. The salivary gland invasion defect shows, that phosphorylation at serine 19 is important for sporozoites to enter salivary glands from where they are transmitted (Fig 4.4).

We decided to focus the *in vitro* work on the stage which shows a mutant *in vivo* phenotype although an effect of the mutation on merozoite invasion and ookinete migration *in vitro* is possible as well. Reasons that these stages were not analyzed *in vitro* in this study are the lack of a proper invasion assay for *P. berghei* parasites (these experiments can also be conducted in cell culture with *P. falciparum* parasites) and the use of mice which is necessary for ookinete cultures. Interestingly, isolated MyoA S19A hemolymph and salivary gland sporozoites were slower than wt parasites on planar glass substrates (Table 4.1). The 3D hydrogel assays developed within this study will help to mimic the skin and thus analyze cell migration of the mutant sporozoites in an environment that is closer to the natural one. Therefore future experiments should be performed to compare the mutant sporozoites in this physiologically relevant setup.

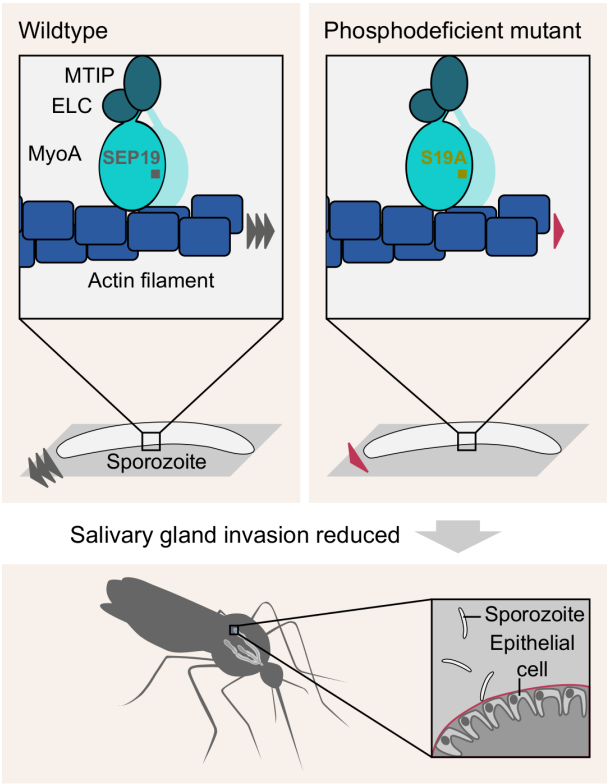

Figure 4.4: Reduced migratory capacity of MyoA S19A hemolymph sporozoites results in a defect of salivary gland invasion. Phosphorylated serine (SEP) 19 located in the N-terminal extension of MyoA forms stabilizing interactions in the rigor state thereby contributing to the kinetic properties of wildtype myosin. This results in efficient translocation of actin filaments in biochemical *in vitro* motility assays (Robert-Paganin et al., 2019). In contrast, the phosphodeficient S19A mutation leads to a reduction in speed. Here, I found that these biochemical properties cause a decrease in migratory capacity and speed of isolated hemolymph sporozoites. *In vivo*, I detected highly reduced numbers of mutant sporozoites in the mosquitoes' salivary glands.

PfMyoA is phosphorylated in merozoites, ookinetes and sporozoites (Lasonder et al., 2015). Given the conservation and mechanistic requirements, it is very likely that PbMyoA is phosphorylated as well although this has not been shown. Robert-Paganin et al. (2019) speculated, that phosphorylation of MyoA at S19 could modulate the motor for higher force as required for merozoite invasion of erythrocytes or higher speed as needed for sporozoites to cross tissues. This would suggest, that prior to invasion, MyoA is dephosphorylated in merozoites. In line with this hypothesis, the phosphomimetic MyoA S19D mutant grew slower in the blood than the S19A mutant (Fig 4.2). However, we obtained only one clone for each parasite line which means that further experiments are needed to receive solid data on whether there is a statistically relevant difference in blood stage growth between these mutants. The MyoA S19D mutant could partially but not completely restore salivary gland invasion and *in vitro* migration of hemolymph and salivary gland sporozoites (Table 4.1). Reasons might be that the aspartic acid not fully simulates the phosphorylated serine or that dynamic changes between phosporylated and unphosphorylated state of MyoA are required for efficient cell migration and invasion. Even in biochemical assays, MyoA S19D did not transport actin filaments at maximum speed (Robert-Paganin et al., 2019).

An increase in gliding capacity of salivary gland versus hemolymph sporozoites was observed for all parasite lines that were investigated, consistent with previous studies (Hegge et al., 2010; Sato et al., 2014). Furthermore, I found that the actin modulating drug Jas increased adhesion of hemolymph sporozoites, while Münter et al. (2009) observed the opposite effect on salivary gland sporozoites. It is unclear what causes these differences and whether the hemolymph sporozoites that are motile *in vitro* are those ones that enter the salivary glands *in vivo*. The difference in gliding capacity between hemolymph and salivary gland sporozoites might be because only the highly motile fraction of hemolymph sporozoites reaches the salivary glands, due to a higher fraction of hemolymph sporozoites with a not fully assembled gliding machinery or due to external stimuli in the salivary gland that allow maturation of sporozoites and thereby influence their motility (Roth et al., 2018).

Taken together, the results obtained within this thesis suggest that the interaction between N-terminal extension and converter as provided by phosphorylated S19 and K764 is more important for MyoA function than the interaction between N-terminal extension and switch I/switch II mediated by E6, R241 and F476. Phosphorylation of MyoA at S19 is important for efficient sporozoite motility *in vitro* and salivary gland invasion *in vivo*. On the other hand, phosphorylation of MyoA is not required for merozoite invasion and ookinete motility *in vivo*, suggesting that MyoA is stage-specifically regulated or merozoites and ookinetes are less sensitive to changes in MyoA kinetics. Tight regulation of MyoA might be carried out by cGMP- and calcium-dependent protein kinases (Alam et al., 2015; Fang et al., 2018). Invasion usually takes less than a minute (Gilson and Crabb, 2009), while ookinetes and sporozoites need to glide for a much longer period of time but move at different speed. Post-translational or transcriptional regulation mechanisms of proteins involved in gliding motility might account for these differences.

Interruption, overexpression or mutagenesis of components of the gliding machinery leads to a salivary gland invasion defect in many cases (Sultan et al., 1997; Steinbuechel and Matuschewski, 2009; Sato et al., 2016; Bane et al., 2016; Douglas et al., 2018b), while only one mutant is known which invades salivary glands at wt levels but

is impaired in skin traversal (Montagna et al., 2012). Penetration of the salivary glands therefore seems to be a major bottleneck in the *Plasmodium* life cycle as it is crucial for transmission of the parasites. Sporozoites seem to be very susceptible to small changes of the components involved in gliding motility in contrast to merozoites and ookinetes, possibly because tight coordination of the gliding machinery is necessary to allow for the incredibly high speed of the sporozoite stage.

Little is known about the role of the N-terminal extension in other myosins. Greenberg et al. (2015) suggested, that this structural element provides functional diversity among the myosin family of proteins. Mammalian Myosin-Ib also contains an N-terminal extension stabilizing the rigor state, however location and orientation differ from the one of MyoA (Robert-Paganin et al., 2019). Also the role that the N-terminal extension plays seems to differ between these myosins. While it mediates force-sensitivity in Myosin-Ib (Greenberg et al., 2015), it is important for efficient translocation of actin filaments in MyoA (Robert-Paganin et al., 2019). Additionally, motor properties can be modulated by phosphorylation of a serine residue within the MyoA N-terminal extension, while such a regulation mechanism has not been identified for Myosin-Ib.

4.3.5 Conclusion

Altogether these observations suggest, that the sporozoite is the stage mostly affected by small changes in MyoA expression or post-translational modification. Although there is evidence that sporozoite motility is required for egress from oocysts (Klug and Frischknecht, 2017), I did not detect a defect at this step of the life cycle for any of my mutant MyoA parasite lines. Instead, the major bottleneck was salivary gland invasion. These findings are in line with previous studies of parasite actin I revealing an important function of actin filament dynamics for salivary gland invasion of sporozoites (Douglas et al., 2018a). The actomyosin motor thus seems to be tightly regulated to allow for efficient sporozoite motility. Furthermore, the difficulties of disrupting single domains of MyoA or actin I in this study and the studies performed by Douglas et al. (2018a) hint at an essential role of these proteins in erythrocyte invasion. In *P. falciparum*, MyoA has been shown to be essential for merozoite invasion as well (Robert-Paganin et al.,

2019). Our findings are in marked contrast to what has been found in *Toxoplasma*, where residual gliding and host cell invasion was observed upon complete disruption of MyoA and actin I (Andenmatten et al., 2013; Egarter et al., 2014; Whitelaw et al., 2017). Reasons might be that residual protein was still present in the parasite lines due to the conditional system that was used. Additionally, different definitions of motility were used. While the authors defined parasites as motile if they moved a distance higher than two µm (Whitelaw et al., 2017), we would define parasites as motile if they move more than a parasite length (ten µm). Importantly, no *myoA(-)* parasite moved with a final displacement of more than one parasite body length (Whitelaw et al., 2017). However, host cell invasion was still possible in *Toxoplasma* if MyoA or actin I were missing. Due to the discrepancies between the studies in *Plasmodium* and the ones in *Toxoplasma* it is likely that alternative invasion and gliding mechanisms independent of the actomyosin motor are specific for *Toxoplasma* or that overlapping functions with other myosins occur due to the larger repertoire of myosin isoforms in *Toxoplasma*. Differences might also be explained by the cell culture system which is used for *Toxoplasma* which does not include all factors relevant *in vivo*. This might also be the reason, why *Toxoplasma* parasites lacking MyoA were not infectious to mice (Meissner et al., 2002).

4.3.6 Future directions: The role of myosin in gliding motility

In the present study, the effect of mutations of MyoA on parasite *in vivo* and *in vitro* motility was tested. In the future, optical tweezer experiments with the myosin mutants generated in this project could be carried out to analyze how a change in MyoA kinetics affects retrograde flow and forces measured at the dorsal apical end of sporozoites.

Here, I studied the role of the myosin heavy chain on invasion and gliding motility of *Plasmodium* parasites. Future work could be performed to investigate the role of the myosin light chains *in vivo*. For example, *in vitro* studies have shown that S108 phosphorylation of MTIP is required for efficient binding to MyoA (Douse et al., 2012). Furthermore, MTIP can be phosphorylated at residues S47 and S51 by a calcium-dependent protein kinase *in vitro* (Green et al., 2008). Whether these phosphorylation

sites are relevant *in vivo* remains an open question. Additionally, it has been shown that mutagenesis of two arginines in the tail domain of MyoA abolishes its peripheral localization in *Toxoplasma*, suggesting that these residues are necessary for the interaction between MyoA and its light chains (Hettmann et al., 2000). As these residues are conserved between *Plasmodium* and *Toxoplasma*, one could test whether the same observations can be made in *Plasmodium*.
Further analysis of the MyoA structure could also aim at resolving the actin-myosin interface and performing site-directed mutagensis of MyoA to elucidate the role of single amino acid residues in actin binding. The actin-myosin interface has only been mapped for very few myosins due to limited resolution of the rigor state and the difficulties to crystallize actin filaments (Robert-Paganin et al., 2020).

Taken together, this thesis provides insights into the regulation of *Plasmodium* gliding motility in dependence of external and internal factors. Investigation of ookinetes and sporozoites inside and on top of polyacrylamide hydrogels revealed that environmental conditions such as tissue elasticity, confinement and pore size have an impact on *Plasmodium* motility. The data shows that parasite migration on flat substrates differs from movement through 3D environments. Furthermore, this study revealed that transcriptional and post-translational regulation of the myosin motor MyoA are important for parasite locomotion. In combination with structural studies performed previously (Robert-Paganin et al., 2019), this work shows how molecular changes affect a living cell in its natural environment. The requirement of MyoA phosphorylation at S19 for efficient salivary gland invasion highlights the importance of a fast actomyosin motor for successful transmission of *Plasmodium* sporozoites.

Acknowledgements

I would like to thank Freddy for the opportunity to work on this exciting project. Thanks for your support, for encouraging critical thinking and for providing scientific advice. I especially enjoyed the freedom to work and organize the project independently. I am grateful that you provided me with the resources to acquire lots of useful skills. Thank you for giving me the opportunity to teach in Woods Hole already in my first year of the PhD and for always encouraging my efforts in science communication.

I would like to thank Ulrich Schwarz and Rasmus Schröder for the pleasant atmosphere and constructive feedback during the TAC sessions. Special thanks to Ulrich for being my first supervisor. Thanks a lot to Ilka Bischofs and Marina Lusic for being part of the Examination Commission.

I would like to thank Jessica and Ross for correcting this thesis. I would also like to thank Jessica for her help with experimental techniques and troubleshooting, for her advice how to shorten protocols, and for making the lab a place not only to work but also to have fun. Thanks to ”AG Kehrer/Ripp”: Emma, Julia H., Chris, Leanne and Xani for all the time we spend drinking ice coffee or sparkling wine and the cheerful lab outings.

Thanks to my students Xani, Maren and Sandra for helping with this project. I would especially want to say thank you to Xani for carrying out so many experiments but also for sharing the joy and excitement for my scientific project.

I would like to thank Julia A. for her friendship inside and outside of the lab. Preparing the science slam together was so much fun.

Thanks to all former and current members of the Frischknecht group, Ben, Catherine,

Dennis, Gunnar, Henni, Jessica, Julia A., Julia S., Katharina, Konrad, Marek, Mendi, Miriam, Mirko, Ross, Saskia, Simon and all students for the enjoyable and collaborative environment in the lab and for interesting discussions. I will miss the breaks with coffee and cake.

Vielen Dank an meine Familie für die großartige Unterstützung. Danke Mami, dass du dich so sehr für mein Projekt interessierst und dich immer über meine Zeichnungen zur Erklärung wissenschaftlicher Sachverhalte freust. Vielen Dank Esther, dass du immer ein offenes Ohr für mich hast und für mich da bist. Danke Papa, dass du mich ermutigst, über mich hinaus zu wachsen. Danke auch an Leo, Claudia, Peter und Luis, für die gemeinsame Zeit, in der ich mich vom stressigen Laboralltag erholen und neue Kraft tanken konnte.

Zuletzt möchte ich mich ganz herzlich bei Claus bedanken. Dein unerschütterliches Vertrauen in mich hat mir unglaublich geholfen. Danke für deine einzigartige Unterstützung, ohne die diese Arbeit nicht möglich gewesen wäre. Danke, dass du mich aus dem Alltag reißt, wenn ich mir mal wieder zu viele Gedanken mache. Dass du mich immer zum Lachen bringst, wenn ich Sorgen habe. Für die wunderschönen gemeinsamen Ausflüge und Reisen. Danke, dass du dein Leben mit mir teilen möchtest.

Bibliography

Alam, M. M., Solyakov, L., Bottrill, A. R., Flueck, C., Siddiqui, F. A., Singh, S., Mistry, S., Viskaduraki, M., Lee, K., Hopp, C. S., Chitnis, C. E., Doerig, C., Moon, R. W., Green, J. L., Holder, A. A., Baker, D. A. and Tobin, A. B. (2015). Phosphoproteomics reveals malaria parasite Protein Kinase G as a signalling hub regulating egress and invasion. Nature Communications *6*, 1–15.

Amino, R., Giovannini, D., Thiberge, S., Gueirard, P., Boisson, B., Dubremetz, J. F., Prévost, M. C., Ishino, T., Yuda, M. and Ménard, R. (2008). Host cell traversal is important for progression of the malaria parasite through the dermis to the liver. Cell Host and Microbe *3*, 88–96.

Amino, R., Thiberge, S., Martin, B., Celli, S., Shorte, S., Frischknecht, F. and Ménard, R. (2006). Quantitative imaging of Plasmodium transmission from mosquito to mammal. Nature Medicine *12*, 220–224.

Andenmatten, N., Egarter, S., Jackson, A. J., Jullien, N., Herman, J. P. and Meissner, M. (2013). Conditional genome engineering in Toxoplasma gondii uncovers alternative invasion mechanisms. Nature Methods *10*, 125–127.

Angrisano, F., Tan, Y. H., Sturm, A., McFadden, G. I. and Baum, J. (2012). Malaria parasite colonisation of the mosquito midgut - placing the Plasmodium ookinete centre stage. International Journal for Parasitology *42*, 519–527.

Baer, K., Klotz, C., Kappe, S. H., Schnieder, T. and Frevert, U. (2007). Release of hepatic Plasmodium yoelii merozoites into the pulmonary microvasculature. PLoS Pathogens *3*, 1651–1668.

Bahl, A., Brunk, B., Crabtree, J., Fraunholz, M. J., Gajria, B., Grant, G. R., Ginsburg, H.,

Gupta, D., Kissinger, J. C., Labo, P., Li, L., Mailman, M. D., Milgram, A. J., Pearson, D. S., Roos, D. S., Schug, J., Stoeckert, C. J. and Whetzel, P. (2003). PlasmoDB: The Plasmodium genome resource. A database integrating experimental and computational data. Nucleic Acids Research *31*, 212–215.

Baker, R. P., Wijetilaka, R. and Urban, S. (2006). Two Plasmodium rhomboid proteases preferentially cleave different adhesins implicated in all invasive stages of malaria. PLoS Pathogens *2*, e113.

Bancells, C., Llorà-Batlle, O., Poran, A., Nötzel, C., Rovira-Graells, N., Elemento, O., Kafsack, B. F. and Cortés, A. (2019). Revisiting the initial steps of sexual development in the malaria parasite Plasmodium falciparum. Nature Microbiology *4*, 144–154.

Bane, K., Lepper, S., Kehrer, J., Sattler, J. M., Singer, M., Reinig, M., Klug, D., Heiss, K., Baum, J., Müller, A.-K. and Frischknecht, F. (2016). The actin filament-binding protein coronin regulates motility in Plasmodium sporozoites. PLoS Pathogens *12*, e1005710.

Bantuchai, S., Nozaki, M., Thongkukiatkul, A., Lorsuwannarat, N., Tachibana, M., Baba, M., Matsuoka, K., Tsuboi, T., Torii, M. and Ishino, T. (2019). Rhoptry neck protein 11 has crucial roles during malaria parasite sporozoite invasion of salivary glands and hepatocytes. International Journal for Parasitology *49*, 725–735.

Barrangou, R., Fremaux, C., Deveau, H., Richards, M., Boyaval, P., Moineau, S., Romero, D. a. and Horvath, P. (2007). CRISPR provides acquired resistance against viruses in prokaryotes. Science *315*, 1709–12.

Battista, A., Frischknecht, F. and Schwarz, U. S. (2014). Geometrical model for malaria parasite migration in structured environments. Physical Review E *90*, 1–12.

Baum, J., Tonkin, C. J., Paul, A. S., Rug, M., Smith, B. J., Gould, S. B., Richard, D., Pollard, T. D. and Cowman, A. F. (2008). A malaria parasite formin regulates actin polymerization and localizes to the parasite-erythrocyte moving junction during invasion. Cell Host and Microbe *3*, 188–198.

Bennink, S., Kiesow, M. J. and Pradel, G. (2016). The development of malaria parasites in the mosquito midgut. Cellular Microbiology *18*, 905–918.

Bergert, M., Erzberger, A., Desai, R. A., Aspalter, I. M., Oates, A. C., Charras, G., Salbreux, G. and Paluch, E. K. (2015). Force transmission during adhesion-independent migration. Nature Cell Biology *17*, 524–9.

Bergert, M., Lendenmann, T., Zündel, M., Ehret, A. E., Panozzo, D., Richner, P., Kim, D. K., Kress, S. J. P., Norris, D. J., Sorkine-Hornung, O., Mazza, E., Poulikakos, D. and Ferrari, A. (2016). Confocal reference free traction force microscopy. Nature Communications *7*, 1–10.

Bergman, L. W., Kaiser, K., Fujioka, H., Coppens, I., Daly, T. M., Fox, S., Matuschewski, K., Nussenzweig, V. and Kappe, S. H. I. (2003). Myosin A tail domain interacting protein (MTIP) localizes to the inner membrane complex of Plasmodium sporozoites. Journal of Cell Science *116*, 39–49.

Beyer, K. (2017). Collective motion and adhesin dynamics of Plasmodium sporozoites.

Billker, O., Dechamps, S., Tewari, R., Wenig, G., Franke-Fayard, B. and Brinkmann, V. (2004). Calcium and a calcium-dependent protein kinase regulate gamete formation and mosquito transmission in a malaria parasite. Cell *117*, 503–514.

Blanchoin, L., Boujemaa-Paterski, R., Sykes, C. and Plastino, J. (2014). Actin dynamics, architecture, and mechanics in cell motility. Physiological Reviews *94*, 235–263.

Bloemink, M. J. and Geeves, M. A. (2011). Shaking the myosin family tree: Biochemical kinetics defines four types of myosin motor. Seminars in Cell and Developmental Biology *22*, 961–967.

Bookwalter, C. S., Kelsen, A., Leung, J. M., Ward, G. E. and Trybus, K. M. (2014). A Toxoplasma gondii class XIV myosin, expressed in Sf9 cells with a parasite co-chaperone, requires two light chains for fast motility. Journal of Biological Chemistry *289*, 30832–30841.

Bookwalter, C. S., Tay, C. L., McCrorie, R., Previs, M. J., Lu, H., Krementsova, E. B., Fagnant, P. M., Baum, J. and Trybus, K. M. (2017). Reconstitution of the core of the

malaria parasite glideosome with recombinant Plasmodium class XIV myosin A and Plasmodium actin. Journal of Biological Chemistry *292*, 19290–19303.

Boucher, L. E. and Bosch, J. (2015). The apicomplexan glideosome and adhesins - structures and function. Journal of Structural Biology *190*, 93–114.

Bryant, J. M., Baumgarten, S., Glover, L., Hutchinson, S. and Rachidi, N. (2019). CRISPR in parasitology: not exactly cut and dried! Trends in Parasitology *35*, 409–422.

Bullen, H. E., Tonkin, C. J., O'Donnell, R. A., Tham, W. H., Papenfuss, A. T., Gould, S., Cowman, A. F., Crabb, B. S. and Gilson, P. R. (2009). A novel family of apicomplexan glideosome-associated proteins with an inner membrane-anchoring role. Journal of Biological Chemistry *284*, 25353–25363.

Burda, P. C., Caldelari, R. and Heussler, V. T. (2017). Manipulation of the host cell membrane during Plasmodium liver stage egress. mBio *8*, e00139–17.

Bushell, E., Gomes, A. R., Sanderson, T., Anar, B., Girling, G., Herd, C., Metcalf, T., Modrzynska, K., Schwach, F., Martin, R. E., Mather, M. W., McFadden, G. I., Parts, L., Rutledge, G. G., Vaidya, A. B., Wengelnik, K., Rayner, J. C. and Billker, O. (2017). Functional profiling of a Plasmodium genome reveals an abundance of essential genes. Cell *170*, 260–272.

Bushell, E. S., Ecker, A., Schlegelmilch, T., Goulding, D., Dougan, G., Sinden, R. E., Christophides, G. K., Kafatos, F. C. and Vlachou, D. (2009). Paternal effect of the nuclear formin-like protein MISFIT on Plasmodium development in the mosquito vector. PLoS Pathogens *5*, e1000539.

Carey, A. F., Singer, M., Bargieri, D., Thiberge, S., Frischknecht, F., Ménard, R. and Amino, R. (2014). Calcium dynamics of Plasmodium berghei sporozoite motility. Cellular Microbiology *16*, 768–783.

Chaparro-Olaya, J., Margos, G., Coles, D. J., Dluzewski, A. R., Mitchell, G. H., Wasserman, M. and Pinder, J. C. (2005). Plasmodium falciparum myosins: Transcription and translation during asexual parasite development. Cell Motility and the Cytoskeleton *60*, 200–213.

Charras, G. and Sahai, E. (2014). Physical influences of the extracellular environment on cell migration. Nature Reviews Molecular Cell Biology *15*, 813–824.

Chen, Y., Ju, L., Rushdi, M., Ge, C. and Zhu, C. (2017). Receptor-mediated cell mechanosensing. Molecular Biology of the Cell *28*, 3134–3155.

Codan, B., Martinelli, V., Mestroni, L. and Sbaizero, O. (2013). Atomic force microscopy of 3T3 and SW-13 cell lines: An investigation of cell elasticity changes due to fixation. Materials Science and Engineering C *33*, 3303–3308.

Combe, A., Moreira, C., Ackerman, S., Thiberge, S., Templeton, T. J. and Ménard, R. (2009). TREP, a novel protein necessary for gliding motility of the malaria sporozoite. International Journal for Parasitology *39*, 489–496.

Cooper, J. A. (1987). Effects of cytochalasin and phalloidin on actin. Journal of Cell Biology *105*, 1473–1478.

Coppi, A., Tewari, R., Bishop, J. R., Bennett, B. L., Lawrence, R., Esko, J. D., Billker, O. and Sinnis, P. (2007). Heparan sulfate proteoglycans provide a signal to Plasmodium sporozoites to stop migrating and productively invade host cells. Cell Host and Microbe *2*, 316–327.

Cowman, A. F. and Crabb, B. S. (2006). Invasion of red blood cells by malaria parasites. Cell *124*, 755–766.

Crick, A. J., Theron, M., Tiffert, T., Lew, V. L., Cicuta, P. and Rayner, J. C. (2014). Quantitation of malaria parasite-erythrocyte cell-cell interactions using optical tweezers. Biophysical Journal *107*, 846–853.

Cui, L., Lindner, S. and Miao, J. (2015). Translational regulation during stage transitions in malaria parasites. Annals of the New York Academy of Sciences *1342*, 1–9.

Das, S., Lemgruber, L., Tay, C. L., Baum, J. and Meissner, M. (2017). Multiple essential functions of Plasmodium falciparum actin-1 during malaria blood-stage development. BMC Biology *15*, 1–16.

de Koning-Ward, T. F., Gilson, P. R. and Crabb, B. S. (2015). Advances in molecular genetic systems in malaria. Nature Reviews Microbiology *13*, 373–87.

Del Rosario, M., Periz, J., Pavlou, G., Lyth, O., Latorre-Barragan, F., Das, S., Pall, G. S., Stortz, J. F., Lemgruber, L., Whitelaw, J. A., Baum, J., Tardieux, I. and Meissner, M. (2019). Apicomplexan F-actin is required for efficient nuclear entry during host cell invasion. EMBO Reports *20*, e48896.

Denisin, A. K. and Pruitt, B. L. (2016). Tuning the range of polyacrylamide gel stiffness for mechanobiology applications. ACS Applied Materials & Interfaces *8*, 21893–21902.

Dessens, J. T., Beetsma, A. L., Dimopoulos, G., Wengelnik, K., Crisanti, A., Kafatos, F. C. and Sinden, R. E. (1999). CTRP is essential for mosquito infection by malaria ookinetes. EMBO Journal *18*, 6221–6227.

Dobrowolski, Janice M. Niesman, I. R. and Sibley, L. D. (1997). Actin in the parasite Toxoplasma gondii is encoded by a single copy gene, ACT1 and exists primarily in a globular form. Cell Motility and the Cytoskeleton *37*, 253–262.

Doench, J. G., Hartenian, E., Graham, D. B., Tothova, Z., Hegde, M., Smith, I., Sullender, M., Ebert, B. L., Xavier, R. J. and Root, D. E. (2014). Rational design of highly active sgRNAs for CRISPR-Cas9-mediated gene inactivation. Nature Biotechnology *32*, 1262–1267.

Doi, Y., Shinzawa, N., Fukumoto, S., Okano, H. and Kanuka, H. (2010). ADF2 is required for transformation of the ookinete and sporozoite in malaria parasite development. Biochemical and Biophysical Research Communications *397*, 668–672.

Douglas, R. G., Amino, R., Sinnis, P. and Frischknecht, F. (2015). Active migration and passive transport of malaria parasites. Trends in Parasitology *31*, 357–362.

Douglas, R. G., Nandekar, P., Aktories, J. E., Kumar, H., Weber, R., Sattler, J. M., Singer, M., Lepper, S., Sadiq, S. K., Wade, R. C. and Frischknecht, F. (2018a). Intersubunit interactions drive divergent dynamics in mammalian and Plasmodium actin filaments. PLoS Biology *16*, 1–30.

Douglas, R. G., Reinig, M., Neale, M. and Frischknecht, F. (2018b). Screening for potential prophylactics targeting sporozoite motility through the skin. Malaria Journal *17*, 1–10.

Douse, C. H., Green, J. L., Salgado, P. S., Simpson, P. J., Thomas, J. C., Langsley, G., Holder, A. A., Tate, E. W. and Cota, E. (2012). Regulation of the Plasmodium motor complex: phosphorylation of myosin A tail-interacting protein (MTIP) loosens its grip on MyoA. Journal of Biological Chemistry *287*, 36968–36977.

Dowse, T. J., Koussis, K., Blackman, M. J. and Soldati-Favre, D. (2008). Roles of proteases during invasion and egress by plasmodium and toxoplasma. Sub-Cellular Biochemistry *47*, 121–139.

Dubois, D. J. and Soldati-Favre, D. (2019). Biogenesis and secretion of micronemes in Toxoplasma gondii. Cellular Microbiology *21*, e13018.

Dubremetz, J. F., Garcia-Réguet, N., Conseil, V. and Fourmaux, M. N. (1998). Apical organelles and host-cell invasion by Apicomplexa. International Journal for Parasitology *28*, 1007–1013.

Dundas, K., Shears, M. J., Sun, Y., Hopp, C. S., Crosnier, C., Metcalf, T., Girling, G., Sinnis, P., Billker, O. and Wright, G. J. (2018). Alpha-v–containing integrins are host receptors for the Plasmodium falciparum sporozoite surface protein, TRAP. PNAS *115*, 4477–4482.

Duraisingh, M. T. and Skillman, K. M. (2018). Epigenetic variation and regulation in malaria parasites. Annual Review of Microbiology *72*, 355–375.

Egarter, S., Andenmatten, N., Jackson, A. J., Whitelaw, J. A., Pall, G., Black, J. A., Ferguson, D. J. P., Tardieux, I., Mogilner, A. and Meissner, M. (2014). The Toxoplasma Acto-MyoA motor complex is important but not essential for gliding motility and host cell invasion. PLOS One *9*, e91819.

Ejigiri, I., Ragheb, D. R. T., Pino, P., Coppi, A., Bennett, B. L., Soldati-Favre, D. and Sinnis, P. (2012). Shedding of TRAP by a rhomboid protease from the malaria sporozoite surface is essential for gliding motility and sporozoite infectivity. PLoS Pathogens *8*, e1002725.

Elosegui-Artola, A., Trepat, X. and Roca-Cusachs, P. (2018). Control of mechanotransduction by molecular clutch dynamics. Trends in Cell Biology *28*, 356–367.

Engler, A. J., Sen, S., Sweeney, H. L. and Discher, D. E. (2006). Matrix elasticity directs stem cell lineage specification. Cell *126*, 677–689.

Fang, H., Gomes, A. R., Klages, N., Pino, P., Maco, B., Walker, E. M., Zenonos, Z. A., Angrisano, F., Baum, J., Doerig, C., Baker, D. A., Billker, O. and Brochet, M. (2018). Epistasis studies reveal redundancy among calcium-dependent protein kinases in motility and invasion of malaria parasites. Nature Communications *9*, 1–14.

Fletcher, D. A. and Mullins, R. D. (2010). Cell mechanics and the cytoskeleton. Nature *463*, 485–492.

Foth, B. J., Goedecke, M. C. and Soldati, D. (2006). New insights into myosin evolution and classification. PNAS *103*, 3681–3686.

Francia, M. E. and Striepen, B. (2014). Cell division in apicomplexan parasites. Nature Reviews Microbiology *12*, 125–136.

Frénal, K., Dubremetz, J. F., Lebrun, M. and Soldati-Favre, D. (2017a). Gliding motility powers invasion and egress in Apicomplexa. Nature Reviews Microbiology *15*, 645–660.

Frénal, K., Jacot, D., Hammoudi, P. M., Graindorge, A., Maco, B. and Soldati-Favre, D. (2017b). Myosin-dependent cell-cell communication controls synchronicity of division in acute and chronic stages of Toxoplasma gondii. Nature Communications *8*, 1–18.

Frenal, K., Marq, J.-B., Jacot, D., Polonais, V. and Soldati-Favre, D. (2014). Plasticity between MyoC- and MyoA-glideosomes : an example of functional compensation in Toxoplasma gondii invasion. PLoS Pathogens *10*, e1004504.

Frenal, K., Polonais, V., Marq, J.-b., Stratmann, R., Limenitakis, J. and Soldati-Favre, D. (2010). Functional dissection of the apicomplexan glideosome molecular architecture. Cell Host & Microbe *8*, 343–357.

Friedl, P. (2004). Prespecification and plasticity: Shifting mechanisms of cell migration. Current Opinion in Cell Biology *16*, 14–23.

Frischknecht, F. (2007). The skin as interface in the transmission of arthropod-borne pathogens. Cellular Microbiology *9*, 1630–1640.

Frischknecht, F., Baldacci, P., Martin, B., Zimmer, C., Thiberge, S., Olivo-Marin, J. C., Shorte, S. L. and Ménard, R. (2004). Imaging movement of malaria parasites during transmission by Anopheles mosquitoes. Cellular Microbiology *6*, 687–694.

Frischknecht, F., Martin, B., Thiery, I., Bourgouin, C. and Menard, R. (2006). Using green fluorescent malaria parasites to screen for permissive vector mosquitoes. Malaria Journal *5*, 1–8.

Gaji, R. Y., Johnson, D. E., Treeck, M., Wang, M., Hudmon, A. and Arrizabalaga, G. (2015). Phosphorylation of a myosin motor by TgCDPK3 facilitates rapid initiation of motility during Toxoplasma gondii egress. PLoS Pathogens *11*, e1005268.

Ganter, M., Rizopoulos, Z., Schüler, H. and Matuschewski, K. (2015). Pivotal and distinct role for Plasmodium actin capping protein alpha during blood infection of the malaria parasite. Molecular Microbiology *96*, 84–94.

Ganter, M., Schüler, H. and Matuschewski, K. (2009). Vital role for the Plasmodium actin capping protein (CP) beta-subunit in motility of malaria sporozoites. Molecular Microbiology *74*, 1356–1367.

Ghorbal, M., Gorman, M., Macpherson, C. R., Martins, R. M., Scherf, A. and Lopez-Rubio, J.-J. (2014). Genome editing in the human malaria parasite Plasmodium falciparum using the CRISPR-Cas9 system. Nature Biotechnology *32*, 819–821.

Ghosh, A. K., Devenport, M., Jethwaney, D., Kalume, D. E., Pandey, A., Anderson, V. E., Sultan, A. A., Kumar, N. and Jacobs-Lorena, M. (2009). Malaria parasite invasion of the mosquito salivary gland requires interaction between the Plasmodium TRAP and the Anopheles saglin proteins. PLoS Pathogens *5*, e1000265.

Gilson, P. R. and Crabb, B. S. (2009). Morphology and kinetics of the three distinct phases of red blood cell invasion by Plasmodium falciparum merozoites. International Journal for Parasitology *39*, 91–96.

Gomes, A. R., Bushell, E., Schwach, F., Girling, G., Anar, B., Quail, M. A., Herd, C., Pfander, C., Modrzynska, K., Rayner, J. C. and Billker, O. (2015). A genome-scale vector resource enables high-throughput reverse genetic screening in a malaria parasite. Cell Host and Microbe *17*, 404–413.

Grady, M. E., Composto, R. J. and Eckmann, D. M. (2016). Cell elasticity with altered cytoskeletal architectures across multiple cell types. Journal of the Mechanical Behavior of Biomedical Materials *61*, 197–207.

Graindorge, A., Frénal, K., Jacot, D., Salamun, J., Marq, J. B. and Soldati-Favre, D. (2016). The conoid associated motor MyoH is indispensable for Toxoplasma gondii entry and exit from host cells. PLoS Pathogens *12*, e1005388.

Green, J. L., Rees-channer, R. R., Howell, S. A., Martin, S. R., Knuepfer, E., Taylor, H. M., Grainger, M. and Holder, A. A. (2008). The motor complex of Plasmodium falciparum. Journal of Biological Chemistry *283*, 30980–30989.

Green, J. L., Wall, R. J., Vahokoski, J., Yusuf, N. A., Ridzuan, M. A. M., Stanway, R. R., Stock, J., Knuepfer, E., Brady, D., Martin, S. R., Howell, S. A., Pires, I. P., Moon, R. W., Molloy, J. E., Kursula, I., Tewari, R. and Holder, A. A. (2017). Compositional and expression analyses of the glideosome during the Plasmodium life cycle reveal an additional myosin light chain required for maximum motility. Journal of Biological Chemistry *292*, 17857–17875.

Greenberg, M. J., Lin, T., Shuman, H. and Ostap, E. M. (2015). Mechanochemical tuning of myosin-I by the N-terminal region. PNAS *112*, E3337–E3344.

Harding, C. R., Gow, M., Kang, J. H., Shortt, E., Manalis, S. R., Meissner, M. and Lourido, S. (2019). Alveolar proteins stabilize cortical microtubules in Toxoplasma gondii. Nature Communications *10*, 1–14.

Harding, C. R. and Meissner, M. (2014). The inner membrane complex through development of Toxoplasma gondii and Plasmodium. Cellular Microbiology *16*, 632–641.

Hartman, M. A. and Spudich, J. A. (2012). The myosin superfamily at a glance. Journal of Cell Science *125*, 1627–1632.

Heaslip, A. T., Nelson, S. R. and Warshaw, D. M. (2016). Dense granule trafficking in Toxoplasma gondii requires a unique class 27 myosin and actin filaments. Molecular Biology of the Cell *27*, 2080–2089.

Hegge, S., Münter, S., Steinbüchel, M., Heiss, K., Engel, U., Matuschewski, K. and Frischknecht, F. (2010). Multistep adhesion of Plasmodium sporozoites. FASEB Journal *24*, 2222–2234.

Hegge, S., Uhrig, K., Streichfuss, M., Kynast-Wolf, G., Matuschewski, K., Spatz, J. P. and Frischknecht, F. (2012). Direct manipulation of malaria parasites with optical tweezers reveals distinct functions of plasmodium surface proteins. ACS Nano *6*, 4648–4662.

Heintzelman, M. B. (2015). Gliding motility in apicomplexan parasites. Seminars in Cell & Developmental Biology *46*, 135–142.

Heiss, K., Nie, H., Kumar, S., Daly, T. M., Bergman, L. W. and Matuschewski, K. (2008). Functional characterization of a redundant Plasmodium TRAP family invasin, TRAP-like protein, by aldolase binding and a genetic complementation test. Eukaryotic Cell *7*, 1062–1070.

Heissler, S. M. and Sellers, J. R. (2016). Various themes of myosin regulation. Journal of Molecular Biology *428*, 1927–1946.

Hellmann, J. K., Münter, S., Kudryashev, M., Schulz, S., Heiss, K., Müller, A.-K., Matuschewski, K., Spatz, J. P., Schwarz, U. S. and Frischknecht, F. (2011). Environmental constraints guide migration of malaria parasites during transmission. PLoS Pathogens *7*, e1002080.

Hellmann, J. K., Perschmann, N., Spatz, J. P. and Frischknecht, F. (2013). Tunable substrates unveil chemical complementation of a genetic cell migration defect. Advanced Healthcare Materials *2*, 1162–1169.

Herm-Götz, A., Weiss, S., Stratmann, R., Fujita-Becker, S., Ruff, C., Meyhofer, E., Soldati, T., Manstein, D. J., Geeves, M. A. and Soldati, D. (2002). Toxoplasma gondii myosin A and its light chain: a fast, single-headed, plus-end-directed motor. EMBO Journal *21*, 2149–2158.

Hettmann, C., Herm, A., Geiter, A., Frank, B., Schwarz, E., Soldati, T. and Soldati, D. (2000). A dibasic motif in the tail of a class XIV apicomplexan myosin is an essential

determinant of plasma membrane localization. Molecular Biology of the Cell *11*, 1385–1400.

Hliscs, M., Sattler, J. M., Tempel, W., Artz, J. D., Dong, A., Hui, R., Matuschewski, K. and Schüler, H. (2010). Structure and function of a G-actin sequestering protein with a vital role in malaria oocyst development inside the mosquito vector. Journal of Biological Chemistry *285*, 11572–11583.

Holmes, D. L. and Stellwagen, N. C. (1991). Estimation of polyacrylamide gel pore size from Ferguson plots of linear DNA fragments. Electrophoresis *12*, 612–619.

Hopp, C. S., Chiou, K., Ragheb, D. R. T., Salman, A. M., Khan, S. M., Liu, A. J. and Sinnis, P. (2015). Longitudinal analysis of Plasmodium sporozoite motility in the dermis reveals component of blood vessel recognition. eLife *4*, e07789.

Horvath, P. and Barrangou, R. (2010). CRISPR/Cas, the immune system of bacteria and archaea. Science *327*, 167–70.

Houdusse, A. and Sweeney, H. L. (2016). How myosin generates force on actin filaments. Trends in Biochemical Sciences *41*, 989–997.

Hughes, K. R., Philip, N., Starnes, L. G., Taylor, S. and Waters, A. P. (2010). From cradle to grave: RNA biology in malaria parasites. Wiley Interdisciplinary Reviews: RNA *1*, 287–303.

Humphrey, J. D., Dufresne, E. R. and Schwartz, M. a. (2014). Mechanotransduction and extracellular matrix homeostasis. Nature Reviews Molecular Cell Biology *15*, 802–812.

Iskratsch, T., Wolfenson, H. and Sheetz, M. P. (2014). Appreciating force and shape - the rise of mechanotransduction in cell biology. Nature Reviews Molecular Cell Biology *15*, 825–833.

Jacot, D., Daher, W. and Soldati-Favre, D. (2013). Toxoplasma gondii myosin F, an essential motor for centrosomes positioning and apicoplast inheritance. The EMBO Journal *32*, 1702–1716.

Jacot, D., Tosetti, N., Pires, I., Stock, J., Graindorge, A., Hung, Y.-F., Han, H., Tewari, R., Kursula, I. and Soldati-Favre, D. (2016). An apicomplexan actin-binding protein serves as a connector and lipid sensor to coordinate motility and invasion. Cell Host & Microbe *20*, 731–743.

Janse, C. J., Ramesar, J. and Waters, A. P. (2006). High-efficiency transfection and drug selection of genetically transformed blood stages of the rodent malaria parasite Plasmodium berghei. Nature Protocols *1*, 646–656.

Janse, C. J. and Waters, A. P. (2002). Episomal transformation of Plasmodium berghei. Methods in Molecular Medicine *72*, 305–315.

Jeninga, M., Quinn, J. and Petter, M. (2019). ApiAP2 transcription factors in apicomplexan parasites. Pathogens *8*, 1–24.

Jinek, M., Chylinski, K., Fonfara, I., Hauer, M., Doudna, J. a. and Charpentier, E. (2012). A programmable dual-RNA-guided DNA endonuclease in adaptive bacterial immunity. Science *337*, 816–21.

Josling, G. A. and Llinás, M. (2015). Sexual development in Plasmodium parasites: Knowing when it's time to commit. Nature Reviews Microbiology *13*, 573–587.

Kad, N. M., Patlak, J. B., Fagnant, P. M., Trybus, K. M. and Warshaw, D. M. (2007). Mutation of a conserved glycine in the SH1-SH2 helix affects the load-dependent kinetics of myosin. Biophysical Journal *92*, 1623–1631.

Kan, A., Tan, Y.-H., Angrisano, F., Hanssen, E., Rogers, K. L., Whitehead, L., Mollard, V. P., Cozijnsen, A., Delves, M. J., Crawford, S., Sinden, R. E., McFadden, G. I., Leckie, C., Bailey, J. and Baum, J. (2014). Quantitative analysis of Plasmodium ookinete motion in three dimensions suggests a critical role for cell shape in the biomechanics of malaria parasite gliding motility. Cellular Microbiology *16*, 734–750.

Katakai, T. and Kinashi, T. (2016). Microenvironmental control of high-speed interstitial T cell migration in the lymph node. Frontiers in Immunology *7*, 1–8.

Kechagia, J. Z., Ivaska, J. and Roca-Cusachs, P. (2019). Integrins as biomechanical sensors of the microenvironment. Nature Reviews Molecular Cell Biology *20*, 457–473.

Kehrer, J., Singer, M., Lemgruber, L., Silva, P. A. G. C., Frischknecht, F. and Mair, G. R. (2016). A putative small solute transporter is responsible for the secretion of G377 and TRAP-containing secretory vesicles during Plasmodium gamete egress and sporozoite motility. PLoS Pathogens *12*, 1–25.

Kinose, F., Wang, S. X., Kidambi, U. S., Moncman, C. L. and Winkelmann, D. A. (1996). Glycine 699 is pivotal for the motor activity of skeletal muscle myosin. Journal of Cell Biology *134*, 895–909.

Kirkman, L. A., Lawrence, E. A. and Deitsch, K. W. (2014). Malaria parasites utilize both homologous recombination and alternative end joining pathways to maintain genome integrity. Nucleic Acids Research *42*, 370–379.

Klug, D. (2017). Modification and analysis of proteins involved in gliding motility and invasion of Plasmodium. PhD thesis, Heidelberg University.

Klug, D. and Frischknecht, F. (2017). Motility precedes egress of malaria parasites from oocysts. eLife *6*, 1–32.

Klug, D., Kehrer, J., Frischknecht, F. and Singer, M. (2018). A synthetic promoter for multi-stage expression to probe complementary functions of Plasmodium adhesins. Journal of Cell Science *131*, jcs210971.

Klug, D., Mair, G. R., Frischknecht, F. and Douglas, R. G. (2016). A small mitochondrial protein present in myzozoans is essential for malaria transmission. Open Biology *6*, 160034.

Kono, M., Herrmann, S., Loughran, N. B., Cabrera, A., Engelberg, K., Lehmann, C., Sinha, D., Prinz, B., Ruch, U., Heussler, V., Spielmann, T., Parkinson, J. and Gilberger, T. W. (2012). Evolution and architecture of the inner membrane complex in asexual and sexual stages of the malaria parasite. Molecular Biology and Evolution *29*, 2113–2132.

Kratzer, J. (2016). Molecular mechanisms of malaria parasite-substrate interactions. MSc thesis, Heidelberg University.

Krüger, T. and Engstler, M. (2015). Flagellar motility in eukaryotic human parasites. Seminars in Cell and Developmental Biology *46*, 113–127.

Kudryashev, M., Lepper, S., Baumeister, W., Cyrklaff, M. and Frischknecht, F. (2010a). Geometric constrains for detecting short actin filaments by cryogenic electron tomography. PMC Biophysics *3*, 1–14.

Kudryashev, M., Lepper, S., Stanway, R., Bohn, S., Baumeister, W., Cyrklaff, M. and Frischknecht, F. (2010b). Positioning of large organelles by a membrane-associated cytoskeleton in Plasmodium sporozoites. Cellular Microbiology *12*, 362–371.

Kudryashev, M., Münter, S., Lemgruber, L., Montagna, G., Stahlberg, H., Matuschewski, K., Meissner, M., Cyrklaff, M. and Frischknecht, F. (2012). Structural basis for chirality and directional motility of Plasmodium sporozoites. Cellular Microbiology *14*, 1757–1768.

Kumar, S. and Barillas-Mury, C. (2005). Ookinete-induced midgut peroxidases detonate the time bomb in anopheline mosquitoes. Insect Biochemistry and Molecular Biology *35*, 721–727.

Lämmermann, T., Bader, B. L., Monkley, S. J., Worbs, T., Wedlich-Söldner, R., Hirsch, K., Keller, M., Förster, R., Critchley, D. R., Fässler, R. and Sixt, M. (2008). Rapid leukocyte migration by integrin-independent flowing and squeezing. Nature *453*, 51–55.

Lang, N. R., Skodzek, K., Hurst, S., Mainka, A., Steinwachs, J., Schneider, J., Aifantis, K. E. and Fabry, B. (2015). Biphasic response of cell invasion to matrix stiffness in three-dimensional biopolymer networks. Acta Biomaterialia *13*, 61–67.

Lasonder, E., Green, J. L., Grainger, M., Langsley, G. and Holder, A. A. (2015). Extensive differential protein phosphorylation as intraerythrocytic Plasmodium falciparum schizonts develop into extracellular invasive merozoites. Proteomics *15*, 2716–2729.

Lee, A. H., Symington, L. S. and Fidock, D. A. (2014). DNA repair mechanisms and their biological roles in the malaria parasite Plasmodium falciparum. Microbiology and Molecular Biology Reviews *78*, 469–486.

Lee, M. C., Lindner, S. E., Lopez-Rubio, J.-J. and Llinás, M. (2019). Cutting back malaria: CRISPR/Cas9 genome editing of Plasmodium. Briefings in Functional Genomics *18*, 281–289.

Lee, M. C. S. and Fidock, D. A. (2014). CRISPR-mediated genome editing of Plasmodium falciparum malaria parasites. Genome Medicine *6*, 1–4.

Liaw, C.-y., Ji, S. and Guvendiren, M. (2018). Engineering 3D hydrogels for personalized in vitro human tissue models. Advanced Healthcare Materials *7*, 1–16.

Lin, J.-w., Annoura, T., Sajid, M., Chevalley-Maurel, S., Ramesar, J., Klop, O., Franke-Fayard, B. M. D., Janse, C. J. and Khan, S. M. (2011). A novel 'Gene Insertion/Marker Out' (GIMO) method for transgene expression and gene complementation in rodent malaria parasites. PLoS ONE *6*, e29289.

Lindner, S. E., Swearingen, K. E., Shears, M. J., Walker, M. P., Vrana, E. N., Hart, K. J., Minns, A. M., Sinnis, P., Moritz, R. L. and Kappe, S. H. (2019). Transcriptomics and proteomics reveal two waves of translational repression during the maturation of malaria parasite sporozoites. Nature Communications *10*, 1–13.

Liu, Y.-J., Le Berre, M., Lautenschlaeger, F., Maiuri, P., Callan-Jones, A., Heuze, M., Takaki, T., Voituriez, R. and Piel, M. (2015). Confinement and low adhesion induce fast amoeboid migration of slow mesenchymal cells. Cell *160*, 659–672.

Lu, H., Fagnant, P. M. and Trybus, K. M. (2019). Unusual dynamics of the divergent malaria parasite PfAct1 actin filament. PNAS *116*, 20418–20427.

Lu, X., Bryant, M. K., Bryan, K. E., Rubenstein, P. A. and Kawai, M. (2005). Role of the N-terminal negative charges of actin in force generation and cross-bridge kinetics in reconstituted bovine cardiac muscle fibres. Journal of Physiology *564*, 65–82.

Matthews, H., Duffy, C. W. and Merrick, C. J. (2018). Checks and balances? DNA replication and the cell cycle in Plasmodium. Parasites and Vectors *11*, 1–13.

Matuschewski, K. (2017). Vaccines against malaria-still a long way to go. FEBS Journal *284*, 2560–2568.

Matuschewski, K., Ross, J., Brown, S. M., Kaiser, K., Nussenzweig, V. and Kappe, S. H. (2002). Infectivity-associated changes in the transcriptional repertoire of the malaria parasite sporozoite stage. Journal of Biological Chemistry *277*, 41948–41953.

Matz, J. M. and Kooij, T. W. (2015). Towards genome-wide experimental genetics in the in vivo malaria model parasite plasmodium berghei. Pathogens and Global Health *109*, 46–60.

Meis, J. F., Wismans, P. G., Jap, P. H., Lensen, a. H. and Ponnudurai, T. (1992). A scanning electron microscopic study of the sporogonic development of Plasmodium falciparum in Anopheles stephensi. Acta Tropica *50*, 227–236.

Meissner, M., Ferguson, D. J. and Frischknecht, F. (2013). Invasion factors of apicomplexan parasites: Essential or redundant? Current Opinion in Microbiology *16*, 438–444.

Meissner, M., Schluter, D. and Soldati, D. (2002). Role of Toxoplasma gondii myosin A in powering parasite gliding and host cell invasion. Science *298*, 837–840.

Melak, M., Plessner, M. and Grosse, R. (2017). Actin visualization at a glance. Journal of Cell Science *130*, 525–530.

Mizuno, Y., Makioka, A., Kawazu, S. I., Kano, S., Kawai, S., Akaki, M., Aikawa, M. and Ohtomo, H. (2002). Effect of jasplakinolide on the growth, invasion, and actin cytoskeleton of Plasmodium falciparum. Parasitology Research *88*, 844–848.

Montagna, G. N., Buscaglia, C. A., Münter, S., Goosmann, C., Frischknecht, F., Brinkmann, V. and Matuschewski, K. (2012). Critical role for heat shock protein 20 (HSP20) in migration of malarial sporozoites. Journal of Biological Chemistry *287*, 2410–2422.

Morahan, B. J., Wang, L. and Coppel, R. L. (2009). No TRAP, no invasion. Trends in Parasitology *25*, 77–84.

Moreau, C. A. (2017). Profilin in Plasmodium berghei gliding motility and development. PhD thesis, Heidelberg University.

Moreau, C. A., Bhargav, S. P., Kumar, H., Quadt, K. A., Piirainen, H., Strauss, L., Kehrer, J., Streichfuss, M., Spatz, J. P., Wade, R. C., Kursula, I. and Frischknecht, F. (2017). A unique profilin-actin interface is important for malaria parasite motility. PLOS Pathogens *13*, e1006412.

Moreau, C. A., Quadt, K. A., Piirainen, H., Kumar, H., Kursula, I. and Frischknecht, F. (2020). A function of profilin in force generation during malaria parasite motility independent of actin binding. Journal of Cell Science *134*, jcs233775.

Moreira, C. K., Templeton, T. J., Lavazec, C., Hayward, R. E., Hobbs, C. V., Kroeze, H., Janse, C. J., Waters, A. P., Sinnis, P. and Coppi, A. (2008). The Plasmodium TRAP/MIC2 family member, TRAP-Like Protein (TLP), is involved in tissue traversal by sporozoites. Cellular Microbiology *10*, 1505–1516.

Morrissette, N. S. and Sibley, L. D. (2002). Cytoskeleton of apicomplexan parasites. Microbiology and Molecular Biology Reviews *66*, 21–38.

Mueller, C., Graindorge, A. and Soldati-Favre, D. (2017). Functions of myosin motors tailored for parasitism. Current Opinion in Microbiology *40*, 113–122.

Muller, I., Jex, A. R., Kappe, S. H., Mikolajczak, S. A., Sattabongkot, J., Patrapuvich, R., Lindner, S., Flannery, E. L., Koepfli, C., Ansell, B., Lerch, A., Emery-Corbin, S. J., Charnaud, S., Smith, J., Merrienne, N., Swearingen, K. E., Moritz, R. L., Petter, M., Duffy, M. F. and Chuenchob, V. (2019). Transcriptome and histone epigenome of Plasmodium vivax salivary-gland sporozoites point to tight regulatory control and mechanisms for liver-stage differentiation in relapsing malaria. International Journal for Parasitology *49*, 501–513.

Münter, S., Sabass, B., Selhuber-Unkel, C., Kudryashev, M., Hegge, S., Engel, U., Spatz, J. P., Matuschewski, K., Schwarz, U. S. and Frischknecht, F. (2009). Plasmodium sporozoite motility is modulated by the turnover of discrete adhesion sites. Cell Host & Microbe *6*, 551–562.

Muthinja, J. M., Ripp, J., Krüger, T., Imle, A., Haraszti, T., Fackler, O. T., Spatz, J. P., Engstler, M. and Frischknecht, F. (2018). Tailored environments to study motile cells and pathogens. Cellular Microbiology *20*, e12820.

Muthinja, M. J., Ripp, J., Hellmann, J. K., Haraszti, T., Dahan, N., Lemgruber, L., Battista, A., Schütz, L., Fackler, O. T., Schwarz, U. S., Spatz, J. P. and Frischknecht, F. (2017). Microstructured blood vessel surrogates reveal structural tropism of motile malaria parasites. Advanced Healthcare Materials *6*, 1601178.

Natarajan, R., Thathy, V., Mota, M. M., Hafalla, J. C., Ménard, R. and Vernick, K. D. (2001). Fluorescent Plasmodium berghei sporozoites and pre-erythrocytic stages: a new tool to study mosquito and mammalian host interactions with malaria parasites. Cellular Microbiology *3*, 371–379.

Nyström, A. and Bruckner-Tuderman, L. (2019). Matrix molecules and skin biology. Seminars in Cell and Developmental Biology *89*, 136–146.

O'Brochta, D. A., Alford, R., Harrell, R., Aluvihare, C., Eappen, A. G., Li, T., Chakravarty, S., Sim, B. K. L., Hoffman, S. L. and Billingsley, P. F. (2019). Is Saglin a mosquito salivary gland receptor for Plasmodium falciparum? Malaria Journal *18*, 1–11.

Odronitz, F. and Kollmar, M. (2007). Drawing the tree of eukaryotic life based on the analysis of 2,269 manually annotated myosins from 328 species. Genome Biology *8*, 1–23.

Orr, R. Y., Philip, N. and Waters, A. P. (2012). Improved negative selection protocol for Plasmodium berghei in the rodent malarial model. Malaria Journal *11*, 1–6.

Otto, T., Böhme, U., Jackson, A., Hunt, M., Franke-Fayard, B., Hoeijmakers, W., Religa, A., Robertson, L., Sanders, M., Ogun, S., Cunningham, D., Erhart, A., Billker, O., Khan, S., Stunnenberg, H., Langhorne, J., Holder, A., Waters, A., Newbold, C., Pain, A., Berriman, M. and Janse, C. (2014). A comprehensive evaluation of rodent malaria parasite genomes and gene expression. BMC Biology *12*, 1–18.

Pasha, S. N., Meenakshi, I. and Sowdhamini, R. (2016). Revisiting myosin families through large-scale sequence searches leads to the discovery of new myosins. Evolutionary Bioinformatics *12*, 201–211.

Patteson, A. E., Pogoda, K., Byfield, F. J., Mandal, K., Ostrowska-Podhorodecka, Z., Charrier, E. E., Galie, P. A., Deptuła, P., Bucki, R., McCulloch, C. A. and Janmey, P. A. (2019). Loss of vimentin enhances cell motility through small confining spaces. Small *15*, e1903180.

Pazicky, S., Dhamotharan, K., Kaszuba, K., Mertens, H., Gilberger, T., Svergun, D., Kosinski, J., Weininger, U. and Löw, C. (2019). Structural role of essential light chains in the apicomplexan glideosome. BioRxiv *Preprint*, 1–47.

Pegoraro, A. F., Janmey, P. and Weitz, D. A. (2017). Mechanical properties of the cytoskeleton and cells. Cold Spring Harbor Perspectives in Biology *9*, a022038.

Pelham, R. J. and Wang, Y. L. (1997). Cell locomotion and focal adhesions are regulated by substrate flexibility. PNAS *94*, 13661–13665.

Peng, D. and Tarleton, R. (2015). EuPaGDT: a web tool tailored to design CRISPR guide RNAs for eukaryotic pathogens. Microbial Genomics *1*, 1–7.

Periz, J., Whitelaw, J., Harding, C., Gras, S., Minina, M. I. D. R., Latorre-Barragan, F., Lemgruber, L., Reimer, M. A., Insall, R., Heaslip, A. and Meissner, M. (2017). Toxoplasma gondii F-actin forms an extensive filamentous network required for material exchange and parasite maturation. eLife *6*, 1–29.

Perrin, A. J., Collins, C. R., Russell, M. R. G., Collinson, L. M., Baker, D. A. and Blackman, M. J. (2018). The actinomyosin motor drives malaria parasite red blood cell invasion but not egress. mBio *9*, 1–13.

Perschmann, N., Hellmann, J. K., Frischknecht, F. and Spatz, J. P. (2011). Induction of malaria parasite migration by synthetically tunable microenvironments. Nano Letters *11*, 4468–4474.

Petrie, R. J. and Yamada, K. M. (2016). Multiple mechanisms of 3D migration: the origins of plasticity. Current Opinion in Cell Biology *42*, 7–12.

Philip, N. and Waters, A. P. (2015). Conditional degradation of Plasmodium calcineurin reveals functions in parasite colonization of both host and vector. Cell Host and Microbe *18*, 122–131.

Pimenta, P. F., Touray, M. and Miller, L. (1994). The journey of malaria sporozoites in the mosquito salivary gland. Journal of Eukaryotic Microbiology *41*, 608–624.

Pospich, S., Kumpula, E. P., Von der Ecken, J., Vahokoski, J., Kursula, I. and Raunser, S. (2017). Near-atomic structure of jasplakinolide-stabilized malaria parasite F-actin reveals the structural basis of filament instability. PNAS *114*, 10636–10641.

Powell, C. J., Jenkins, M. L., Parker, M. L., Ramaswamy, R., Warshaw, D. M., Ward, G. E., Burke, J. E. and Boulanger, M. J. (2017). Dissecting the molecular assembly of the Toxoplasma gondii MyoA motility complex. Journal of Biological Chemistry *292*, 19469–19477.

Powell, C. J., Ramaswamy, R., Kelsen, A., Hamelin, D. J., Warshaw, D. M., Bosch, J., Burke, J. E., Ward, G. E. and Boulanger, M. J. (2018). Structural and mechanistic insights into the function of the unconventional class XIV myosin MyoA from Toxoplasma gondii. PNAS *115*, E10548–E10555.

Pradel, G., Garapaty, S. and Frevert, U. (2002). Proteoglycans mediate malaria sporozoite targeting to the liver. Molecular Microbiology *45*, 637–651.

Preller, M., Bauer, S., Adamek, N., Fujita-Becker, S., Fedorov, R., Geeves, M. A. and Manstein, D. J. (2011). Structural basis for the allosteric interference of myosin function by reactive thiol region mutations G680A and G680V. Journal of Biological Chemistry *286*, 35051–35060.

Probst, D. (2018). Continuum modeling of cell contractility. PhD thesis, Heidelberg University.

Prudêncio, M., Rodriguez, A. and Mota, M. M. (2006). The silent path to thousands of merozoites: the Plasmodium liver stage. Nature Reviews Microbiology *4*, 849–856.

Quadt, K. A., Streichfuss, M., Moreau, C., Spatz, J. P. and Frischknecht, F. (2016).

Coupling of retrograde flow to force production during malaria parasite migration. ACS Nano *10*, 2091–2102.

Rathnapala, U. L., Goodman, C. D. and McFadden, G. I. (2017). A novel genetic technique in Plasmodium berghei allows liver stage analysis of genes required for mosquito stage development and demonstrates that de novo heme synthesis is essential for liver stage development in the malaria parasite. PLoS Pathogens *13*, e1006396.

Ribeiro, A. J., Denisin, A. K., Wilson, R. E. and Pruitt, B. L. (2016). For whom the cells pull: hydrogel and micropost devices for measuring traction forces. Methods *94*, 51–64.

Robert-Paganin, J., Pylypenko, O., Kikuti, C., Sweeney, H. L. and Houdusse, A. (2020). Force generation by myosin motors: A structural perspective. Chemical Reviews *120*, 5–35.

Robert-Paganin, J., Robblee, J. P., Auguin, D., Blake, T. C. A., Bookwalter, C. S., Krementsova, E. B., Moussaoui, D., Previs, M. J., Jousset, G., Baum, J., Trybus, K. M. and Houdusse, A. (2019). Plasmodium myosin A drives parasite invasion by an atypical force generating mechanism. Nature Communications *10*, 1–12.

Roth, A., Adapa, S. R., Zhang, M., Liao, X., Saxena, V., Goffe, R., Li, S., Ubalee, R., Saggu, G. S., Pala, Z. R., Garg, S., Davidson, S., Jiang, R. H. and Adams, J. H. (2018). Unraveling the Plasmodium vivax sporozoite transcriptional journey from mosquito vector to human host. Scientific Reports *8*, 1–20.

Rotsch, C. and Radmacher, M. (2000). Drug-induced changes of cytoskeletal structure and mechanics in fibroblasts : an atomic force microscopy study. Biophysical Journal *78*, 520–535.

RTSS Clinical Trials Partnership (2017). Efficacy and safety of RTS,S/AS01 malaria vaccine with or without a booster dose in infants and children in Africa: final results of a phase 3, individually randomised, controlled trial. Lancet *386*, 31–45.

Ruiz, J. L. and Gómez-Díaz, E. (2019). The second life of Plasmodium in the mosquito host: gene regulation on the move. Briefings in Functional Genomics *18*, 313–357.

Ruprecht, V., Monzo, P., Ravasio, A., Yue, Z., Makhija, E., Strale, P. O., Gauthier, N., Shivashankar, G. V., Studer, V., Albiges-Rizo, C. and Viasnoff, V. (2017). How cells respond to environmental cues – insights from bio-functionalized substrates. Journal of Cell Science *130*, 51–61.

Ruprecht, V., Wieser, S., Callan-Jones, A., Smutny, M., Morita, H., Sako, K., Barone, V., Ritsch-Marte, M., Sixt, M., Voituriez, R. and Heisenberg, C. P. (2015). Cortical contractility triggers a stochastic switch to fast amoeboid cell motility. Cell *160*, 673–685.

Sato, Y., Hliscs, M., Dunst, J., Goosmann, C., Brinkmann, V., Montagna, G. N. and Matuschewski, K. (2016). Comparative Plasmodium gene overexpression reveals distinct perturbation of sporozoite transmission by profilin. Molecular Biology of the Cell *27*, 2234–2244.

Sato, Y., Montagna, G. N. and Matuschewski, K. (2014). Plasmodium berghei sporozoites acquire virulence and immunogenicity during mosquito hemocoel transit. Infection and Immunity *82*, 1164–1172.

Sattler, J. M., Ganter, M., Hliscs, M., Matuschewski, K. and Schüler, H. (2011). Actin regulation in the malaria parasite. European Journal of Cell Biology *90*, 966–971.

Schindelin, J., Arganda-Carreras, I., Frise, E., Kaynig, V., Longair, M., Pietzsch, T., Preibisch, S., Rueden, C., Saalfeld, S., Schmid, B., Tinevez, J.-Y., White, D. J., Hartenstein, V., Eliceiri, K., Tomancak, P. and Cardona, A. (2012). Fiji: an open-source platform for biological-image analysis. Nature Methods *9*, 676–682.

Schmitz, S., Grainger, M., Howell, S., Calder, L. J., Gaeb, M., Pinder, J. C., Holder, A. A. and Veigel, C. (2005). Malaria parasite actin filaments are very short. Journal of Molecular Biology *349*, 113–125.

Schmitz, S., Schaap, I. A., Kleinjung, J., Harder, S., Grainger, M., Calder, L., Rosenthal, P. B., Holder, A. A. and Veigel, C. (2010). Malaria parasite actin polymerization and filament structure. Journal of Biological Chemistry *285*, 36577–36585.

Schüler, H. and Matuschewski, K. (2006). Regulation of apicomplexan microfilament dynamics by a minimal set of actin-binding proteins. Traffic *7*, 1433–1439.

Schüler, H., Mueller, A.-K. and Matuschewski, K. (2005). A Plasmodium actin-depolymerizing factor that binds exclusively to actin monomers. Molecular Biology of the Cell *16*, 4013–4023.

Schwach, F., Bushell, E., Gomes, A. R., Anar, B., Girling, G., Herd, C., Rayner, J. C. and Billker, O. (2015). PlasmoGEM, a database supporting a community resource for large-scale experimental genetics in malaria parasites. Nucleic Acids Research *43*, D1176–D1182.

Schwarz, U. S. and Gardel, M. L. (2012). United we stand – integrating the actin cytoskeleton and cell–matrix adhesions in cellular mechanotransduction. Journal of Cell Science *125*, 3051–3060.

Schwarz, U. S. and Soiné, J. R. D. (2015). Traction force microscopy on soft elastic substrates: a guide to recent computational advances. Biochimica et Biophysica Acta *1853*, 3095–3104.

Sebastian, S., Brochet, M., Collins, M. O., Schwach, F., Jones, M. L., Goulding, D., Rayner, J. C., Choudhary, J. S. and Billker, O. (2012). A Plasmodium calcium-dependent protein kinase controls zygote development and transmission by translationally activating repressed mRNAs. Cell Host & Microbe *12*, 9–19.

Sebé-Pedrós, A., Grau-Bové, X., Richards, T. A. and Ruiz-Trillo, I. (2014). Evolution and classification of myosins, a paneukaryotic whole-genome approach. Genome Biology and Evolution *6*, 290–305.

Seetharaman, S. and Etienne-Manneville, S. (2018). Integrin diversity brings specificity in mechanotransduction. Biology of the Cell *110*, 49–64.

Sellers, J. R. (2000). Myosins: a diverse superfamily. Biochimica et Biophysica Acta *1496*, 3–22.

Shen, B. and Sibley, L. D. (2014). Toxoplasma aldolase is required for metabolism but dispensable for host-cell invasion. PNAS *111*, 3567–72.

Siden-Kiamos, I., Ganter, M., Kunze, A., Hliscs, M., Steinbüchel, M., Mendoza, J., Sinden, R. E., Louis, C. and Matuschewski, K. (2011). Stage-specific depletion of

myosin A supports an essential role in motility of malarial ookinetes. Cellular Microbiology *13*, 1996–2006.

Siden-Kiamos, I., Pinder, J. C. and Louis, C. (2006). Involvement of actin and myosins in Plasmodium berghei ookinete motility. Molecular and Biochemical Parasitology *150*, 308–317.

Sidik, S. M., Huet, D., Ganesan, S. M., Huynh, M. H., Wang, T., Nasamu, A. S., Thiru, P., Saeij, J. P. J., Carruthers, V. B., Niles, J. C. and Lourido, S. (2016). A genome-wide CRISPR screen in Toxoplasma identifies essential apicomplexan genes. Cell *166*, 1423–1435.

Sinden, R. E., Canning, E. U. and Spain, B. (1976). Gametogenesis and fertilization in Plasmodium yoelii nigeriensis: a transmission electron microscope study. Proceedings of the Royal Society B *193*, 55–76.

Sinden, R. E., Talman, A., Marques, S. R., Wass, M. N. and Sternberg, M. J. (2010). The flagellum in malarial parasites. Current Opinion in Microbiology *13*, 491–500.

Singer, M., Marshall, J., Heiss, K., Mair, G., Grimm, D., Mueller, A.-K. and Frischknecht, F. (2015). Zinc finger nuclease-based double-strand breaks attenuate malaria parasites and reveal rare microhomology-mediated end joining. Genome Biology *16*, 1–18.

Smyrnakou, X. (2019). The role of the actomyosin motor and substrate characteristics in Plasmodium berghei gliding motility. MSc thesis, Heidelberg University.

Song, G., Koksal, A. C., Lu, C. and Springer, T. a. (2012). Shape change in the receptor for gliding motility in Plasmodium sporozoites. PNAS *109*, 21420–5.

Spreng, B., Fleckenstein, H., Kübler, P., Di Biagio, C., Benz, M., Patra, P., Schwarz, U. S., Cyrklaff, M. and Frischknecht, F. (2019). Microtubule number and length determine cellular shape and function in Plasmodium. The EMBO Journal *38*, e100984.

Stadler, R. V., White, L. A., Hu, K., Helmke, B. P. and Guilford, W. H. (2017). Direct measurement of cortical force generation and polarization in a living parasite. Molecular Biology of the Cell *28*, 1912–1923.

Stanway, R. R., Bushell, E., Chiappino-Pepe, A., Roques, M., Sanderson, T., Franke-Fayard, B., Caldelari, R., Golomingi, M., Nyonda, M., Pandey, V., Schwach, F., Chevalley, S., Ramesar, J., Metcalf, T., Herd, C., Burda, P. C., Rayner, J. C., Soldati-Favre, D., Janse, C. J., Hatzimanikatis, V., Billker, O. and Heussler, V. T. (2019). Genome-scale identification of essential metabolic processes for targeting the Plasmodium liver stage. Cell *179*, 1112–1128.

Steinbuechel, M. and Matuschewski, K. (2009). Role for the Plasmodium sporozoite-specific transmembrane protein S6 in parasite motility and efficient malaria transmission. Cellular Microbiology *11*, 279–288.

Stortz, J. F., Del Rosario, M., Singer, M., Wilkes, J. M., Meissner, M. and Das, S. (2019). Formin-2 drives polymerisation of actin filaments enabling segregation of apicoplasts and cytokinesis in Plasmodium falciparum. eLife *8*, e49030.

Sturm, A., Amino, R., Van De Sand, C., Regen, T., Retzlaff, S., Rennenberg, A., Krueger, A., Pollok, J. M., Menard, R. and Heussler, V. T. (2006). Manipulation of host hepatocytes by the malaria parasite for delivery into liver sinusoids. Science *313*, 1287–1290.

Sultan, A. A., Thathy, V., Frevert, U., Robson, K. J. H., Crisanti, A., Nussenzweig, V., Nussenzweig, R. S. and Ménard, R. (1997). TRAP is necessary for gliding motility and infectivity of Plasmodium sporozoites. Cell *90*, 511–522.

Sutoh, K., Ando, M., Sutoh, K. and Toyoshima, Y. Y. (1991). Site-directed mutations of Dictyostelium actin: Disruption of a negative charge cluster at the N terminus. PNAS *88*, 7711–7714.

Sweeney, H. L. and Houdusse, A. (2010). Structural and functional insights into the myosin motor mechanism. Annual Review of Biophysics *39*, 539–557.

Tavares, J., Formaglio, P., Thiberge, S., Mordelet, E., Rooijen, N. V., Medvinsky, A., Ménard, R. and Amino, R. (2013). Role of host cell traversal by the malaria sporozoite during liver infection. The Journal of Experimental Medicine *210*, 905–915.

Tayalia, P., Mazur, E. and Mooney, D. J. (2011). Controlled architectural and chemotactic studies of 3D cell migration. Biomaterials *32*, 2634–2641.

Theocharis, A. D., Skandalis, S. S., Gialeli, C. and Karamanos, N. K. (2016). Extracellular matrix structure. Advanced Drug Delivery Reviews *97*, 4–27.

Theveneau, E. and Mayor, R. (2012). Cell migration. Comprehensive Physiology *2*, 2369–2392.

Tomley, F. M. and Soldati, D. S. (2001). Mix and match modules: structure and function of microneme proteins in apicomplexan parasites. Trends in Parasitology *17*, 81–88.

Tossavainen, H., Pihlajamaa, T., Huttunen, T. K., Raulo, E., Rauvala, H., Permi, P. and Kilpeläinen, I. (2006). The layered fold of the TSR domain of P. falciparum TRAP contains a heparin binding site . Protein Science *15*, 1760–1768.

Tse, J. R. and Engler, A. J. (2010). Preparation of hydrogel substrates with tunable mechanical properties. Current Protocols in Cell Biology *47*, 1–16.

Vahokoski, J., Bhargav, S. P., Desfosses, A., Andreadaki, M., Kumpula, E. P., Martinez, S. M., Ignatev, A., Lepper, S., Frischknecht, F., Sidén-Kiamos, I., Sachse, C. and Kursula, I. (2014). Structural differences explain diverse functions of Plasmodium actins. PLoS Pathogens *10*, e1004091.

van Lin, L. H. M., Pace, T., Janse, C. J., Birago, C., Ramesar, J., Picci, L., Ponzi, M. and Waters, A. P. (2001). Interspecies conservation of gene order and intron-exon structure in a genomic locus of high gene density and complexity in Plasmodium. Nucleic Acids Research *29*, 2059–2068.

Vanderberg, J. P. (1974). Studies on the motility of Plasmodium sporozoites. The Journal of Protozoology *21*, 527–537.

Vlachou, D., Zimmermann, T., Cantera, R., Janse, C. J., Waters, A. P. and Kafatos, F. C. (2004). Real-time, in vivo analysis of malaria ookinete locomotion and mosquito midgut invasion. Cellular Microbiology *6*, 671–685.

Volohonsky, G., Paul-Gilloteaux, P., Stafkova, J., Soichot, J., Salamero, J. and Levashina, E. A. (2020). Kinetics of Plasmodium midgut invasion in Anopheles mosquitoes. BioRxiv *Preprint*, 1–27.

Vu, L. T., Jain, G., Veres, B. D. and Rajagopalan, P. (2015). Cell migration on planar and three-dimensional matrices: A hydrogel-based perspective. Tissue Engineering *21*, 67–74.

Wagner, J. C., Platt, R. J., Goldfless, S. J., Zhang, F. and Niles, J. C. (2014). Efficient CRISPR-Cas9-mediated genome editing in Plasmodium falciparum. Nature Methods *11*, 915–918.

Walklate, J., Ujfalusi, Z. and Geeves, M. A. (2016). Myosin isoforms and the mechanochemical cross-bridge cycle. Journal of Experimental Biology *219*, 168–174.

Wall, R. J., Zeeshan, M., Katris, N. J., Limenitakis, R., Rea, E., Stock, J., Brady, D., Waller, R. F., Holder, A. A. and Tewari, R. (2019). Systematic analysis of Plasmodium myosins reveals differential expression, localisation, and function in invasive and proliferative parasite stages. Cellular Microbiology *21*, e13082.

Welch, M. D., Mallavarapu, A., Rosenblatt, J. and Mitchison, T. J. (1997). Actin dynamics in vivo. Current Opinion in Cell Biology *9*, 54–61.

Wells, M. B. and Andrew, D. J. (2019). Anopheles salivary gland architecture shapes Plasmodium sporozoite availability for transmission. mBio *10*, e01238–19.

Wen, J. H., Vincent, L. G., Fuhrmann, A., Choi, Y. S., Hribar, K. C., Taylor-Weiner, H., Chen, S. and Engler, A. J. (2014). Interplay of matrix stiffness and protein tethering in stem cell differentiation. Nature Materials *13*, 979–987.

Wesseling, J. G., Snijders, P. J. F., van Someren, P., Jansen, J., Smits, M. A. and Schoenmakers, J. G. G. (1989). Stage-specific expression and genomic organization of the actin genes of the malaria parasite Plasmodium falciparum. Molecular and Biochemical Parasitology *35*, 167–176.

White, M. W. and Suvorova, E. S. (2018). Apicomplexa cell cycles: something old, borrowed, lost, and new. Trends in Parasitology *34*, 759–771.

Whitelaw, J. A., Latorre-Barragan, F., Gras, S., Pall, G. S., Leung, J. M., Heaslip, A., Egarter, S., Andenmatten, N., Nelson, S. R., Warshaw, D. M., Ward, G. E. and Meiss-

ner, M. (2017). Surface attachment, promoted by the actomyosin system of Toxoplasma gondii is important for efficient gliding motility and invasion. BMC Biology *15*, 1–23.

WHO (2019). World Malaria Report.

Williams, M. J., Alonso, H., Enciso, M., Egarter, S., Sheiner, L., Meissner, M., Striepen, B., Smith, B. J. and Tonkin, C. J. (2015). Two essential light chains regulate the MyoA lever arm to promote Toxoplasma gliding motility. mBio *6*, e00845–15.

Winder, S. J. and Ayscough, K. R. (2005). Actin-binding proteins. Journal of Cell Science *118*, 651–654.

Wykes, M. N. and Good, M. F. (2009). What have we learnt from mouse models for the study of malaria? European Journal of Immunology *39*, 1991–2058.

Yahata, K., Treeck, M., Culleton, R., Gilberger, T. W. and Kaneko, O. (2012). Time-lapse imaging of red blood cell invasion by the rodent malaria parasite Plasmodium yoelii. PLoS ONE *7*, e50780.

Yeoman, J. A., Hanssen, E., Maier, A. G., Klonis, N., Maco, B., Baum, J., Turnbull, L., Whitchurch, C. B., Dixon, M. W. and Tilley, L. (2011). Tracking glideosome-associated protein 50 reveals the development and organization of the inner membrane complex of Plasmodium falciparum. Eukaryotic Cell *10*, 556–564.

Yusuf, N. A., Green, J. L., Wall, R. J., Knuepfer, E., Moon, R. W., Schulte-Huxel, C., Stanway, R. R., Martin, S. R., Howell, S. A., Douse, C. H., Cota, E., Tate, E. W., Tewari, R. and Holder, A. A. (2015). The Plasmodium class XIV Myosin, MyoB, has a distinct subcellular location in invasive and motile stages of the malaria parasite and an unusual light chain. Journal of Biological Chemistry *290*, 12147–12164.

Zahouani, H., Pailler-Mattei, C., Sohm, B., Vargiolu, R., Cenizo, V. and Debret, R. (2009). Characterization of the mechanical properties of a dermal equivalent compared with human skin in vivo by indentation and static friction tests. Skin Research and Technology *15*, 68–76.

Zhang, C., Gao, H., Yang, Z., Jiang, Y., Li, Z., Wang, X., Xiao, B., Su, X.-z., Cui, H. and Yuan, J. (2017). CRISPR/Cas9 mediated sequential editing of genes critical for ookinete motility in Plasmodium yoelii. Molecular and Biochemical Parasitology *212*, 1–8.

Zhang, C., Xiao, B., Jiang, Y., Zhao, Y., Li, Z., Gao, H., Ling, Y., Wei, J., Li, S., Lu, M., Su, X.-z., Cui, H. and Yuan, J. (2014). Efficient editing of malaria parasite genome using the CRISPR/Cas9 system. mBio *5*, 1–9.

Zhang, M., Wang, C., Otto, T. D., Oberstaller, J., Liao, X., Adapa, S. R., Udenze, K., Bronner, I. F., Cassandra, D., Mayho, M., Brown, J., Li, S., Swanson, J., Rayner, J. C., Jiang, R. H. Y. and Adams, J. H. (2018). Uncovering the essential genome of the human malaria parasite Plasmodium falciparum by saturation mutagenesis. Science *360*, eaap7847.

Zieler, H. and Dvorak, J. A. (2000). Invasion in vitro of mosquito midgut cells by the malaria parasite proceeds by a conserved mechanism and results in death of the invaded midgut cells. PNAS *97*, 11516–11521.